

Aus dem Bereich Med. Physiologie
Theoretische Medizin und Biowissenschaften
der Medizinischen Fakultät
der Universität des Saarlandes, Homburg/Saar

**A pHluorin-based method to monitor exocytosis by
release of peptidergic cargo molecules from
chromaffin cells**

**Dissertation zur Erlangung des Grades eines Doktors der
Naturwissenschaften**

der Medizinischen Fakultät
der UNIVERSITÄT DES SAARLANDES

2015

vorgelegt von: Soumyajit Dutta
geb.am: 01.01.1983 in Nadia, India

Tag des Promotionskolloquiums: _____

Dekan:

Vorsitzender:

Berichtersteller:

Erklärung gemäß § 7 Abs. 1 Nr. 4

Ich erkläre hiermit an Eides statt, dass ich die vorliegende Arbeit ohne unzulässige Hilfe Dritter und ohne Benutzung anderer als der angegebenen Hilfsmittel angefertigt habe. Die aus anderen Quellen direkt oder indirekt übernommenen Daten und Konzepte sind unter Angabe der Quelle gekennzeichnet.

Bei der Auswahl und Auswertung folgenden Materials haben mir die nachstehend aufgeführten Personen in der jeweils beschriebenen Weise unentgeltlich/entgeltlich geholfen:

1.
2. usw.

Weitere Personen waren an der inhaltlich-materiellen Erstellung der vorliegenden Arbeit nicht beteiligt. Insbesondere habe ich nicht die entgeltliche Hilfe von Vermittlungs- bzw. Beratungsdiensten (Promotionsberater/innen oder anderer Personen) in Anspruch genommen. Außer den Angegebenen hat niemand von mir unmittelbar oder mittelbar geldwerte Leistungen für Arbeiten erhalten, die im Zusammenhang mit dem Inhalt der vorgelegten Dissertation stehen.

Die Arbeit wurde bisher weder im Inland noch im Ausland in gleicher oder ähnlicher Form in einem anderen Verfahren zur Erlangung des Doktorgrades einer anderen Prüfungsbehörde vorgelegt.

Ich versichere an Eides statt, dass ich nach bestem Wissen die Wahrheit gesagt und nichts verschwiegen habe.

Vor Aufnahme der vorstehenden Versicherung an Eides Statt wurde ich über die Bedeutung einer eidesstattlichen Versicherung und die strafrechtlichen Folgen einer unrichtigen oder unvollständigen eidesstattlichen Versicherung belehrt.

Ort, Datum



Unterschrift der/des Promovierenden

Unterschrift der die Versicherung an Eides statt aufnehmenden Beamtin bzw. des aufnehmenden Beamten

Acknowledgements

First and foremost, I would like to thank my supervisor Prof. Dr. Dieter Bruns for giving me an opportunity and space to conduct my doctoral work under his mentorship. Beside, I appreciate his guidance, pushand support during my entire PhD. I also appreciate his the scientific liberty and critical evaluation in the progress of this work, this made me learn plenty of new things scientifically and also philosophically. I would always be grateful to him for providing me this learning curve and I hope it will be beneficial for all my future endeavors, and I also hope he will continue to advise me throughout my scientific career. I would also like to thank Dr. Ralf Mohrmann for highly generous helping-hand regarding guidance and suggestions for this work. Starting from sharing notion on projected experiments, technical advice, trouble-shooting and high standard programming in IGOR that saved my valuable time and energy.

I would also like to thank Prof Dr. Jens Rettig for his critical evaluation and suggestions to improemy project at our departmental lab meetings. Alongside, I am also thankful to all lab members from Prof. Bruns and Prof. Rettig groups. They made the lab atmosphere highly amicable, which allowed me have a free pass within the building to use different facilities and share reagents with mutual understanding. I would like to thank Dr. Ute Becherer for helping me with the TIRF experiments and analysis. Alongside, I am also grateful to her for keeping the door open for me, which allowed me throw all my queries without any inhibition. I also thank Prof. Frank Schmitz, Dr. David Stevens and Dr Claudia Schirra for their valuable suggestions during our lab meetings.

Alongside, I am immensely thankful to Varsha Pattu, for some technical help and for reading and correcting my thesis thoroughly, in spite of her extremely busy schedule. I am immensely thankful to Yvonne for sharing her technical experience and taking all my questions, irrespective of the quality and content of the questions, for helping me in various perspective that were helpful for me to settle down in Germany and also with various personal problem. I also thank Barbara for helping me with various professional, personal problems and also for being a reciprocal listener to some out-of-the-box topics. I would like to thank Dr. Ulf Matti for helping

me with some molecular biology work in the beginning. I would also like to thank Ms. Judith Arend and Marina Wirth for their enormous cooperation and generosity in various bureaucratic stuffs on my behalf. I would like to the graduate school GRK 1326 for the guidance and support during my PhD I am also thankful to Debadutta Deb, Madhurima for making their efforts to correct my thesis; along with them I also thank Halimani for being the best buddy on and off the campus and also for the experimental help in TIRF microscopy. I would also like to thank Antonio for providing experimental help at some phases of my PhD and also for giving me clusters of good times. I would like to thank all members of Abt. Bruns, viz Venessa, Patrick, Walentina, Katja, Kathrine, and Holger for excellent technical support. I would also thank Mayur, Ekta, Sandra, Anneka, Surya for some intellectual contribution and for good companionship. I am also thankful to Birgit, Martina and Marina for helping me immensely in picking animals and also with the animal house assignments. I would also like to thank other people on and off-campus, which I could not mention due to the space restriction. I would like to thank all my friends, seniors and relatives within and out of Germany for their help in various phases of life. Lastly, I would like to show immense gratitude towards my parents and brother, without their sacrifice and support I would never reach this platform.

Table of Content

i	Erklärung gemäß § 7 Abs. 1 Nr. 4	-I-
ii	Acknowledgement	-II-
iii	Table of Content	-IV-
iv	Summary	-VIII-
v	Zusammenfassung	-X-
<hr/>		
1.	Introduction	-1-
1.1	Exocytosis and Endocytosis	-1-
1.1.1	Different types of exocytosis	-2-
1.1.1.1	Constitutive exocytosis	-2-
1.1.1.2	Regulated exocytosis	-3-
1.2	Cardinal steps of Regulated exocytosis	-3-
1.2.1	Biogenesis of vesicles	-3-
1.2.2	Docking of vesicles	-5-
1.2.3	Priming of vesicles	-6-
1.2.4	Fusion of vesicles	-7-
1.3	Governing bodies of membrane fusion in regulated exocytosis	-9-
1.3.1	SNARE proteins	-9-
1.3.2	SM proteins	-13-
1.3.3	Calcium control of vesicular exocytosis	-15-
1.3.3.1	Synaptotagmins	-15-
1.3.3.2	Complexins	-18-
1.4	Neuropeptide Y	-20-
1.5	Objective of the study	-21-
<hr/>		
2.	Materials and Methods	-24-
2.1	Materials	-24-
2.1.1	Reagents	-24-
2.1.2	Kits	-24-
2.1.3	Locke's solution for adrenal gland dissection	-25-
2.1.4	Culture medium (Serum free)	-25-
2.1.5	Enzyme medium	-25-
2.1.6	Inactivation medium	-26-
2.1.7	Solution for activation of virus	-26-

2.1.8	Solution for NPY release assay	-26-
2.1.8.1	Ringer's Solution (normal bath solution)	-26-
2.1.8.2	High Potassium Ringer's Solution (Depolarization solution)	-26-
2.1.8.3	Ammonium Chloride Ringer's Solution (Alkalization Solution)	-27-
2.1.9	Molecular Biology Solution	-27-
2.1.10	Biochemistry Solution	-28-
2.1.11	Plasmids	-31-
2.1.12	Primers and oligonucleotides	-31-
2.1.13	PCR reaction	-32-
2.1.13.1	Standard cloning PCR reaction	-33-
2.1.13.2	Genotyping PCR reaction	-33-
2.1.14	Agarose gel electrophoresis	-36-
2.1.15	Antibodies	-36-
2.2	Methods	-36-
2.2.1	Cell culture	-36-
2.2.1.1	Chromaffin cell culture	-36-
2.2.1.2	Semliki forest virus activation	-37-
2.2.2	Molecular Biology	-37-
2.2.3.	Production of recombinant virus particles	-38-
2.2.4	Biochemistry	-39-
2.2.4.1	Tissue homogenate preparation	-39-
2.2.4.2	Lysate preparation from plated cells	-40-
2.2.4.3	SDS PAGE	-40-
2.2.4.4	Immunoblot	-40-
2.3	Real time NPY release measurement	-41-
2.3.1	Preparation of perfusion pipette	-41-
2.3.2	Preparatory phase of experiment	-42-
2.4.	Digital Image acquisition, processing and analysis	-43-
2.4.1	Confocal Microscopy	-43-
2.4.2	Evanescence wave Microscopy	-44-
2.4.3	Image Analysis	-44-
2.4.4	Line Scan Analysis	-45-
2.5	Statistics	-45-

3. Results	-46-
3.1.1 Imaging stimulus-evoked NPY-pHluorin release from large dense-core vesicles (LDCVs)	-46-
3.1.2 Stimulus-evoked NPY release events fulfill the hallmark of classical v-SNARE mediated and Ca ²⁺ -regulated fusion process	-50-
3.1.3 NPY-pHluorin release shows highly variable kinetics	-52-
3.1.4 Reacidification does not influence the kinetics of NPY-pHluorin time course	-56-
3.1.5 Radial dispersion of NPY molecules from the fusion site	-58-
3.1.6 TIRF images acquired with 20 Hz sampling rate confirms rapid discharge of cargo	-63-
3.1.7 NPY-like molecule with high diffusion coefficient demonstrates 'point-source' dispersion	-66-
3.1.8 NPY-pHluorin release time course is unaffected by the mode of stimulation	-69-
3.1.9 Main calcium sensors play a fundamental role in the facilitation of the NPY-pHluorin release	-71-
3.2.1 Stimulation evoked rise in [Ca ²⁺] _i leads to the dissipation of vesicle membrane membrane-bound VAMP _{II} -pHluorin signal	-73-
3.2.2 Kinetics of SynaptopHluorin (Syb-pHluorin) time course is highly heterogeneous	-78-
3.2.3 Spatial distribution of vesicular Syb _{II} in the fusion site accompanying vesicular exocytosis	-79-
3.2.4 Reacidification of the internalized vesicular lumen contributes in the kinetics of Syb-pHluorin signal time course	-84-
3.3.1 Complexin _{III} (Cpx) is the only isoform that expresses in murine chromaffin cells	-91-
3.3.2 Complexin _{III} ablation leads to a marginal increase in the event frequency and it also increases the spike and the plateau ratio	-92-
3.3.3 Complexin _{III} deficiency does not influence the kinetics of NPY-pHluorin signal time course	-94-
4. Discussion	-97-
4.1 Stimulation evokes NPY release from chromaffin granule	-97-
4.2 Variable kinetics of cargo release are due to variability in the opening	

	of the fusion pore	-100-
4.3	Efflux of the cargo molecules and its discharge-based diffusion are the main rate-limiting steps of NPY discharge	-103-
4.4	Schematic illustration of NPY-pHluorin release from LDCVs	-105-
4.5	Syb-pHluorin, a tool to study exo-and endocytosis	-106-
4.6	Spatial reorganization of vesicular SybII at fusion site as a consequence of vesicular exocytosis	-107-
4.7	Bafilomycin treatment prolongs the time course of Syb-pHluorin events	-108-
5	References	-113-
6	Appendix	-133-
7	Curriculum Vitae	-134-

Summary

The fundamental role of SNAREs and other SNARE accessory molecules, such as SM proteins (Sec and Munc family of proteins), Synaptotagmins (Syt) and Complexins (Cpx) in vesicular exocytosis have been extensively studied. Information on the fusion machinery was primarily congregated from different *in vitro* (biochemical fusion assays), *in vivo* and *ex vivo* electrophysiological and imaging studies. In particular, electrophysiological studies provided information on the fusion machinery in primary cells and/or tissue slices by measuring capacitance, admittance and synaptic currents. On the other hand, imaging studies acquired information on vesicular exocytosis by tracking the signal time course of vesicle bound fluorescent components. In addition, mechanistic information on the exocytotic fusion pore was primarily gathered from the amperometric recordings that rely on the rapid oxidation of small transmitter molecules like epinephrine, serotonin or dopamine. Given the rapid release of such molecules amperometric recordings allow us to study only the exocytotic event for a few milliseconds, but cannot provide insight into the fate of vesicles few seconds after initiation of discharge. In this thesis, we used slowly diffusible cargo molecules, such as oligopeptides, to study the exocytotic event at later times after exocytosis initiation. For this, pHluorin, the pH-sensitive variant of GFP was attached to the vesicular cargo molecule NPY in order to detect changes in the intravesicular pH that is parallel to exocytosis. Our data revealed that NPY-pHluorin is a well-suited reporter molecule to monitor stimulus-evoked vesicular exocytosis by the gain and subsequent loss of fluorescence signal. The rapid uprise in the fluorescence of NPY-pHluorin, upon local superfusion of exocytosis-inducing agents such as 10 μ M ionomycin or a depolarizing high K^+ solution, indicates fusion pore opening. The rapid efflux of hydrated (H_3O^+) proton (0.1 x 0.2 x 0.2 nm) through the initial fusion pore (diameter \sim 2 nm) neutralizes the intravesicular pH and leads to dequenching that was observed with an increase of pHluorin' signal, whereas the subsequent loss in the signal indicates discharge of the cargo molecule from the vesicle. Interestingly, a significant fraction of NPY fusion events exhibit, before the rapid decay of the signal, a characteristic, stationary plateau phase that most likely reflects hindered efflux of cargo molecules due to restricting fusion pore diameters. Based on the molecular dimensions of NPY-pHluorin (\sim 4 x 3 nm) we can estimate that in this case the exocytotic pore exhibits diameters below 3 nm.

Transient, spike-like events instead represent a different type of fusion event that releases cargo rapidly as the pore reaches a maximally dilated state without any measurable temporal delay.

Both types of events [spike and plateau events] were found to be dependent on classical vesicular SNARE proteins (SynaptobrevinII and Cellubrevin) and were facilitated by an increase in intracellular Ca^{2+} . In good correlation, our results demonstrate that NPY-pHluorin release from large dense core vesicles depends on calcium sensing proteins, such as SytI and SytVII. Moreover, the data revealed that reacidification has no role in the signal time course of NPY-pHluorin. Finally, we provide evidence that cargo efflux from the vesicle core is the rate-limiting step in governing the time course of NPY-pHluorin release from the secretory vesicles.

In a separate set of experiments, we studied the kinetics and spatial distribution of the membrane-bound slowly diffusing SynaptopHluorin molecules (comprising the integral membrane protein SynaptobrevinII together with pHluorin). Compared with the kinetics of NPY- events, the time course of the Syb-pHluorin signal is significantly longer and thereby provided insight into a different state of vesicular trafficking, such as endocytosis. Using this experimental paradigm, we could show that the Syb-pHluorin signal is strongly prolonged by blocking the vesicular ATPase with bafilomycin. These results and further analyses show that both, spatial dispersion of the Syb-pHluorin in the plasma membrane (after exocytosis) and reacidification of the vesicle (after endocytosis) contribute to the observed loss of the Syb-pHluorin signal. However, elucidating the mechanistic components for these distinct release events, regarding SNARE complexes and their accessory molecules, particularly in the context of their supra-molecular organization is essential for a better understanding of the neurotransmitter release and cellular trafficking.

Zusammenfassung

Die essentielle Rolle der SNARE-Proteine und ihrer assoziierten Regulatoren wie den SM Proteinen (Sec und Munc Familie), Synaptotagmine (Syt) und Complexinen (Cpx) bei der vesikulären Exozytose wurde bereits intensiv untersucht. Dabei konnten Befunde über die Fusionsmaschinerie durch verschiedene biochemische Fusionsassays und durch elektrophysiologische bzw. bildgebende Studien sowohl in vivo als auch ex vivo gesammelt werden. Besonders haben elektrophysiologische Kapazitäts- und synaptische Strommessungen neue Ergebnisse zur Fusionsmaschinerie in Primärzellen und/oder Gewebeschnitten liefern können. Bildgebende Untersuchungen erlaubten es, Informationen über die vesikuläre Exozytose zu sammeln, indem Intensitätsänderungen des Signals vesikulär gebundener fluoreszierender Komponenten verfolgt wurden. Einblicke in das Verhalten der exozytotischen Fusionspore wurden auch durch amperometrische Messungen erzielt, die auf einer schnellen Oxidation von Botenstoffmolekülen wie Adrenalin, Serotonin oder Dopamin beruhen. Aufgrund der schnellen Freisetzung dieser Botenstoffe liefert ihre elektrochemische Detektion jedoch nur für wenige Millisekunden Informationen zum Membranfusionsvorgang und gewährt keinen Einblick in das Schicksal des Vesikels einige Sekunden nach Initiierung der Exozytose. In dieser Doktorarbeit wurden langsam-diffundierende Frachtmoleküle, wie Oligopeptide, untersucht, um Mechanismen der Exozytose auch zu späteren Zeitpunkten nach Initiierung der Membranfusion untersuchen zu können. Die pH-sensitive Variante des GFP, pHluorin, wurde dazu mit dem vesikulären Frachtprotein NPY fusioniert, um die mit der Exozytose einhergehenden Änderungen des intravesikulären pH-Wertes zu detektieren.

Diese Untersuchungen zeigen, das NPY-pHluorin sich sehr gut als Reporter eignet, um die Stimulus-induzierte vesikuläre Exozytose als Zu- und nachfolgende Abnahme des Fluoreszenzsignals zu verfolgen. Die erste, schnelle Zunahme der NPY-pHluorin Fluoreszenz durch lokale Perfusion mit Exozytose-induzierenden Substanzen, wie z.B. 10 μ M Ionomycin oder einer depolarisierenden K^+ -Lösung, weist auf die Öffnung der Fusionspore hin. Der schnelle Ausstrom von hydrierten (H_3O^+) Protonen ($0.1 \times 0.2 \times 0.2$ nm) durch die initiale Fusionspore (Durchmesser 2nm) neutralisiert den intravesikulären pH und resultiert in einer Zunahme der pHluorin Intensität. Der nachfolgende Verlust des Signals hingegen lässt sich durch die Freisetzung des

Frachtmoleküls aus dem Vesikel erklären. Interessanterweise weist eine signifikante Fraktion der Fusionsereignisse vor der schnellen Abnahme des Fluoreszenzsignals eine ausgeprägte, stationäre Plateauphase auf, die eine verzögerte Freisetzung der Frachtmoleküle durch einschränkende Fusionsporendurchmesser nahelegt. Ausgehend von den molekularen Dimensionen des NPY-pHluorin ($\sim 4 \times 3$ nm) konnten wir abschätzen, dass in diesem Fall der Fusionsporendurchmesser geringer als 3 nm ist. Transiente, nadel-ähnliche Signalverläufe repräsentieren hingegen ein Szenario, bei dem NPY-pHluorin schnell freigesetzt wird, da die Fusionspore sofort, ohne messbare, zeitliche Verzögerung, ein maximal dilatiertes Stadium erreicht.

Das Auftreten beider Ereignis-Typen (Plateau- und Nadel-Typ) ist von klassischen vesikulären SNARE Proteinen (SynaptobrevinII und Cellubrevin) abhängig und wird durch den Anstieg der intrazellulären Ca^{2+} gefördert. Des Weiteren wurde deutlich, dass die Freisetzung von NPY-pHluorin aus großen elektronendichten Vesikeln von den Ca^{2+} -Sensoren SytI und SytVII abhängig ist. Außerdem legen die Daten nahe, dass nicht die Reacidifizierung des Vesikels nach Endozytose sondern die Freisetzung der Frachtmoleküle aus dem Vesikel den ratenbestimmenden Schritt für den zeitlichen Verlauf der Signalabnahme darstellt.

In einer weiteren Reihe von Experimenten wurden Kinetik und räumliche Verteilung des membran-gebundenen und besonders langsam diffundierenden SynaptopHluorin (Fusionsprotein aus membranintegriertem Synaptobrevin und pHluorin) untersucht. Verglichen mit NPY-pHluorin ist der zeitliche Verlauf von SynaptopHluorin deutlich verlangsamt und lieferte dabei zusätzliche Einblicke in Stadien des vesikulären Transports, wie der Endozytose. So konnten wir zeigen, dass das SynaptopHluorin-Signal durch Blockade der vesikulären ATPase mit Bafilomycin signifikant verlängert wird. Dieser Befund und weitere Analysen zeigen, dass neben einer diffusionsabhängigen, räumlichen Verteilung des SynaptopHluorin in der Plasmamembran nach Exozytose auch die Reacidifizierung des Vesikels nach Endozytose für die Abnahme des Fluoreszenzsignals verantwortlich ist.

Für ein besseres Verständnis der Neurotransmitterfreisetzung und der zellulären Transportvorgänge wird es in Zukunft jedoch nötig sein, die zugrundeliegenden Mechanismen Exozytose auch im Kontext der supramolekularen Organisation mehrerer SNARE Komplexe und ihrer akzessorischen Moleküle zu untersuchen.

1. Introduction

1.1 Exocytosis and Endocytosis

Cellular trafficking is a fundamental process in cell physiology by which intracellular, intercellular and extracellular communication takes place. These processes may vary between prokaryotes and eukaryotes. In a prokaryotic cell, all of these communications take place across the cellular barrier: for instance, enzymes required for digestion are transported to the plasma membrane and thereafter secreted to the cell exterior. These transportations enable enzymes to take up small undigested and/or partially digested metabolites generated in the preceding steps of digestion (Alberts et al., 2001). In eukaryotes, a structured membrane system developed during evolution. Here, cellular trafficking allows cells to take up macromolecules by a process called endocytosis. It also plays a regulatory role in the delivery of proteins and carbohydrate to the cell exterior, a process known as exocytosis. However, the molecules to be secreted pass through multiple compartments and travel along this biosynthetic-secretory pathway. Upon following this route, these molecules can also be modified in a series of controlled steps. Furthermore, these molecules are stored in the luminal domain or membrane bound intracellular organelles (vesicles or granules) until they are needed for physiological processes. On requirement, they are delivered to a specific cell-surface domain, where organelle membrane merges with the plasma membrane (Alberts et al., 2001). Alternatively based on functionality, exocytosis can also be defined as a cardinal process, where cellular substances are discharged into the extra-cellular milieu from the substance-containing pouch, i.e. membrane bound vesicles. These substances are required to be transferred to the site of action at the required time. To this end, vesicles fuse with the plasma membrane by the formation of a lipid bridge, and any material within the vesicle diffuses into the extracellular space (Almers, 1990).

The trafficking of secretory vesicles to the plasma membrane of eukaryotic cells is indispensable for many physiological functions (Burgoyne et al., 2003). It also provides the basis of intercellular communication in multicellular organisms

through the release of a plethora of extracellularly acting molecules. As a preceding step to release, these vesicles are captured and subsequently carried by molecular motor proteins to the vicinity of plasma membrane in the range of a few hundred nanometers in the cell interior.

1.1.1 Different types of exocytosis

Two different exocytotic processes have been demonstrated in the eukaryotic system depending on the nature of the stimulus, one is constitutive exocytosis and the second is regulated exocytosis. Constitutive exocytosis is mainly involved in the transportation of proteins including diverse receptors, whereas regulated exocytosis is mainly involved in the secretion of neurotransmitter and hormones (Alberts et al., 2001).

1.1.1.1 Constitutive exocytosis

Constitutive exocytosis delivers newly synthesized proteins to the plasma membrane and external medium. It differs from stimulus-evoked exocytosis by a couple of parameters. For instance, constitutive exocytosis was found to be unaltered, even when the level of cytosolic calcium concentration drops well below the resting levels (Edwardson et al., 1992). Moreover, this process is abrogated by the activation of GTP-binding proteins, such as the non-hydrolysable GTP analogue GTP γ S (Helms et al., 1990). However, regulated exocytosis is facilitated by the rise of intracellular calcium level and often GTP analogues have stimulatory effects on it (Gomperts et al., 1990). Nevertheless, it is generally accepted that mechanistically constitutive exocytosis is similar to regulated exocytosis (Palade, 1975) but not identical. Similar molecular components, such as SNAREs and SNAPS mediate both the processes (Rothman et al., 1996).

Furthermore, some particular cell-type or cellular organelles are competent to facilitate constitutive secretion in the form of proteins (Burges et al., 1987), such as plasma proteins and antibodies. Alongside synthesized proteins, constitutive pathway also secretes some extracellular molecules, such as extracellular matrix components.

1.1.1.2 Regulated exocytosis

Regulated exocytosis is mainly involved in the cellular communication in specialized cell types, where neurotransmitters (Glutamate, GABA, Glycine, D-Serine, Aspartate and Acetylcholine etc), neuropeptides (NPY, α -MSH, Galanin-like peptide) and hormones (Insulin, Epinephrine, Nor-epinephrine) are filled in differently sized cellular packages. They are released upon stimulation which induces an intracellular calcium influx that in-line promotes a rise in the cytosolic calcium. For instance, in exocrine, neuroendocrine and neuronal cells, hormones and neurotransmitters are packed and stored in vesicles. Upon stimulation, which results an increase in the cytosolic calcium levels, the secretory machinery recognizes this calcium rise and triggers the collapse of vesicle bound content into the cell exterior by fusion of the vesicle membrane with the plasma membrane.

1.2 Cardinal steps of regulated exocytosis

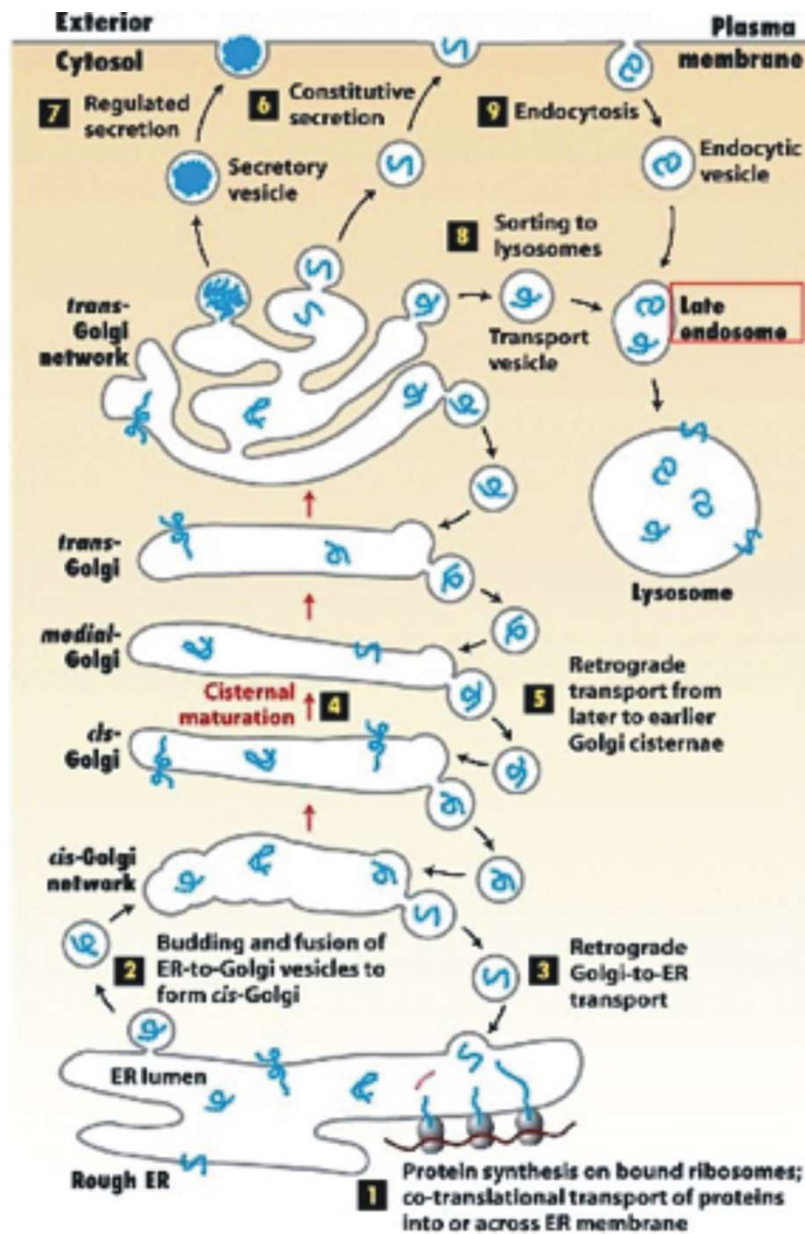
Prior to exocytosis, synaptic and secretory vesicles undergo a series of maturation steps. After their biogenesis, they become sequentially release competent by being docked and primed in the vicinity of the plasma membrane.

1.2.1 Biogenesis of vesicles

For secretory vesicles and vesicular cargo proteins, *de novo* syntheses of cargo molecules occur at the endoplasmic reticulum followed by a series of maturation steps through-out the golgi apparatus, i.e. *cis*-Golgi, *medial*-Golgi and *trans*-Golgi network. Cargo-containing vesicular structures generally bud off from the *trans*-golgi network. Secretory vesicles store a subset of their secreted proteins at a very high, almost crystalline concentration in their luminal core. The enormous density of proteins results in the characteristic dense core that can be visualized in the electron micrographs of the cells (Kelly, 1991).

Generation of small synaptic vesicles and their subsequent accumulation at nerve terminals provide hallmarks for synapse formation. Moreover, synaptic vesicles are also initially generated at the Golgi-network; they actively get recycled at the nerve terminals by rapid endocytosis and refilled with neurotransmitter by the

electrochemical and pH gradient across the vesicular membrane. This gradient is induced in the vesicles by vesicular membrane containing proton transporters such as biogenic amine transporter, acetylcholine transporter, glutamate transporter and combined GABA / Glycine transporter (Kelly, 1991).



Taken from: Molecular Cell Biology, Harvey Lodish et al., Sixth edition, 2008 W. H. Freeman and company.

Fig 1. Overview of cellular trafficking process: *Secretory pathway:* Synthesis of proteins bearing an ER signal sequence is completed in the rough ER **1**, and the newly made polypeptide chains are inserted into the ER membrane or cross into the lumen. Some proteins (e.g., ER enzymes or structural proteins) remain within the ER. The remainders are packaged into transport vesicles **2** that

bud from the ER and fuse to form new *cis*-Golgi cisternae. Mis-sorted ER-resident proteins and vesicle membranes that need to be reused are retrieved to the ER by vesicles **3**, that bud from the *cis*-Golgi and fuse with the ER. Each *cis*-Golgi cisterna, with its protein content, physically moves from the *cis* to the *trans* face of the Golgi complex **4** by a non-vesicular process called cisternae maturation. Retrogradetransport vesicles **5**, move Golgi-resident proteins to the proper Golgi compartment **6**, and are secreted continuously (constitutive secretion). In certain cell types, some soluble proteins are stored in secretory vesicles **7**, and are released only after cell receives an appropriate neural or hormonal signal (regulated secretion). Lysosome-destined membrane and soluble proteins are transported in the vesicles that bud from the *trans*-Golgi **8**, they first move to the late endosome and then end up in the lysosome. *Endocytic pathway*: Membrane and soluble extracellular proteins taken up by vesicles that bud from the plasma membrane **9** can also move to the lysosome via endosomes. [Taken from **Molecular Cell Biology, Harvey Lodish et al., Sixth edition © 2008 W. H. Freeman and company**]

1.2.2 Docking of vesicles

In order to achieve sub-millisecond temporal precision of the stimulus dependent release, vesicles must localize in close proximity to the plasma membrane before elicitation of the calcium influx (de Wit et al., 2006). This process is known as membrane docking of the 'to-be-released' vesicles. This is an essential step of exocytosis and is morphologically defined by electron micrographs as vesicles that appear closely apposed to the plasma membrane (de Wit et al., 2006, Verhage and Sorensen 2008). Recently, vesicle mobility with millisecond temporal resolution was visualized with the development of evanescent field microscopy. This visualization includes imaging the arrival of vesicles at the target membrane (docking) till the time of fusion in real time in live cells (exocytosis) (Nofal et al., 2007).

Munc 18-1 has been found to play a crucial role in the secretory vesicle docking (Voets et al., 2001) by promoting the formation of syntaxin-1/SNAP-25 "acceptor" complex. The C2 domain containing protein Synaptotagmin1 (Syt1 or SytI) then binds to this complex (Fig. 2). In contrast, the unproductive syntaxin-1/SNAP-25 2:1 complex is incompetent to facilitate the initiation of the docking process (de Wit et al., 2009). This later pathway is known as an "off-pathway" (Fasshauer et al., 1997; Fasshauer et al., 1997; Xiao et al., 2001; Zilly et al., 2006 and Jahn et al., 2012). In an alternative scenario to docking, vesicles are also known to be held in

the close proximity of the plasma membrane by 'tethers', i.e. adhering vesicles to the cytoskeletal components (Verhage and Sorensen, 2008).

1.2.3 Priming of vesicles

Priming is a process that is defined by the transfer of vesicles from the docked but unprimed pool (UPP) to a slowly and readily releasable primed pool (SRP and RRP respectively) (Becherer et al., 2006). In another way, priming can also be demarcated as a process that makes the vesicles release-competent in such a way that it can fuse with the plasma membrane instantaneously upon increase in the intracellular calcium. Experimentally priming was defined from the work in chromaffin cells (Holz et al., 1989; Bittner et al., 1992) and PC12 cells (Hay et al., 1992), where primed vesicles exhibited a lower latency for release. Alternatively, priming can be defined as a process that support sustained secretion on stimulation. This process is known to be dependent on Mg-ATP and intracellular calcium, phosphatidylinositol-4,5-bisphosphate (PIP₂) and NSF-dependent cis-SNARE disassembly (Fig. 2) (Eberhard et al., 1990; Hay et al., 1995; Banerjee et al., 1996; Verhage and Sorensen 2008). The 'primed' pool of vesicles that are ready-to-fuse at a sub-millisecond time scale, are also known as readily releasable vesicle pool (RRP). Substantial progress in this field of study has been made in the last decade providing evidences for the involvement of different molecular machineries contributing towards the facilitation of the priming process. Amongst them one fundamental process is the formation of a trimeric SNARE complex from the individual Q- and R-SNARE proteins. In neuroendocrine cells and neuronal synapses, it was evident that the R-SNARE synaptobrevin or VAMP (Vesicular associated membrane protein), which resides on vesicular membranes, forms a highly stable complex by zippering with the Q-SNAREs, i.e. SNAP25 and Syntaxin, in order to provide a four helical bundle at the core of the complex (for review see Bruns and Jahn, 2002; Rettig and Neher, 2002; Becherer and Rettig, 2006;). Furthermore, the priming process consists of two ATP dependent reactions, (1) the ATP-dependent production of PIP₂, (2) the ATP-dependent action of NSF in the rearrangement of the SNARE complex. These are prerequisites and cardinal steps in the priming process. Involvement of other molecular players in the priming

process is also well documented, particularly Munc13. Munc 13 deficiency leads to the abolishment of neuronal exocytosis (Varoqueaux et al., 2002). In addition, Rab3-interacting molecules (RIMs) have been reported to be involved in the priming process as well (Südhof, 1995; Martin, 2002).

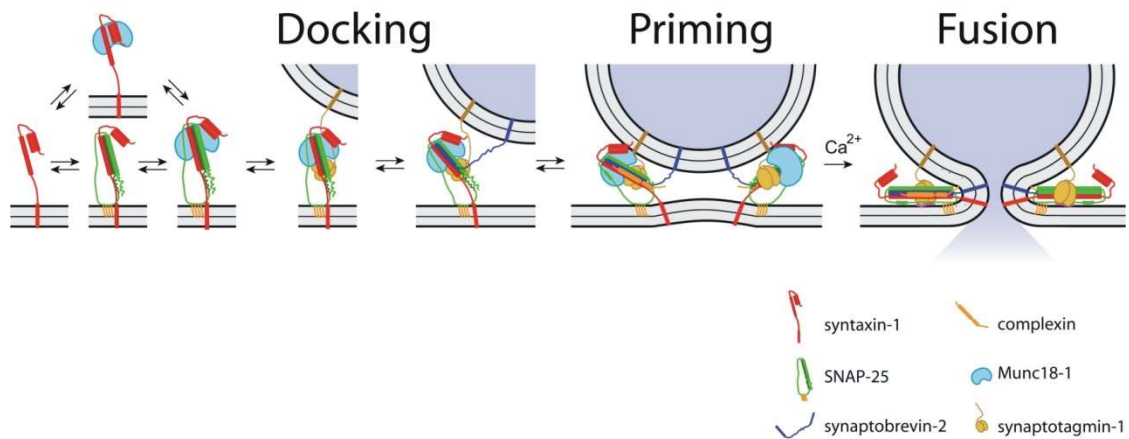


Fig. 2: Overview of regulated secretory pathway of vesicular release: This experimentally derived model depicts three main and sequential steps of regulated exocytosis, such as docking, priming and fusion. This starts with the formation of different protein complexes consisting of Syntaxin-1 (red), SNAP-25 (Green), and/or Munc18-1 (Blue), until the final fusion that procures participation of Synaptobrevin/VAMP-2 (dark blue). Assembly of VAMP-2 (v-SNARE) with the Syntaxin-1/Munc18-1 (1:1), the productive complex and SNAP-25 (t-SNARE), altogether leads to the formation of a complete SNARE complex, which is also known as *trans*-SNARE complex. Furthermore, this scheme also represents Synaptotagmin1 [Sytl] (yellow) and Complexin (orange), and their contribution in the execution of release with sub-millisecond temporal precision. **Adapted from De Wit et al., 2009; Cell.**

1.2.4 Fusion of vesicles

The terminating step of regulated exocytosis is the fusion of the vesicle with the plasma membrane. Initial merging of vesicle and plasma membrane is accompanied with opening of a conduit, which is essential for the deliverance of the vesicular cargo into the synaptic cleft and extracellular milieu. This step is common in neuronal exocytosis as well as in the neuroendocrine secretion. In amperometry, the oxidizable current detected in amperometric recordings from chromaffin granules provides information on exocytotic machinery, and the fusion

pore opening (Chow et al., 1992). As it is illustrated in Fig. 3B, full fusion proceeds through the opening of a fusion pore and the appearance of a pre-spike-foot (PSF), followed by a spike in the amperometric recordings that describes the fusion pore dilation step as the vesicular content is completely expelled (Chow et al., 1992; Bruns et al., 1995; Schroeder et al., 1996; Wang et al., 2001; Bruns et al., 2004). Additionally, the stand-alone-feet (SAF) detected in amperometric events defines the opening of the fusion pore that closes without further dilation, illustrating the kiss-and-run event or vesicular retrieval (Wang et al., 2003).

In uncaging experiments, as is demonstrated in Fig. 3A, exocytosis can be monitored in chromaffin cells in the whole cell patch-clamp configuration by measuring the membrane capacitance. Here, photolytic uncaging of $[Ca]_i$ by UV-photolysis of NP-EGTA, rapidly elevates $[Ca^{2+}]_i$ from 300 nM to 20 μ M. Close observation of the capacitance trace in Figure 3A illustrates two components. These are termed as “rapid/readily releasable pool” (RRP) and “slowly releasable pool” (SRP) based on their different kinetics (Fig. 3A). Nevertheless, it is a debatable issue in the field of neurosecretion whether vesicles fully collapse into the plasma membrane or whether there is just a narrow fusion pore opening, leading to neurotransmitter discharge prior to the retrieval of partially collapsed vesicles. The latter mode of exocytosis is referred as “kiss-and-run” (Becherer et al., 2006). The development of different state-of-the-art high resolution imaging techniques, such as confocal and total internal reflection fluorescence (TIRF)-evanescent field microscopy have made it possible to distinguish between the full-fusion and the kiss-and-run modes of fusion. They provide new avenues to monitor and to quantify the time course of single vesicular release event from their docked state to priming and finally fusion at the plasma membrane. In addition, TIRF-microscopy provides accurate information of vesicular residence time and mobility in the vicinity of the plasma membrane. Furthermore, with this technique the differentiation between functional docking and priming of LDCVs has been achieved. (Toonen et al., 2006; Nofal et al., 2008; Yizhar et al., 2008; Pasche et al., 2012;). In line with TIRF-microscopy, other microscopic techniques providing real time information on the evanescent field has been beneficial to acquire information on release kinetics of various other molecules in other cell types, such

as insulin from β -pancreatic cells and phogrin release from INS1 cells (Tsuboi et al., 2000). Moreover, low frequency time-lapse confocal microscopy has been previously used to monitor vesicular trafficking in the vicinity of the plasma membrane (Pouli et al., 1998). With the availability of faster acquisition time-lapse confocal microscopy in hand, we were intrigued to demonstrate the dynamics of vesicles from their pre-fusion to post-fusion state. Additionally with the help of evanescent field microscopy, radial dispersion of fluorescently labeled cargo molecules can be observed at the post-fusion stage. This dispersion occurs from the vesicle core into the evanescent field and/ or extra cellular milieu, which was observed as lateral dissipation of fluorescence signal (Zhu et al., 2007). This method drove us to demonstrate the NPY release at real time with high-resolution time-lapse confocal and TIRF microscopy.

1.3 Governing bodies of membrane fusion in regulated exocytosis

1.3.1 SNARE proteins

The functional involvement of SNARE proteins in exocytosis has been well documented. To date, in spite of variable interpretation over some molecular components, the fundamental role of SNAREs in membrane fusion has been proven beyond reasonable doubts. The idea originally initiated with the discovery of 'SNARE hypothesis', SNAREs form a superfamily of small proteins with varying member numbers i.e. 25, 36 and 54 in *Saccharomyces cerevisiae*, humans and *Arabidopsis Thaliana*, respectively. The hallmark of SNAREs is the presence of a SNARE motif representing a stretch of evolutionarily conserved 60-70 amino acids that are arranged in heptad repeats (Jahn and Scheller, 2006). After obtaining substantial amount of evidences on neuronal synapses, it became clear that SNARE proteins were primary targets of botulinum and tetanus toxins (Schiavo et al., 1992). These neurotoxins enter the presynaptic terminal and act as highly specific endo-proteases, cleaving specifically SNARE proteins. This conformational mutilation of SNAREs abrogates presynaptic membrane fusion without altering the morphological structure of the terminal (Südhof and Rizo, 2011). The neuronal SNARE proteins comprise of a vesicular synaptobrevin (also

referred as **Vesicle Associated Membrane Protein**, i.e. **VAMP**), and a plasma membrane.

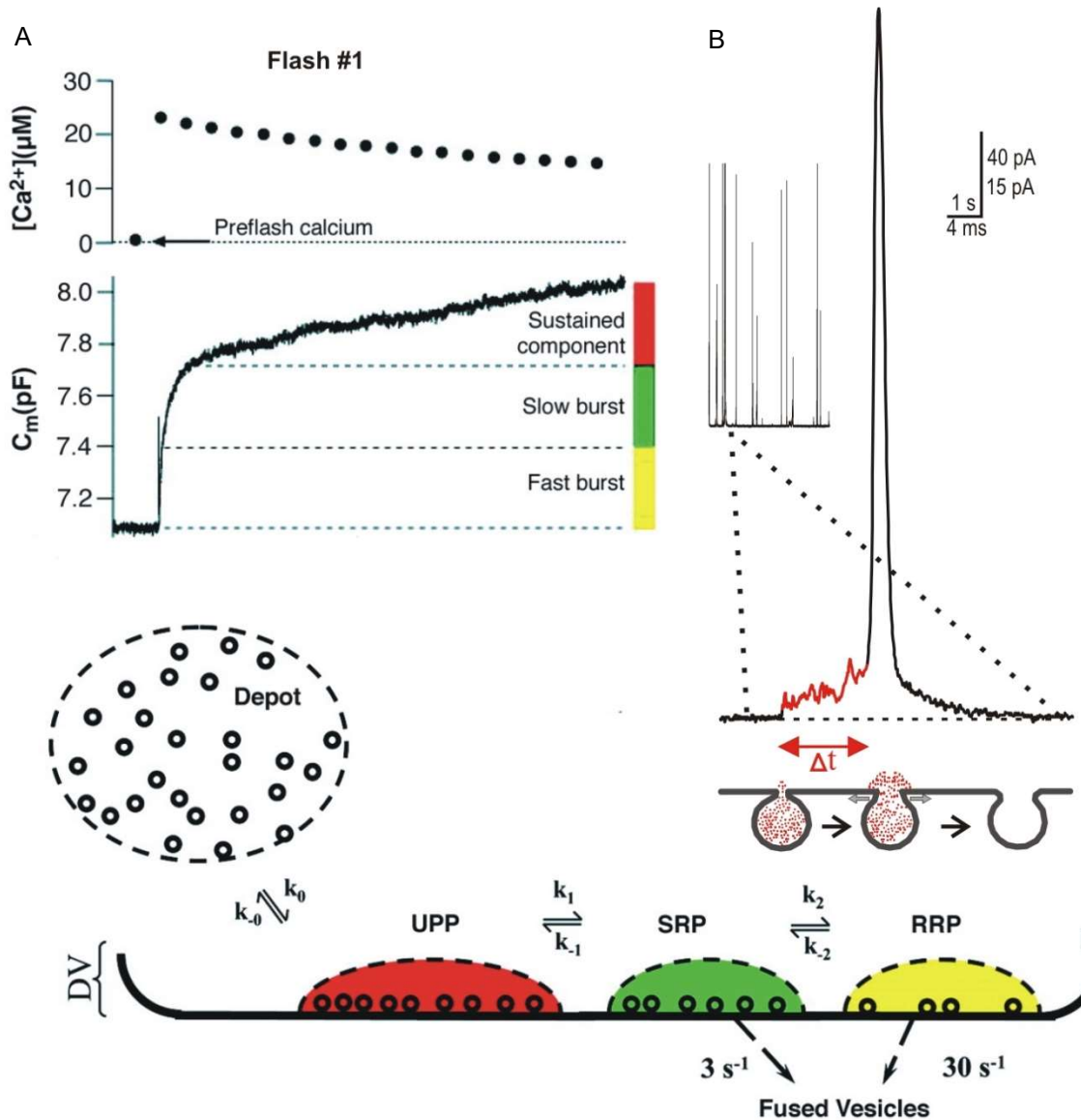


Fig 3: Schematic depiction of vesicle pools and demonstration of different read-out methods to measure neuroendocrine exocytosis: (A). Exemplary traces depicting vesicle pools on typical flash evoked responses, elicited by $20 \mu M [Ca]_i$ (upper trace). The subsequent increase in membrane capacitance (middle trace), as membrane capacitance increases in proportion to the number of chromaffin granules that fuse with the plasma membrane. The color code assigns parts of the trace to the fusion of vesicles, from RRP (yellow) or SRP (green) or slow priming (with release immediately following) of previously unprimed vesicles (red). (B) Exemplary signal traces of amperometric recordings,

measured with a carbon fiber microelectrode in direct contact with the plasma membrane of a chromaffin cell. A 'foot' signal (red line) precedes the main amperometric spike indicative for restricted transmitter discharge through the narrow fusion pore that slowly expands ($t = \text{'foot'}$ duration, see scheme) before full collapse of vesicles, coinciding with rapid pore dilation. (C). Vesicles are depicted in four different states. Vesicles of the depot pool (about 2000) enter the unprimed pool (UPP), when they dock at the membrane. A total of 850 morphologically docked vesicles (as observed in electron micrographs) are subdivided into the UPP (about 650 vesicles) and a primed pool, with the latter again subdivided into the slowly releasable pool, SRP, and rapidly releasable pool, RRP (each about 100 vesicles). Priming can be functionally defined by the fraction of vesicles, which are released within milliseconds of $[Ca^{2+}]_i$ elevation. **Adapted from Rettig J and Neher E, 2002 Science; Borisovska M et al., 2005, EMBO.**

The SNARE motif classifies SNAREs into four subtypes, namely Qa, Qb, Qc and R-SNARE (Fig. 4); based on the presence of a conserved central hydrophilic layer of interacting amino acids that is composed of two or three glutamines (Q) and one arginine (R) residue (Jahn and Fasshauer, 2012). The four-helical bundles of a SNARE complex are formed primarily by hydrophobic interactions. All physiological SNARE complexes are composed of one Qa, one Qb, one Qc and one R domain contributed by specific members of the SNARE family of proteins. R-SNAREs are localized in the vesicle (donor) membrane, which then interact with two or three Q-SNAREs in the plasma (target) membrane. Sometimes the R-SNARE is also called as the v-SNARE (for vesicular SNARE); and the Q-SNAREs are referred as the t-SNAREs (for target membrane) (Südhof and Rizo, 2011) (Fig. 4).

For synaptobrevin and syntaxin, a short linker connects the SNARE-motif to the carboxy-terminal transmembrane region (TMR). For SNAP-25, a palmitoylated linker region between its two SNARE motifs (Qa and Qb), provides a molecular link with the plasma membrane. As illustrated in Fig 4, syntaxin possesses an additional anti-parallel three-helix bundle to the amino terminal domain, referred to as H-abc domain, which is connected to the SNARE motif by a flexible linker (Jahn and Fasshauer, 2012).

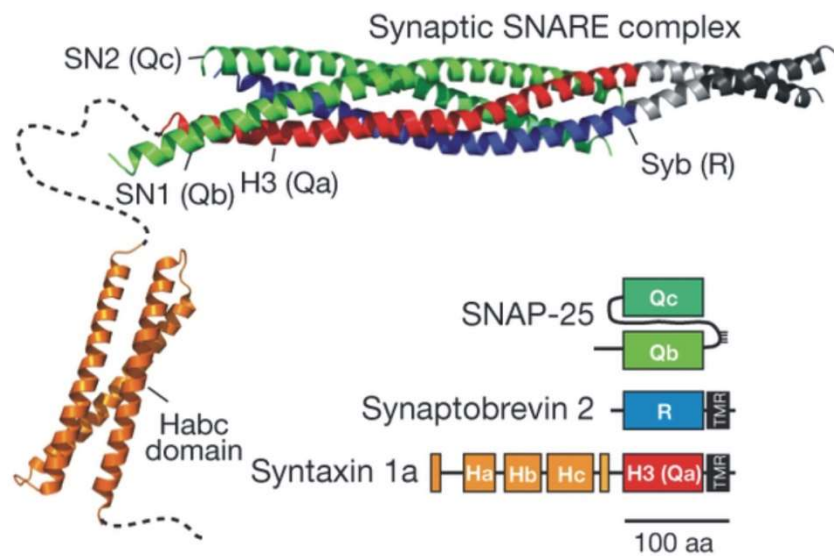


Fig 4: Schematic depiction of domain structures and crystal structures of different SNARE proteins: Syntaxin1, one of the t-SNARE proteins consists of three main regions: a trans-membrane region (grey), a N-peptide (red) or Qa SNARE, flexible region (dashed line) between a Qa SNARE motif and a H-abc domain (orange). The other t-SNARE, SNAP-25 has two main functional domains (green), the Qb and Qc SNARE motifs respectively. These two parallel helices are attached to each other with a flexible palmitoylated region that functions as an anchor to the plasma membrane. The v-SNARE or R-SNARE, which is primarily synaptobrevinII in neurons consists of three main functional domains i.e. a trans-membrane region (grey), a juxta-membrane region (black line) and a core R SNARE motif (blue), which participate in the SNARE complex formation. **Adapted from Jahn R and Fasshauer D, 2012, 490, 7419, Nature.**

In addition, the linker residing between the SNARE motif and the trans-membrane region is crucial as a force transducer as it translates the energy that is released upon trans-SNARE complex zippering (McNew et al., 1999; Deak et al., 2006; Kesavan et al., 2007) into a catalytic force, which helps in overcoming the repulsive force generated between the two apposing bilayers (Südhof and Rothman, 2009). Facilitation of fusion is also governed by an ATP-dependent cycle of regulated assembly-disassembly of the SNARE complex (Jahn and Fasshauer, 2012). The bilayer merger is thermodynamically coupled to exergonic folding of SNARE proteins that is trailed by the endergonic unfolding of AAA⁺- Adenosine triphosphate (ATPase) and *N*-ethylmaleimide-sensitive factor (NSF), which bring them back to their initial state for a new round of cycle (Südhof and Rothman, 2009;

Jahn and Fasshauer, 2012). Experimentally, this machinery of thermodynamics has been validated in the spontaneous fusion of artificial lipid vesicles containing purified v-SNARE and t-SNAREs (Weber et al., 1998). SNARE assembly, which transforms a *cis*-SNARE into a *trans*-SNARE complex (also known as “SNAREpin”), initiates at the N-terminal ends of the SNARE motifs. Involvement of different SNARE motifs leads to the formation of a tight bundle of four parallel α -helices, which subsequently progresses towards the C-terminal membrane anchors. The energy released with this assembly process is used to initiate membrane fusion. As it zippers up the amount of energy released from each SNAREpin is equivalent to $35 k_B T$ or 20 kcal/mol (Li Feng et al., 2007; Südhof and Rothman, 2009). The activation energy required for bilayer fusion is in the range of 50 to 100 $k_B T$. Thus, three or more individual SNAREpin might be aligned to provide sufficient energy, in order to elicit fusion of a single vesicle (Hua et al., 2001; Mohrmann et al. 2010). NSF catalyzes this reaction by its interaction with *trans*-SNARE complex that execute the dissociation of conjugated SNAP cofactors from SNARE complex (Jahn and Fasshauer, 2012). NSF is a hexamer that is likely to use three to six ATPs with each catalytic cycle (approximately 20 to 40 kcal/mol). After opening of the fusion pore, both membranes completely merge and then the *trans*-SNARE complex is converted into the low energy *cis*-SNARE complex. After execution of exocytosis, synaptobrevin is endocytosed and recycled, so that it can participate in subsequent rounds of exocytosis (Südhof and Rothman, 2009; Südhof and Rizo, 2011; Jahn and Fasshauer, 2012).

In addition to this highly complicated machinery of SNAREs in vesicular exocytosis, other accessory and regulatory components also play a major role in the vesicle fusion, such as SM proteins (Sec and Munc family of proteins), Synaptotagmins (Syt) and Complexins (Cpx).

1.3.2 SM proteins

In orchestrating vesicular fusion during exocytosis, SM proteins act as indispensable partners for SNARE proteins. Based on earlier findings, it is assumed that SM proteins organized *trans*-SNARE complexes spatially and temporally (Südhof and Rothman, 2009). SM proteins are evolutionarily conserved

cytosolic proteins of approximately 600 amino acid residues that are arranged in three lobes, folded into an arch-shaped “clasp” structure (Südhof and Rizo, 2011). The pivotal role of SM proteins in membrane fusion was first understood after isolating Munc18-1 from Munc18-1 bound syntaxin-1 complexes (Hata et al., 1993). This binding was found to be restricted to the ‘closed’ conformation of syntaxin-1. In the process of binding, Munc18-1 forms a complex that includes a part of the SNARE motif, thus disabling SNARE complex formation. (Hata et al., 1993; Dulubova et al., 1999). Furthermore, Munc18-1 was reported to control the pool size of vesicles (Toonen et al., 2006). Based on these findings, it was suggested that Munc-18 is an inhibitor of fusion rather than a component of the fusion machinery (Wu et al., 2001). Other studies also demonstrated that the deletion of Munc-18 facilitates a loss of fusion events, meaning that Munc18-1 is a cardinal component of vesicular exocytosis, specifically docking (Verhage et al., 2000; Voets et al., 2001). The dilemma was partially resolved at least for the mammalian system upon finding that a conserved sequence at the N-terminal end of syntaxin binds to SM protein by a compatible mechanism with SNARE assembly (Südhof and Rothman, 2009). Genetic ablation of Munc18-1, leads to a remarkable reduction in synaptic transmission, as loss of Munc18-1 leads to a decrease in the number of available synaptic vesicles for release and escalation of their release probability (Gerber et al., 2008). It is also assumed that a complex involving Munc-18 and syntaxin is the most promising scenario that constitutes a docking platform for regulated secretion (Verhage and Sorensen 2008; Südhof and Rizo, 2011).

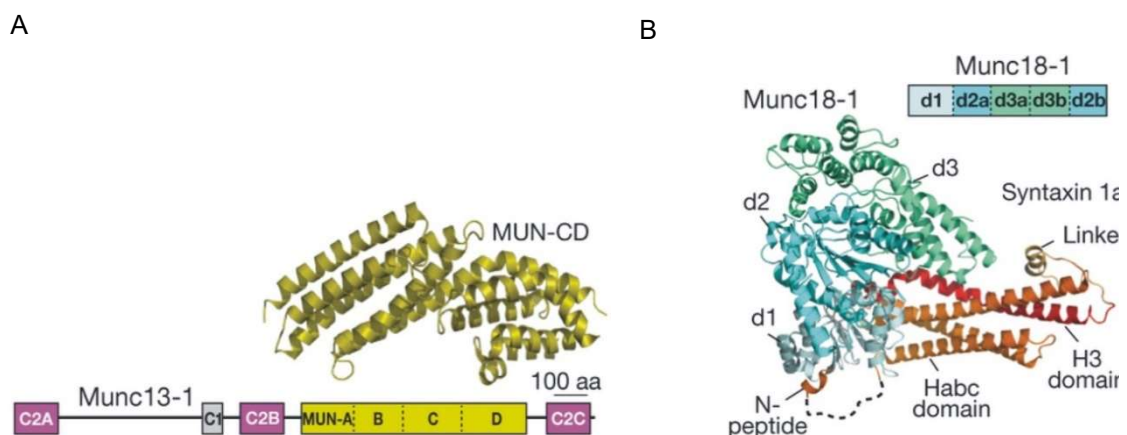


Fig 5: Schematic depiction of domain and crystal structures of two cardinal SM proteins:
 (A). For Munc 13-1, calcium-binding C2 domains are demarcated as C2A, C2B and C2C (pink). Phorbol-ester-binding domain is the C1 domain (grey), and then there is the MUN domain (yellow). The key elements of the protein have been subdivided into four parts A, B, C and D.
 (B). Munc18-1 forms a ternary complex with Syntaxin 1a, which is known to be a *closed conformation*. The central helices of Munc18-1 d2a and d2b (blue-green) participate actively in the formation of the *closed* conformational complex. **Adapted from Jahn R and Fasshauer D, 2012, Nature.**

In line with Munc18-1, another gene *unc13* was found in *C. elegans* that codes for a diacylglycerol-binding protein, and mutation in which leads to an “uncoordinated” release phenotype (Südhof 2012). However, no information on its precise localization and functionality is available (Maruyama et al., 1991; Südhof 2012). Munc-13s, a mammalian homolog of *unc13* has been found to be an active zone protein that is essential for synaptic vesicle and large dense core vesicle priming. (Brose et al., 1995; Augustine et al., 1999; Ashery et al., 2000). The Munc-13s are modulatory components sharing a conserved C-terminal containing phorbol-ester-binding C1 domain and two calcium binding C2 domains that flank a larger, so-called MUN domain (Wojcik et al., 2007). Later on, it was found that only expression of the MUN domain in neurons that are deficient of Munc 13s, could completely restore the arrest of exocytosis, thereby identifying MUN domain as the fundamental elements of Munc 13s in vesicle exocytosis (Basu et al., 2005).

1.3.3 Calcium control of vesicular exocytosis

Short latency of exocytosis together with its high speed and precision, are primarily governed by the Ca^{2+} sensing protein Synaptotagmin (Syt) and its cofactor Complexin (Cpx) (Südhof 2012). Later on, other calcium sensors were also found to be involved in the various modes of exocytosis, such as the Doc2 family of proteins.

1.3.3.1 Synaptotagmins

In order to cope with the extraordinary speed of the final stage of the fusion reaction, a Ca^{2+} sensor is required at the site of exocytosis that binds to Ca^{2+}

cooperatively and undergoes a Ca^{2+} -dependent conformational change. Synaptotagmin (Syt) isoforms are known to have this function, primarily as synaptic and secretory vesicle proteins. Some isoforms can also be found in cytosolic fractions, however. Syts are evolutionarily conserved and their existence has also been observed in invertebrates (Pang et al., 2010). To date, 8 of the identified 16 mammalian isoforms of Syts were found to bind calcium with apparent affinities that is distinct between groups but similar within the group, such as Syt [I-III], Syt [V-VII], Syt IX and Syt X (Pang et al., 2010). Firstly, Syt was identified as a 65-kDa protein, localized to synaptic vesicles and LDCVs in neurons and neuroendocrine cells, respectively (Matthew et al., 1981). A single TMR (transmembrane region) has been found to anchor Syt to synaptic vesicles. The hallmarks of Syts are two C2 domains known as C2A and C2B that are connected to each other and the membrane by flexible linkers (Coussens et al., 1986; Davletov et al., 1993). The C2 domains are rigid, oval-shaped β -sandwiches that possess a cluster of calcium-binding loops, serving as partial coordination site for two and three calcium ions, for the C2A and C2B domains, respectively. The C2 domains bind to membranes comprising of acidic phospholipids that complete the calcium coordination sites (Jahn and Fasshauer, 2012). Additionally, the C2B domain comprises of a spatially separated basic patch, which directs the domain to membranes enriched in PIP2. Membrane binding is an electrostatic phenomenon and can be reversed by chelating the calcium or influencing the ionic strength (Jahn and Fasshauer, 2012). In addition, the C2 domains bind to syntaxin alone or syntaxin incorporated in SNARE complexes (Vrljic et al., 2010; Lai et al., 2011). Syt1 deletion abrogates fast synchronous neurotransmitter release (Geppert et al., 1994). Nevertheless, delayed asynchronous release is retained in absence of Syt1, and is increased upon repetitive stimulation, probably due to other deputizing Syt isoforms (Maximov et al., 2005; Südhof 2012). In addition, previous investigations on murine cortical neurons have revealed that majority of the spontaneous release (95%) is elicited by Ca^{2+} binding to Syt1. Hence, spontaneous and evoked releases follow the same Ca^{2+} -dependent release mechanisms. Additionally, alteration in the Ca^{2+} affinity of Syt1, induced by certain mutations was found to alter both spontaneous and evoked release properties (Xu et al., 2009). However, loss of Syt1 was found

to be ineffective on hypertonic sucrose induced release, later on this releasable vesicle pool [RRP] was found to be Ca^{2+} -independent (Xu et al., 2009; Südhof 2012). Moreover, data collected from other model systems suggested that Syt is needed to convert the asynchronous release events into rapidly triggered synchronous events, thus loss of Syt1 leads to an elevation in asynchronous release (Yoshihara et al., 2002; Chapman 2008). In addition, deficiency of different Syt isoforms led to the alteration of different phases of flash evoked response of neuroendocrine release, such as the exocytosis burst (EB), which is abolished and the RRP is significantly reduced (Voets et al., 2001; Schonn et al., 2008; Dhara et al., 2014). Moreover, other studies revealed that Syt1 and Syt1X exhibited high degree of functional redundancy in the regulation of fusion pore for peptidergic release from LDCV fusion pores in PC12 cells. Deletion of both led to a significant loss in the event frequency and also induces change in the ratio of kiss-and-run, kiss-and-stay and full fusion events (Zhu et al., 2007). Additionally, functional overlap of Syt1 and SytVII was also observed in LDCV release from adrenal chromaffin cells. Upon genetic ablation of both isoforms, only slowly release components (slow burst and sustained component) existed, which accounts for 30% of wildtype exocytosis (Schonn et al., 2008).

In an attempt to find out more on the distinctive regulatory mechanisms of synchronous and asynchronous release, the other molecular player, the Doc2 family of protein was identified. They contain two C2 domains (C2A and C2B) that are similar to those found in the Syt family (Groffen et al., 2010; Yao et al., 2011).



Fig. 6. Schematic representation of the domain and crystal structure Syt1 and CpxII: A. Vesicular protein Syt1 (Syt1) is anchored to the synaptic vesicle by a single trans-membrane region (TMR). The key elements of this protein are two calcium-binding domains that are β -sandwiches in nature, C2A (pink) and C2B (light pink), are connected to each other with a

flexible linker (black line). Calcium binding loops are marked with a dotted circle. B. Cpx primarily consists of four regions, which exhibit significant functions. They are the N-terminus (black line, left), the C-terminus (black line, right) and the central domain (yellow), which contains an accessory α -helix and central-helix. **Adapted from Jahn R and Fasshauer D, 2012, Nature.**

1.3.3.2 Complexins

Since SNARE proteins can assemble spontaneously, fast Ca^{2+} -triggered fusion requires regulating proteins, such as Cpx (McMahon et al., 1995; Chen et al., 2002), which prevents premature SNARE complex formation (Dhara et al., 2014). Cpxs are relatively small cytosolic α -helical proteins comprising a family of four small (134-160 residues) isoforms, such as CpxI, CpxII, CpxIII and CpxIV. They are highly charged proteins with a molecular weight in the range of 16 kD. CpxI is expressed specifically in the central nervous system, whereas CpxII is expressed in non-neuronal tissues, alongside the CNS. Nonetheless, there are many types of neurons that express both proteins at different levels, such as murine hippocampal neurons. In addition, other isoforms i.e. CpxIII and CpxIV, have 58% protein sequence identity among each other, but share a limited homology of 24-28% with CpxI and CpxII. They are predominantly expressed in the retina where they are specifically sorted to ribbon synapses of photoreceptor and bipolar neurons (Reim et al., 2005; Brose, 2008). Most Cpx isoforms bind to the assembled SNARE complexes with high affinity and have multiple domains with distinct functions (Brose, 2008). The N-terminal region of Cpx exhibits a stimulatory effect on evoked release in murine neurons (Xue et al., 2007; Maximov et al., 2009), but has no effect on evoked release occurring at the *C. elegans* neuromuscular junction (Hobson et al., 2011; Martin et al., 2011). The accessory α -helix provides an inhibitory action in *in-vivo* investigations (Xue et al., 2007; Maximov et al., 2009; Yang et al., 2010).

Cpxs bind via a central helix to a groove, located on the surface of the SNARE complex that is formed by the helices of syntaxin and synaptobrevin (Chen et al., 2002; Bracher et al., 2002). In order to exert its physiological function, Cpx requires a partially assembled SNARE complex. However, the C-terminal region of Cpx that

covers almost half of the size of total protein is also known to bind Syt (Tokumaru H et al., 2008) or/and phospholipids (Malsam et al., 2009; Seiler et al., 2009). The C-terminal regions have also been suggested to be functionally inert (Xue M et al., 2007) but in contrary they are also involved in clamping spontaneous fusion (Cho et al., 2010; Martin et al., 2011; Kaeser-Woo et al., 2012). Additionally in neuroendocrine chromaffin cells, our group could demonstrate that the C-terminal domain of CpxII promotes the increase of the pool of primed vesicles by hindering premature exocytosis at sub-micromolar Ca^{2+} concentrations, whereas the N-terminal domain shortens the secretory delay and accelerates the kinetics of Ca^{2+} -triggered exocytosis by increasing the Ca^{2+} affinity of synchronous secretion (Dhara et al., 2014). Our data further revealed that the C-terminal domain attenuates the fluctuation of early fusion pore and slows its expansion, which is functionally antagonized by SytI (Dhara et al., 2014). In particular knockdown and knockout perturbations have elicited controversies of Cpx function in transmitter release. Genetic ablation of all Cpx isoforms expressed in the brain leads to a reduction of both spontaneous and evoked release in hippocampal neurons, while the calcium affinity of evoked release is also reduced (Xue et al., 2007; Xue et al., 2010). But nevertheless, RNAi knockdown of Cpx in mass-cultured cortical neurons increases spontaneous release and decreases evoked release, which requires a higher calcium affinity (Maximov et al., 2009; Yang et al., 2010; Cao et al., 2013). Moreover, the clamping function of Cpx occurs due to the blocking of SNARE zippering, presumably due to the direct competition with the synaptobrevin-binding site at the C-terminal part of the SNARE complex, which is released on binding of Syts that is altered in its conformation upon calcium influx (Yang et al., 2010; Kummel et al., 2011; Jahn and Fasshauer, 2012). In addition, previous work on Cpx in neuroendocrine PC12 cells (An J et al., 2010) revealed that Cpx recruits itself at a late step of exocytosis and modulates the fusion pore. In a nutshell, they observed that full-length wildtype Cpx was visualized momentarily during full fusion; whereas a truncated version of Cpx consisting of only the SNARE-complex binding region stayed at the fusion site for a prolonged duration (An J et al., 2010). Alongside this finding, other investigations revealed that the overexpression of CpxII led to the alteration of single fusion event kinetics,

i.e. the time course measured over amperometric spike was decreased (Archer et al., 2002). Considering these results, it seems worthwhile to study Cpx function in peptidergic release from adrenal chromaffin cells.

1.4 Neuropeptide Y

Neuropeptide Y (NPY) is a 36 amino acids polypeptide and it is structurally similar to peptide YY (PYY) and pancreatic polypeptide (PP) neurotransmitter. They are most abundantly found in the brain and as well as in the autonomous nervous system (ANS) of humans with minor variations in other mammalian species. In the ANS, neurons that are part of sympathetic nervous system mainly produce and release NPY, upon different stimuli. There are five different subtypes of receptors that mediate the action of NPY. NPY is stored and released along with epinephrine and nor-epinephrine in the brainstem, peripheral post-ganglionic sympathetic fibers, as well as from adrenal chromaffin cells (Renshaw et al., 2001).

Similar to many other polypeptide hormones and neuropeptides, as well as many hydrolytic enzymes, NPY is also synthesized as an inactive protein precursor from which the component has to be activated by proteolysis. The beginning of this transformation takes place in the *trans* Golgi network, and continues in secretory vesicles as well as in the extracellular fluid. In a nutshell, many secreted polypeptides carry an amino-terminal *pro-piece* that is cleaved off during the processing, in order to yield the functionally mature protein. These proteins are synthesized as pre-pro-proteins, the pre-piece contains an ER signal peptide, which is cleaved off in the rough endoplasmic reticulum (RER) (Alberts et.al. 2001). NPY has substantial physiological implications, such as appetite regulation and obesity (Kalra and Kalra, 2004). In addition to some other physiological implications, NPY has also been found to be associated with the development of cognitive behavior i.e. energy balance, memory and learning.

Considering the physiological and pathophysiological perspective of NPY, and to get a better understanding of the mechanisms of NPY release from LDCVs, we investigated the release of NPY from large dense core vesicles of murine chromaffin cells. Furthermore, NPY has been suggested to play a role in neuronal development and in the progression of epilepsy (Hansel et al., 2001). It was also

demonstrated that intra-ventricular or systemic injection of NPY induces a reduction in the plasma level of luteinizing hormone (LH) in castrated rats of both sexes (Guy et al., 1988).

1.5 Objective of the study

Till date, many state-of-the-art methods have been employed to emphasize on structural and functional read-outs for measuring fusion pore opening. The very initial attempt was made by ultra-structural studies that revealed omega-figures in the nerve terminals where exocytotic pits have been captured by rapid freezing (Ornberg et al., 1981). Furthermore, capacitance measurements provide a read-out that relies on the direct relationship between membrane capacitance and membrane surface area (Gillis 1995; Gentet et al., 2000). Consequently, fusion of differentially sized vesicles leads to an increase in capacitance measurement ranging from ~ 1 fF for chromaffin cells to ~ 16 fF in beige mouse mast cells (Fernandez et al., 1984). Intermittently occurring successive downward steps provide substantial evidence for kiss-and-run phenomenon (Neher et al., 1982). Lately, conductance measurement of exocytotic fusion pore revealed valuable insight into fusion pore dynamics and the duration of the opening (Spruce et al., 1990). As we mentioned above, important information on the fusion pore opening and single exocytotic events was also acquired with carbon fiber amperometry that relies on the oxidation of released transmitter molecules as it has been successfully documented in chromaffin cells (Chow et al., 1992). The appearance of a pre-spike-foot (PSF) and subsequent spike in the amperometric recordings illustrates opening of the fusion pore and subsequent dilation with the expulsion of cargo (Chow et al., 1992; Bruns et al., 1995; Schroeder et al., 1996; Wang et al., 2001; Bruns et al., 2004). The size of the fusion pore is reflected in foot amplitude and the duration translates into the stability of the pore (Jackson and Chapman, 2006). In addition, the kiss-and-run mode or vesicular retrieval is reflected in stand-alone-feet (SAF) of amperometric recordings (Wang et al., 2003). Nonetheless, amperometric recordings are primarily restricted to the oxidizable elements, which are relatively small in size. Furthermore, the release of such small molecules occurs rapidly even through a non-dilated fusion pore. Indeed, due to the rapid

time course of catecholamine release, amperometric recordings cannot provide any information on the fate of vesicles at the post-fusion stage, i.e. 1-2 seconds after the initiation of exocytosis.

Optical methods, instead, were extensively employed to unravel the behavior of the fusion pore in this time domain. As described in section 1.2.4, a number of fluorescently labeled molecules were used to monitor exocytosis. Earlier works have been done with FM1-43 and its variants. The kiss-and-run phenomenon was studied by uptake and discharge of longer side-chain dye-based methods. Apart from this, experiments in which only a small fraction of vesicles were labeled, fluorescence measurements generated evidences for kiss-and-run mode of exocytosis. (Jackson and Chapman 2006). Moreover, single vesicle imaging method includes the environmental pH-reflective labeling of the luminal part of the vesicular protein synaptophysin, which reports multiple components of endocytosis (Miesenböcker et al., 1998; Gandhi et al., 2003). Additionally, another study reported a coordinated action SytI and SytIX by using NPY-pHluorin for LDCV release events in PC12 cells (Zhu et al., 2007).

In order to study peptidergic release from chromaffin cells in detail, we used NPY tagged with pHluorin, which is the pH sensitive variant of GFP. The fluorescence of pHluorin molecule is governed by the pH of the milieu where it resides. Since luminal pH is acidic (~5.5), the fluorescence of pHluorin is quenched inside vesicular lumen. On opening of the fusion pore pHluorin molecules come across the pH of extracellular milieu (~7.4). This sudden change in the pH leads to the dequenching of the pHluorin molecule. As a cargo bound reporter molecule, the loss of the NPY-pHluorin fluorescence signal should occur due to discharge and radial dispersion of the cargo molecule from the fusion site.

Therefore, measuring single vesicle peptide release should help to unravel the complex mechanisms of exocytosis, from fusion pore opening to the fate of vesicles at post fusion state.

At first, we tried to provide a detailed characterization of such release events with respect to their signal amplitudes and kinetics. In the course of my PhD thesis, I intended to answer the principal questions:

1. Does peptide release provide new insight into the behavior of the fusion process and if so, are these signals informative regarding the fate of the vesicle (full fusion versus kiss and run)?
2. Do different fluorescently labelled molecules like NPY-pHluorin and the membrane bound Synaptobrevin-pHluorin behave differently during vesicle exocytosis?
3. Furthermore, can we find evidence that the time course of peptide release is sensitive towards genetic deficiencies of vesicular SNARE proteins and SNARE regulating proteins?

2. Materials and Methods

2.1 Material

2.1.1 Reagents

Acrylamide/Bisacrylamide	Roth (Karlsruhe, Germany)
Agarose	GE Healthcare
Ammoniumpersulfate (APS)	Sigma
Ampicillin	Sigma
Bradford reagent	Bio-rad, Richmond, USA
Bafilomycin	Sigma
Coomassie Brilliant Blue R-250	Fluka
Dithiothreitol (DTT)	Roth
EDTA	Sigma
Glycine	Sigma
HEPES	Sigma
Ionomycin	Calbiochem/Sigma
Proteinase K	Roche
Sodiumdodecylsulfate (SDS)	Sigma
TEMED (N, N, N, N-Tetramethylethylenediamine)	Bio-rad
Triton X-100	Sigma
Tween-20	Sigma
Tris Base	Merck

2.1.2 Kits

Qiagen Gel Extraction kit

Qiagen PCR purification kit

Qiagen Plasmid mini kit

Qiagen Plasmid midi kit

Qiagen gel extraction kit

Direct PCR tail-Peqlab kit

KAPA Mouse Genotyping Kit

Life technologies mMessage mMachine ® SP6 kit

All kits were used according to modified protocols.

2.1.3 Locke's solution for adrenal gland dissection

NaCl	- 154 mM
KCl	- 5.6 mM
NaHCO ₃	- 3.6 mM
Glucose	- 5.6 mM
HEPES	- 5.0 mM
pH	- 7.3
Osmolality	- 320 mOsm/kg (of water)

2.1.4 Culture medium (Serum free)

DMEM (31966, 4.5g/L glucose and pyruvate)	- 100 ml
Penicillin-streptomycin (Gibco 10,000 units)	- 400 μ l
Insulin- transferrin- selenium (Gibco 100X)	- 1 ml
Sterile filter and equilibrate in CO ₂ incubator	

2.1.5 Enzyme medium

DMEM (31966, 4.5g/L glucose and pyruvate)	- 250 ml
L-cysteine	- 1.65 mM
CaCl ₂ dihydrate	- 1 mM
Na ₂ EDTA	- 0.5 mM
pH	- 7.3

2.1.6 Inactivation medium

DMEM (31966, 4.5g/L glucose and pyruvate)	- 225 ml
Fetal Calf Serum	- 25 ml
Trypsin Inhibitor	- 625 mg
Albumin	- 625 mg

2.1.7 Solution for activation of virus

Chymotrypsin	- 2 mg/ml
Aprotinin	- 6 mg/ml
BSA 6.5% (w/v)	- 6.5 mg/ml

Every solution was made in Optimem medium, filtered and batched in 120 μ l aliquots

2.1.8 Solution for NPY release assay**2.1.8.1 Ringer's Solution (normal bath solution)**

NaCl	- 130 mM
KCl	- 4 mM
CaCl ₂	- 2mM
MgCl ₂	- 1 mM
Glucose	- 34 mM
HEPES	- 10 mM
pH	- 7.3
Osmolality	- 310-320 mOsm/kg (of water)

2.1.8.2 High Potassium Ringer's Solution (Depolarization solution)

NaCl	- 50 mM
KCl	- 80 mM
CaCl ₂	- 2mM
MgCl ₂	- 1 mM
Glucose	- 34 mM
HEPES	- 10 mM

pH	- 7.3
Osmolality water)	- 310-320 mOsm/kg (of

2.1.8.3 Ammonium Chloride Ringer's Solution (Alkalization Solution)

NaCl	- 80 mM
NH ₄ Cl	- 50 mM
KCl	- 4 mM
CaCl ₂	- 2mM
MgCl ₂	- 1 mM
Glucose	- 34 mM
HEPES	- 10 mM
pH	- 7.3
Osmolality water)	- 310-320 mOsm/kg (of

2.1.9 Molecular Biology Solution:

TAE buffer:

Tris HCl	- 40 mM
Acetic acid (v/v)	- 0.11 %
EDTA	- 1 mM
pH	- 8

1 kb DNA-Marker:

1 kb ladder	- 1x
H ₂ O	- 3x
Loading Dye	- 3x

LB (Luria Bertani) medium:

Tryptone	- 10 g
Yeast extract	- 5 g

NaCl	- 10 g
NaOH	- 100 mM
DDW	- 1000 ml

5X MOPS buffer:

Sodium Acetate	- 3.28 g
MOPS	- 20.6 g

2.1.10 Biochemistry Solution:

Homogenization Solution

Tris-Cl	- 50 mM
NaCl	- 150 mM
PMSF	- 25 mM
TritonX 100 (v/v)	- 20 %
EDTA pH 8	- 500 mM
DTT	- 1 mM
Deoxycholate	- 1 mM
Protease inhibitor tablets	- 1 pill for 5 ml

2M Tris-HCl (pH 8.8)

Tris-Base	- 24.2 g
DDW initial	- 50 ml
pH adjusted with conc. HCl	- 8.8
DDW add to	- 100 ml

1M Tris-HCl (pH 6.8)

Tris-Base	- 12.1 g
DDW initial	- 50 ml
pH adjusted to 8.8 by adding conc. HCl slowly	
Total volume has been made to	- 100 ml

10% (w/v) SDS

10 gm of SDS pellet dissolved in 100 ml of double distilled water

4X Resolving buffer

2M Tris- HCl (pH 8.8)	- 75 ml (1.5 M)
10% SDS	- 4 ml (0.4%)
DDW add to	- 100 ml

4X Stacking buffer

1M Tris- HCl (pH 6.8)	- 50 ml (0.5 M)
10% SDS	- 4 ml (0.4%)
DDW add to	- 100 ml

10% Ammonium persulfate

APS	- 0.1 g
DDW	- 1 ml

10X Electrophoresis Buffer

Tris-Base	- 3 g
Glycine	- 14.4 g
SDS	- 1 g
DDW add to	- 1000 ml
pH 8.3	

5X Laemmli Sample buffer

1M Tris-HCl (pH 6.8)	- 0.6 ml (60 mM)
50% glycerol	- 5 ml (25%)
10% SDS	- 2 %
2- Mercaptoethanol	- 14.4 mM
Bromophenol Blue	- 0.1 %

2X Laemmli Sample buffer

10% SDS	- 4 %
Glycerol	- 20 %
1 M Tris-HCl	- 120 mM

Materials and Methods

DDW	- 2.8 ml
Bromophenol Blue	- 0.02 %
2- Mercaptoethanol	- 10 %

Transfer Buffer

Tris Base (47.8 mM)	- 11.6 g
Glycine (38.9 mM)	- 5.85 g
SDS (0.38%)	- 0.76 g
Methanol (20%)	- 400 ml
Total Volume	- 2000 ml

Tab. 1: SDS Gel Components: left: resolving gel ingredients; right: stacking gel ingredients

Resolving Gel	13%	15%	Stacking Gel	5%
Acrylamide (30%)			Acrylamide (30%)	
Bisacrylamide (0.8%)	4.1 ml	5.1 ml	Bisacrylamide (0.8%)	670 μ l
4X Resolving Gel Buffer	2.5 ml	2.5 ml	4X Stacking Gel Buffer	1 ml
H ₂ O	3.0 ml	2.4 ml	H ₂ O	2.3 ml
10% APS	75 μ l	75 μ l	10% APS	30 μ l
TEMED	7.5 μ l	7.5 μ l	TEMED	5 μ l

1X TBST

Tris Base	- 6.05 g
NaCl	- 8.76 g
Tween 20	- 1 ml
1M HCl to adjust pH	- 7.5
DDW add to	- 1000 ml

1XPBST

10X PBS	-	10 ml
Tween 20	-	0.05 %
DDW to volume made	-	100 ml

Blocking Buffer (8% skimmed milk)

Skimmed milk	-	8 g
1X TBST	-	100 ml

Blocking buffer (5% skimmed milk)

Skimmed milk	-	5 g
1X TBST	-	100 ml

2.1.11 Plasmids**2.1.11.1 Plasmid semliki forest virus (pSFV1)**

- pSFV1 Eukaryotic Expression Vector (Invitrogen)- Modified by Ralf B. Nehring, MPI Gottingen with an extended *multiple cloning site*. [Plasmid map: appendix]

2.1.11.2 Helper plasmid

- pSFV-Helper 2 DNA (Invitrogen), constructed from a full-length SFV clone with a deletion in the region coding for non-structural proteins.

2.1.11.3 Bacteria

- *E. Coli* strain DH5 α used as competent cells.

2.1.12 Primers and oligonucleotides**2.1.12.1 Genotyping Primers****2.1.12.1.1 CpxII Genotyping Primers**

- CPXII_wt_Fw_lang: 5'-CGG CAG CAG ATC CGA GAC AAG-3'
- CPXII_wt_Rv_1130: 5'-GAG AGG GGC ATG AAG TCA AGT CAG-3'
- CPXII_mut_Fw_1111: 5'-CGC GGC GGA GTT GTT GAC CTC G-3'

- CPXII_mut_RV_1128: 5'-CAG GCA CAC TAC ATC CCA CAA ACA-3'

2.1.12.1.2 Syt1 Genotyping Primers

- Syt1_wt_Fw: 5'- GTATTCAGTGCGTCTCAGAGAC-3'
- Syt1_wt/mut_Rv: 5'- AACTATAATTTGTCACAGGCATTGCCTTTCA-3'
- Syt1_mut_Fw: 5'- GAGCGCGCGCGGCGGAGTTGT-3'

2.1.12.2 Mutagenesis Primers Semliki forest virus

- NPY-pHluorin_BamHI_Fw: 5'-TATATGGATCCATGCTAGGTAACAAGCGA-3'
- NPY-pHluorin_BssHII_Rv: 5'-ATATAGCGCGCTTATTTGTATAGTTCATC-3'

2.1.12.3 Enzymes and recommended buffers

- BamHI NEB buffer 3.1 and Cutsmart
- BssHII Cutsmart and NEB buffer 3.1
- SpeI Cutsmart and NEB buffer 2.1
- NruI NEB buffer 3.1
- CIP NEB buffer 3.1
- T4-DNA ligase NEB T4 ligase buffer

All restriction endonucleases and buffers were purchased from New England Biolabs (NEB).

2.1.13 PCR reaction

PCR is a biochemical technique by which *in-vitro* enzymatic amplification of DNA fragment occurs, by using the capability of DNA polymerase to synthesize new strand of complementary DNA to the offered template strand. Since DNA polymerase can add a nucleotide only to the preexisting 3'-OH groups, thus it requires a primer to which first nucleotide can be added, subsequent nucleotide can be added to the preceding nucleotide.

[<http://www.ncbi.nlm.nih.gov/genome/probe/doc/TechPCR.shtml>]

2.1.13.1 Standard cloning PCR reaction

DNA		100 ng
Primer_Fw		0.5 μ l (50pmol)
Primer_Rv		0.5 μ l (50pmol)
10X buffer		5 μ l
dNTPs		1.0 μ l (2.5mM each)
DDW	add to	50 μ l

Tab. 2: PCR program for the cloning procedure

Steps	Temperature	Time (Mins)
Initial Denaturation	94° C	3.00
Denaturation	94° C	0.30
Annealing (Variable for reactions)	45-55 ° C (Variable for primer sets)	0.45
Elongation	72° C	2.00-3.00
Final Elongation	72° C	7.00-10.00

For detail in cloning procedure, see 2.2.2 (Fig. 7)

2.1.13.2 Genotyping PCR reaction

2.1.13.2.1 Genomic DNA isolation

2.1.13.2.1.1 Genomic DNA isolation by Direct-tail-PCR kit

DNA template for genotyping PCR was obtained from a tail biopsy (2 mm) from mouse embryos. Genomic DNA was extracted using the Direct-Tail-PCR buffer in the presence of proteinase K, tail pieces were digested for overnight at 55° C with 100 rpm agitation, subsequent heat inactivation step of the enzymatic digested products have been performed at 85° C for one hour. Digested samples were centrifuged at 13,000 rpm for 5 minutes at room temperature. The supernatant of the centrifugation step contains extracted genomic DNA. Henceforth, this

supernatant samples used as sample for genotyping PCR by probing them with specific primers.

Tab. 3: PCR reaction for the genotyping

CPX- wt	Ingredient for one sample	CPX- mutant	Ingredient for one sample
DDW-PCR	Adjust final volume 25 µl	DDW-PCR	Adjust final volume 25 µl
10X PCR buffer	2.5 µl	10X PCR buffer	2.5 µl
CPX_wt_Fw	0.5 µl	DMSO	0.7 µl
CPX_wt_Rv	0.5 µl	CPX_mut_Fw	0.5 µl
dNTPs (2.5mM each)	1.0 µl	CPX_mut_Rv	0.5 µl
Red Taq pols	1.0 µl	dNTPs (2.5mM each)	1.0 µl
DNA	100 ng	Red Taq pols	1.0 µl
		DNA	100 ng

SYT1- wt	Ingredient for one sample	SYT1- mutant	Ingredient for one sample
DDW-PCR	Adjust final volume 25 µl	DDW-PCR	Adjust final volume 25 µl
10X PCR buffer	2.5 µl	10X PCR buffer	2.5 µl
MgCl ₂	1.0 µl	MgSO ₄	0.2 µl
Syt1_wt_Fw	0.5 µl	Syt1_mut_Fw	0.5 µl
Syt1_Rv	0.5 µl	Syt1_Rv	0.5 µl
dNTPs (2.5mM each)	1.0 µl	dNTPs (2.5mM each)	1.0 µl
Red Taq pols	1.0 µl	Red Taq pols	1.0 µl
DNA	100 ng	DNA	100 ng

3.1.13.2.1.2 Genomic DNA isolation by KAPA kit

Apart from aforementioned method, genomic DNA for genotyping was also from embryos by using KAPA Mouse Genotyping kit. Modified kit protocol was followed from the manufacturer's instructions (peqlab KK7302). The 10X KAPA express extract buffer and the KAPA express extract enzyme were added to the tailpieces, along with 88 µl PCR-grade. Then the samples were thoroughly mixed by vortexing briefly. Furthermore, digestion was performed at 75° C for 15 minutes. Subsequent, heat-inactivation was performed at 95° C for 10 minutes. Finally, samples were vortexed briefly for 5 seconds and centrifuged at 13,000 rpm for 2 minutes. Supernatant of the reaction products were used as samples for the PCR reaction, 1 µl of these samples was used as the template for the PCR reaction.

Tab. 4: PCR programs for the genotyping

<u>SYT I wildtype/mutant</u>		<u>CPX wildtype</u>		<u>CPX mutant</u>	
Temp.	Time (m)	Temp	Time (m)	Temp.	Time (m)
94° C	10.00	94° C	05.00	94° C	05.00
94° C	00.30	94° C	00.30	94° C	00.30
60° C	00.45	64° C	00.45	59.1° C	00.30
72° C	03.00	72° C	01.00	72° C	01.00
72° C	10.00	72° C	07.00	72° C	07.00

**KAPA mix reaction Ingredient for
one sample**

DDW-PCR	7.25 µl
MgCl ₂ (25 mM)	0.5 µl
Forward primer	1.25 µl
Reverse primer	1.25 µl
DMSO	1.25 µl
KAPA mix	12.5 µl
DNA	1 µl

2.1.14 Agarose gel electrophoresis

Gel percentage was determined based on the size of the amplicon [PCR amplification product] and the product yielded from the restriction digestion [(gel percentage usually, 0.8-2.0%); ethidium bromide (EtBr)]. Samples were electrophoresed at 120 V for 30-50 minutes. Subsequently, in-gel DNA bands were detected under UV-illumination.

2.1.15 Antibodies

2.1.15.1 Primary Antibodies

SynaptobrevinII 69.1: mouse monoclonal (MPI, Göttingen)

SNAP 25 71.2: mouse monoclonal (synaptic system)

SyntaxinI 78.2: mouse monoclonal (synaptic system)

CpxI, II: Recognizes SNARE binding domain of protein (synaptic system)

2.1.15.2 Secondary Antibodies

HRP-conjugated Goat Anti-mouse (Bio-Rad)

HRP-conjugated Goat Anti-rabbit (GE Life science)

2.2 Methods

2.2.1 Cell culture

2.2.1.1 Chromaffin cell culture

Chromaffin cell preparation was primarily performed from first postnatal day (P≈0) animals with few exceptions for some genotypes. Because of lethality, synaptobrevinII/ cellubrevin v-SNARE double knockout animals, Syt1/ Syt7 and Syt1 null mutant cells were prepared on 18th embryonic day. For E≈18 preparation, heterozygous pregnant mothers were sacrificed by asphyxiation followed by decapitation. Instantaneously, embryos were obtained from the mother by cesarean section. Upon decapitating the embryos, adrenal glands were removed from pups, and transferred to a 35 mm petri dish containing 400 µl of Locke's solution. Furthermore, the connective tissues adjacent to the gland were detached and the outer part of adrenal gland i.e. cortex, was peeled out of the gland with fine forceps. Afterwards, the medulla part of the glands were transferred to 15 ml of

falcon tube, in 400 μ l enzyme solutions containing 7.5-10 units of Papain/ml. For enzymatic digestion, glands were agitated at 70 rpm in 37° C for 20 minutes. After digestion, enzyme solution was replaced with the same volume of inactivation solution and incubated for 5 minutes. Subsequently, after a series of washing steps with DMEM medium (without supplement); chromaffin cells were extracted from glands by gradient trituration. Initially, 1 ml micropipette tips was used for trituration and 200 μ l tips were used to perform subsequent trituration steps. After achieving homogeneity in the digested solution, 100 μ l of the solution was plated in the center of each coverslip placed in a six-well plate. After 20 minutes of incubation, 3 ml DMEM medium-containing supplements were poured on each well of six-well plate. All experiments were performed at 2-3 Days *in-vitro* (DIV).

2.2.1.2 Semliki forest virus activation (400 μ l of virus aliquot)

Optimem medium	- 300 μ l
Chymotrypsin	- 110 μ l
BSA	- 110 μ l
Aprotinin	- 110 μ l

Chymotrypsin was added on the virus aliquot after addition of Optimem medium. After 50 minutes of incubation, BSA and aprotinin were added subsequently. Virus batches were always activated on the day before the experiment.

2.2.2 Molecular Biology

Cloning of different construct

Cloning of NPY-pHluorin

NPY-pHluorin construct incorporated in pEF-BOS, a mammalian vector had been kindly provided by Thomas Söllner, BZH, Heidelberg, Germany. NPY-pHluorin part was amplified by *in-vitro mutagenesis* procedure, where restriction sites for BamHI and BssHII were introduced at the upstream and the downstream of the NPY-pHluorin respectively by appropriate set of primers (Materials and Methods 2.1.12.2). The amplified products and the pSFV1-vector backbone (appendix 1), were digested by BamHI and BssHII enzymes. In order to avoid unspecified ligation, the digested vector backbone was treated with Calf intestinal

phosphatase (CIP). All enzymatic reactions were performed by modified version of NEB recommended protocol. The digested products were extracted and purified by Qiagen gel extraction kit, according to a modified manufacturer's protocol. Compatible insert and vector backbone were ligated overnight at 16° C with T4 DNA ligase. Ligated product was transformed into *E. Coli* DH5 α strain of competent cells and bacteria were grown in LB medium containing 150 μ g/ml of Ampicillin, at 37° C for overnight with 100 rpm agitation. DNA was purified by using mini and midi Qiagen Plasmid purification kits. Sequence of the construct was confirmed by commercially available sequencing service (MWG Biotech, Germany).

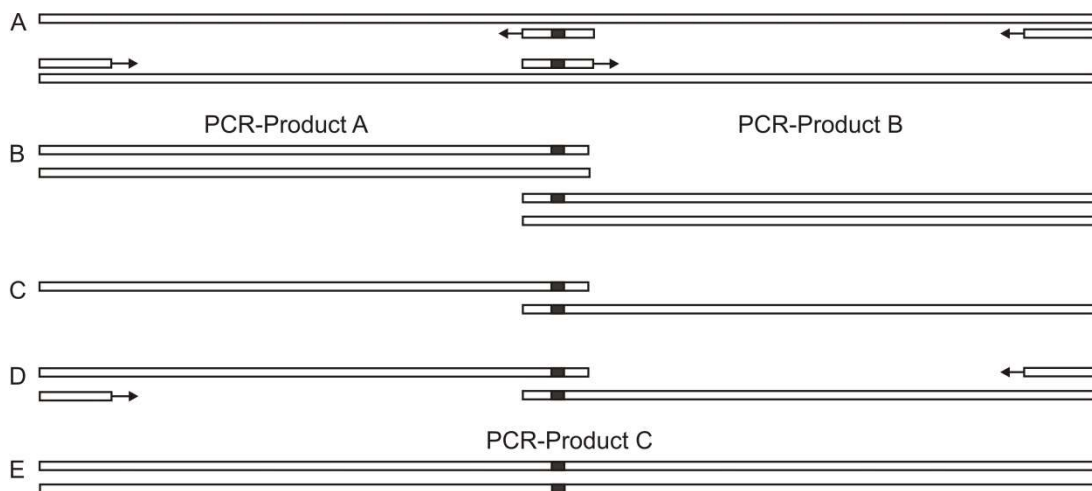


Fig 7: Schematic representation of in-vitro mutagenesis by over-lapping PCR: Two independent PCR reactions were performed with two different sets of primers. Complementary region for ligation two primers has been depicted by black box. Product A and Product B were generated by two reactions, which were ligated afterwards, in order to generate final product, Product C.

2.2.3 Production of recombinant virus particles

Linearization of the candidate and vector the DNA molecule

Primary step of the virus production is to linearize the vector molecule, which was obtained by a restriction enzyme, which has a unique cleavage site (unicutter) that restriction enzyme was *SpeI* (New England Biolabs) for NPY-pHluorin. The restriction digestion was performed by enzyme's manufacturers' protocol. The linearized DNA was purified by phenol-chloroform method.

In-vitro transcription of the DNA molecule

In-vitro transcription was performed by Life technologies mMessage mMachine ® SP6 kit with a modified manufacturer's protocol. Thereafter, purification of RNA molecule was obtained by phenol-chloroform method.

Electrophoresis of RNA molecule

RNA was electrophoresed in 2% (w/v) agarose gel made in the MOPS buffer and formaldehyde. MOPS buffer was used as running buffer for the RNA gel. Samples were pre-heated at 65° C for 10 minutes before loading sample on the gel.

Electroporation of *Semliki-Forest-virus*

*Semliki-forest-virus*RNA was electroporated in BHK cells (ATCC). A pre-optimized electroporation protocol was followed. At prerequisite level of electroporation, cells were counted to obtain 10 million cells for this step. The RNA and helper RNA were mixed carefully in 400 µl of cell suspension, subsequently electroporated with single electric pulse. Thereafter, electroporated samples were transferred to 1 ml, then to 8 ml of Optimem medium with FCS as supplement. Cells were incubated for 18-22 hrs at 31° C and 5 % CO₂.

*Semliki-Forest-virus*Harvest

Supernatant containing virus particles were collected after centrifuging the medium, where transfected cells were grown overnight. The fluorescence level from individual flask were checked, virus harvesting medium was centrifuged at 2500 rpm, 4° C for 5 minutes. Supernatant was aliquoted into batches of 400 µl fraction. Aliquots were snap frozen in liquid nitrogen and then stored at -80° C.

2.2.4 Biochemistry

2.2.4.1 Tissue homogenate preparation

Animals were sacrificed by asphyxiation followed by decapitation. Subsequently, whole brain was removed, after opening the skull. Successively, brain samples were snap frozen in liquid nitrogen by putting them in cryo-vials. Adrenal glands were removed in the same procedure as it was described earlier in chromaffin cell preparation section (Section 2.2.1.1). In line, extracted brain and glands were dissolved in homogenization buffer; 100 mg of brain was dissolved in 150 µl of buffer and both glands were homogenized in 50 µl of homogenization buffer.

Tissue samples were broken with mechanical shearing by glass rod in glass homogenizers, sized 3 ml and 100 μ l, respectively. Brain samples were homogenized until the solution turns completely turbid and devoid of any big particles. After homogenization, solutions were stranded in ice for 1 hr. Finally, samples were centrifuged at 13,000 rpm for 10 minutes at 4° C, supernatants were collected without disturbing the pellets. Finally, samples were aliquoted and stored in -80 ° C.

2.2.4.2 Lysate preparation from plated cells

Chromaffin cells were extracted from newly born animals (P~ 1-2) and plated on coverslips in a proportion of 3 coverslips/animal. Cell lysate was prepared from DIV 3 cells. Before harvesting, cells in the coverslips were washed in ringer's solution. Cells were harvested in 30 μ l of 2X lamelli buffer, containing 2-mercaptoethanol. In order to avoid the loss of material or/and to restrict the over-dilution of the content, samples from subsequent coverslips were pooled with same same solution in repetitive manner. Samples were collected in a 500 μ l microfuge tubes. Samples were heated at 95° C for 3 minutes, before loading them into a 13%-15% SDS-PAGE resolving gel.

2.2.4.3 SDS PAGE

This technique allows denatured unstructured linear polypeptides to be separated, based on its length and mass-to-charge ratio. Components mentioned in Table 1 were used to prepare the resolving gel and poured into the gel plates in Bio-Rad mini gel-casting apparatus. On the same degree, stacking gel prepared and poured on top of resolving gel, after polymerization of resolving gel. Depending on the experiment, polypeptide samples were heated in 5X sample buffer (tissue lysate) and 2X sample buffer (cell lysate), for tissue lysate and cell lysate for 10 minutes and 3 minutes, respectively. After a pulse spin, samples were loaded in gel wells; proteins from these gels were transferred to nitrocellulose membrane.

2.2.4.4 Immunoblot

Immunoblot or western blots is a widely technique used to detect protein by probing them against specific antibody, from the tissue homogenates and cell lysates. From section 2.2.3.2, unstained gel was sandwiched between nitrocellulose membrane and Whatman filter papers. The nitrocellulose and Whatman filter papers were pre-wet in Bjerrum and Schafer-Nielsen (semi-dry) transfer buffer. Components and accessories of transfer were aligned from cathode to anode in this way, i.e. 3 filter papers, nitrocellulose, unstained gel, 3 filter papers. Transfer was performed at constant voltage of 12 Volts for 60 minutes in Bio-Rad Semi-Dry-Blotting apparatus. Post transfer, membrane was reversibly stained with Ponceu S to verify efficiency of the transfer. After which, the membrane was rinsed in DDW. To minimize the unspecific binding of antibodies, blots/membranes were subjected to blocking for 2 hours in non-fat milk, with a percentage of 5-8 (w/v), depending on the experiment. After blocking, they were probed with the desired primary antibody diluted in blocking buffer for overnight at 4°C under gentle agitation. In order to remove unbound antibodies, blots were washed 4 times in washing buffer [1% (w/v) non-fat milk] for 2 hours at room temperature. After washing, blots were probed with secondary antibody, desired dilutions of antibodies were achieved in blocking buffer or 1X TBST and blots were incubated for 1 hour in secondary antibody. Finally, blot was washed 5 times in 1X TBST for 2 hrs. ECL kit (Pierce) was used to visualize the signals from blots with a manufacturer's protocol. Signals were in captured in photographic film (Kodak) against the membrane. Films were developed, fixed and band intensity was quantified.

2.3 Real time NPY release measurement

2.3.1 Preparation of perfusion pipette

Perfusion pipettes were custom-build, where plexi-glass was cut in desired size, and subsequently heated to give horseshoe shape. Depending on the required number of needles, a hole was generated at the center of the twisted part. For our experimental paradigm, a 2 mm diameter hole was made, that can accommodate three needle cannulas of 0.45x12 mm BL/LB 26 Gx1/2" dimensions. Needles were cut to the same length, reopened by rubbing against sandpaper. In parallel, tooth-cement components were mixed thoroughly in 1:1 ratio until it turns into a paste,

which was spread uniformly in layers. After positioning all cannulas at equidistant from each other, cannulas were sealed with tooth-cement. Afterwards, it was incubated at 56°C for 1 hour, then it was put in 4°C for overnight. In line, shrink tube was put at the needle bases, heated it make it stable. Non-heparinized glass capillaries, inner diameter of 1.1 mm were pulled, cut and polished under microscopic observation, providing an inner diameter of 100 μm. Apex region of the tip was bent in acute angle, in order to make it parallel to the coverslip surface.

2.3.2 Preparatory phase of experiment

Depending on the demand of the experiment, perfusion was performed locally that standardized to provide three different solutions out-flow on cell surface, i.e. Ringers' solution, exocytosis causal stimulus and ammonium chloride. Three different 10 ml syringes were put in a stable stand, which was installed at 10 cm high from the microscope piezo.

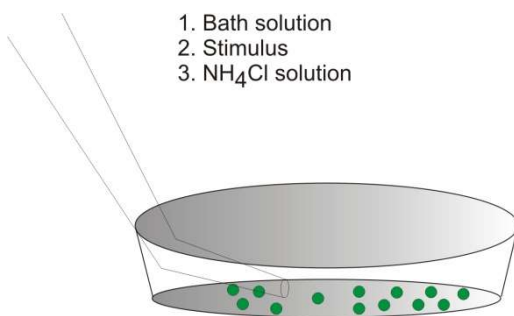
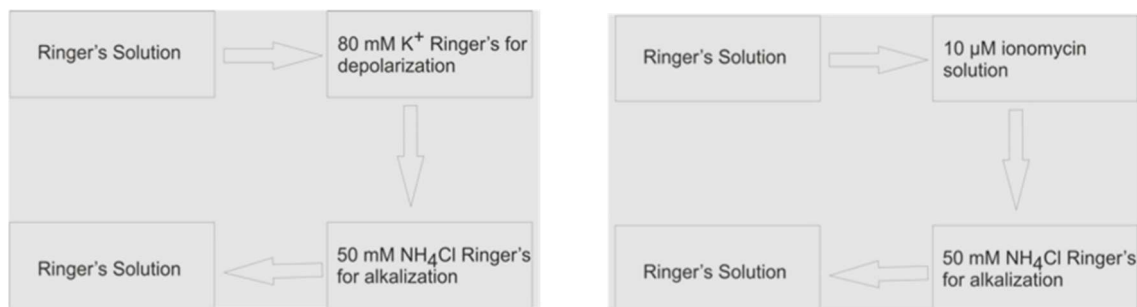


Fig 8. Schematic representation of experimental paradigm of NPY release measurement: Two different stimulation protocols were followed to evoke exocytosis by achieving intracellular Ca^{2+} -influx. For both stimulation protocols, after stimulation cells were undergone Ammonium chloride treatment, in order visualize unreleased vesicles. Schematic representation of imaging experiment for NPY-pHluorin release from LDCV upon exocytosis.

Perfusion pipette was installed on a direct attachment adapter unit of a micromanipulator. The direct adapter attachment on the unit may be conveniently positioned at X, Y and Z direction with a joystick. Perfusion pipette was placed at a distance 700 μm from the center of the cell. After positioning and filling of the perfusion tubes, chromaffin cells containing coverslips were mounted, which were acutely over-expressed with NPY-pHluorin. Virus particles were activated on the day before the experiment. Virus activation procedure is already depicted in the section 2.2.2.2. Cells were infected 5.5-6.5 hours prior to the measurement. Coverslips were mounted on a chamber after a brief washing step with ringer's solution. Chamber was put on confocal LSM-710 microscope's piezo stage. Images were visualized by 100X oil objective with numerical aperture of 1.41.

2.4. Digital Image acquisition, processing and analysis

2.4.1 Confocal Microscopy

The LSM 710 microscopic set up (www.zeiss.com) was mainly used for microscopic experiments. This works in the principle of using laser beam hits scanning head from pigtailed laser diode that has 34-channel QUASAR detector by Carl Zeiss. Images were acquired as 8-bit-encoded digital image with Zen software (Zeiss). In order to maximize the acquisition rate to 10 Hz, frame area of $15.4 \times 15.4 \mu\text{m}^2$ [$\{168 \times 168 \text{ pixel}^2\}$, as 1 pixel corresponds to 80 nanometers] was selected that can accommodate most of the chromaffin cell footprint. Consequently, scanning was performed in a unidirectional line-scan, 488 argon lasers used to excite pHluorin molecule. Uniformity in the image capturing was maintained through all set of experiments, i.e. in the hardware (same laser intensity and with identical pinhole opening) and also the parameters in software (Image settings) were kept identical. Cellular footprint was located first; the fluorophore was excited with the required laser, to perform the measurement. For complete measurement, 1080 frames were captured without any interval, where every frame took 100 milliseconds to be captured. Cells were measured under continuous solution flow, from start to end it follows, such as ringer's solution for 12 sec, stimulus to evoke exocytosis for 78 sec and ammonium chloride solutions for 18 seconds, respectively.

2.4.2 Evanescent wave Microscopy

In order to monitor the cloud like dispersion or diffusional spreading of cargo molecules into extracellular space, evanescent wave or Total Internal Reflection Microscopy (TIRF) was performed; field of view was restricted to 200 nm from the coverslip base. IX70 microscope based TIRF setup equipped with a 100x / 1.45 NA Plan Apochromat Olympus objective, a TILL-TIRF condenser and a solid state 85 YCA emitting at 488nm. Images were captured in micromax 512BFT, which was controlled with Metamorph software. The obtained acquisition rate was 20 Hz. The exposure time was 50 ms Pixel size was 130 nm and the resulting penetration depth was 263 nm. Secretion was induced by simultaneous superfusion of High Potassium solution.

2.4.3 Image Analysis

Secretion of a vesicle was detected by rapid gain and subsequent loss of fluorescence. Stimulation evoked gain of signal from baseline to maximum occurs very rapidly, which cannot be measured at our experimental set up. After initial visual observation from brightening spots, quintessential feature of pHluorin that is uprise and subsequent decay in the fluorescence intensity was monitored by putting a region of interest of 8 pixels diameter around every individual puncta. Metamorph software was used to determine the average fluorescence from individual ROI by tracking the individual vesicles throughout the stack (Stacking interval 100 ms). Furthermore, quantified average fluorescence values were imported to IgorPro6 program (Wave metrics) through a custom-written routine. Detailed analyses were performed on individual traces upon transforming fluorescence values into traces, i.e. Amplitude Maxima, Half-width and Time constants for Decay or τ (Tau). Moreover, analyzing the dispersion of the cargo molecules from the core of the vesicle to the periphery provided a read-out to monitor secretion. This set of data was obtained by TIRF microscopy, where 20 Hz acquisitions were performed. For analysis, two concentric circles were drawn surrounding the events; circles were of 5 and 10 pixels respectively corresponding to a numeric diameter of 0.8 μm and 1.6 μm . Integrated fluorescence was

measured for individual puncta or events. Upon subtracting the total fluorescence value of inner circle from the outer circle, total fluorescence values were obtained for adjacent annular structure, formed in the juxtaposition of two circles. Fluorescence values from TIRF recordings were obtained after background correction throughout the stack with ImageJ software and the integrated fluorescence measured from individual circle in Metamorph software.

2.4.4 Line Scan Analysis

Based on the duration of the events, event-containing frames were extracted from the whole stack of images. For short lasting and long lasting events respectively 21 frames 51 frames, were extracted from a whole stack. Mean fluorescent intensity was obtained from NPY-pHluorin and synaptopHluorin events on a rectangle, which has a dimension of 24 pixels X 6 pixels (1 pixel = 0.08 μm). Values were obtained with custom written routine in Metamorph. Average traces were acquired from each group of events, i.e. long and short lasting event. After offset correction average traces were fitted with a Gaussian function [Equation 2 (Result section 3.2.1)].

2.5 Statistics

Reported data are presented as mean \pm SEM (Standard error of the mean) unless stated otherwise. To determine statistically significant differences, one-way analysis of variance, i.e. student- *t-test* or Rank-sum test between two groups were performed, unless indicated otherwise. The distribution of the data set always considered for statistical analysis. The following significance levels were applied. Error probability $p < 0.05$ (*), $p < 0.01$ (**) and $p < 0.001$ (***).

3. Results

3.1.1 Imaging stimulus-evoked NPY-pHluorin release from large dense-core vesicles (LDCVs)

Predominantly electrochemical techniques, such as amperometric recordings on PC12 and chromaffin cells have previously provided substantial information on fusion pore kinetics and cargo discharge from LDCVs (Chow et al., 1992; Schroeder et al., 1996; Wang et al., 2001; Wang et al., 2003; Bruns et al., 2004; Borisovska et al., 2005; Kesavan et al., 2007). Single amperometric spikes frequently possess a biphasic onset, exhibiting a small initial oxidation current (pre-spike foot signal; PSF) followed by the main amperometric spike. While the first one reflects catecholamine efflux through a narrow fusion pore, the second one indicates bulk release. Therefore, amperometry allows us to resolve discrete phases of transmitter discharge from single vesicles. However, amperometric recordings are limited to oxidizable molecules, such as catecholamines, dopamines and serotonin, and this high-resolution electrochemical method cannot report any information about the fate of vesicles after the discharge of the rapidly diffusible cargo molecules. Therefore, it is highly interesting to study exocytotic discharge of slowly diffusing molecules, like oligopeptides seconds after initiation of exocytosis. In recent years, complementary optical methods have been developed to study intracellular trafficking and vesicular release using fluorescently tagged cargo molecules (Taraska et al., 2003; Taraska et al., 2004; Perrais et al., 2004; Zhu et al., 2007; An et al., 2010). Here in this work, we designed our experimental strategy to use NPY-pHluorin [(a fusion protein between NPY and the pH-sensitive variant of EGFP, pHluorin), (which was kindly provided by Thomas Söllner from Heidelberg University)] to study vesicular exocytosis. NPY-pHluorin is sorted to the vesicular lumen due to the targeting sequence of NPY (Zhu et al., 2007) and is found to co-localize with different LDCV markers, such as chromogranin-A and B as described by Steiner et al., 1989. The fluorescence of the intravesicular pHluorin-based constructs results from their dequenching reaction due to the change in the intravesicular environmental pH upon opening of the fusion pore; thus such constructs are able to report the initial opening of fusion pore, as well as the subsequent efflux of the cargo molecules. Here, NPY-pHluorin was acutely expressed in cultured mouse

chromaffin cells by using a viral expression system (Semliki Forest). Cells were infected with virus particles on DIV2-3 and imaged at the cellular footprint after 5 hours (hrs) of infection. After contacting the coverslip, the cell develops an extended footprint area, yielding a planar region, which is suitable for the observation of a large number of fusion events.

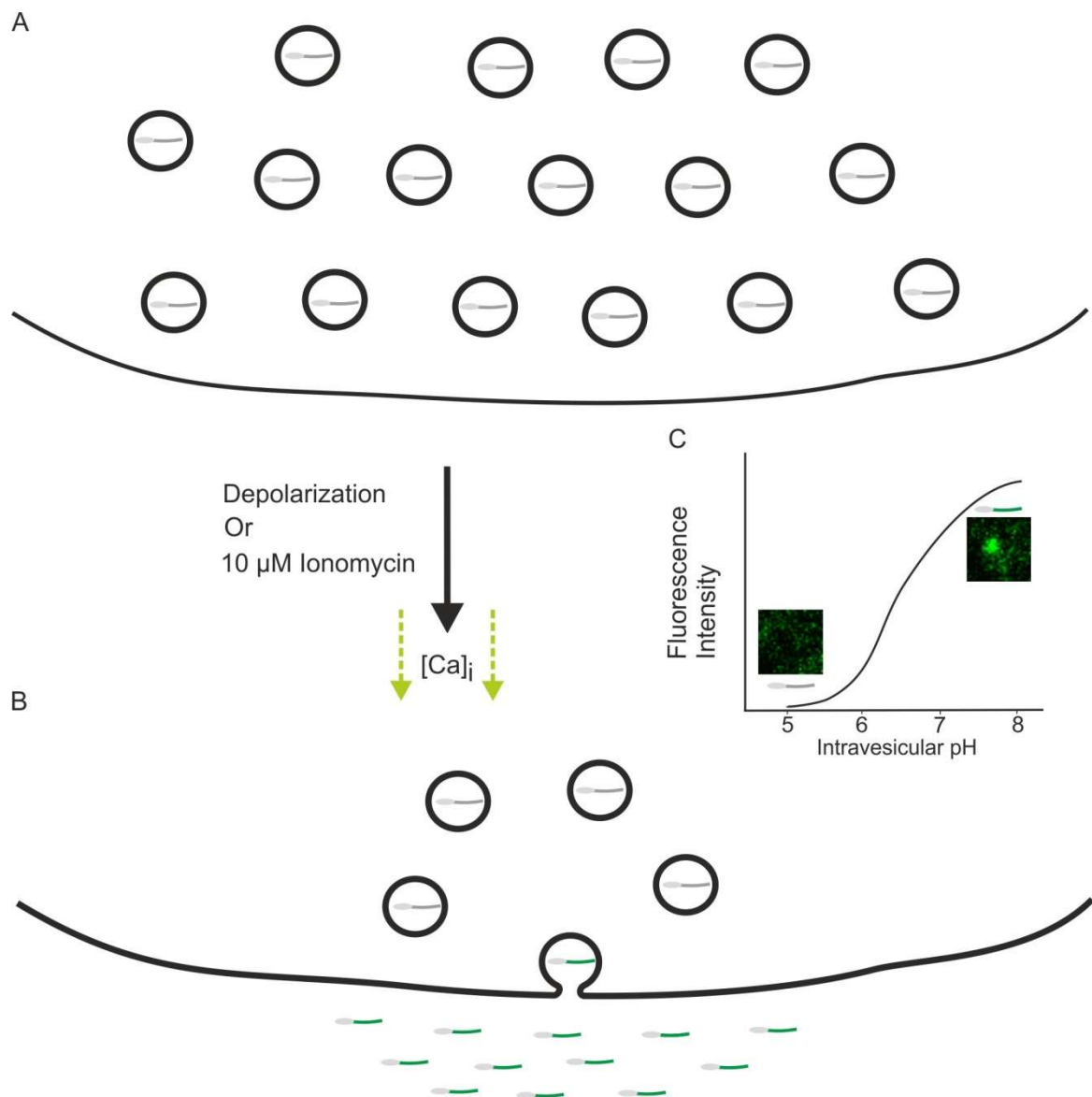
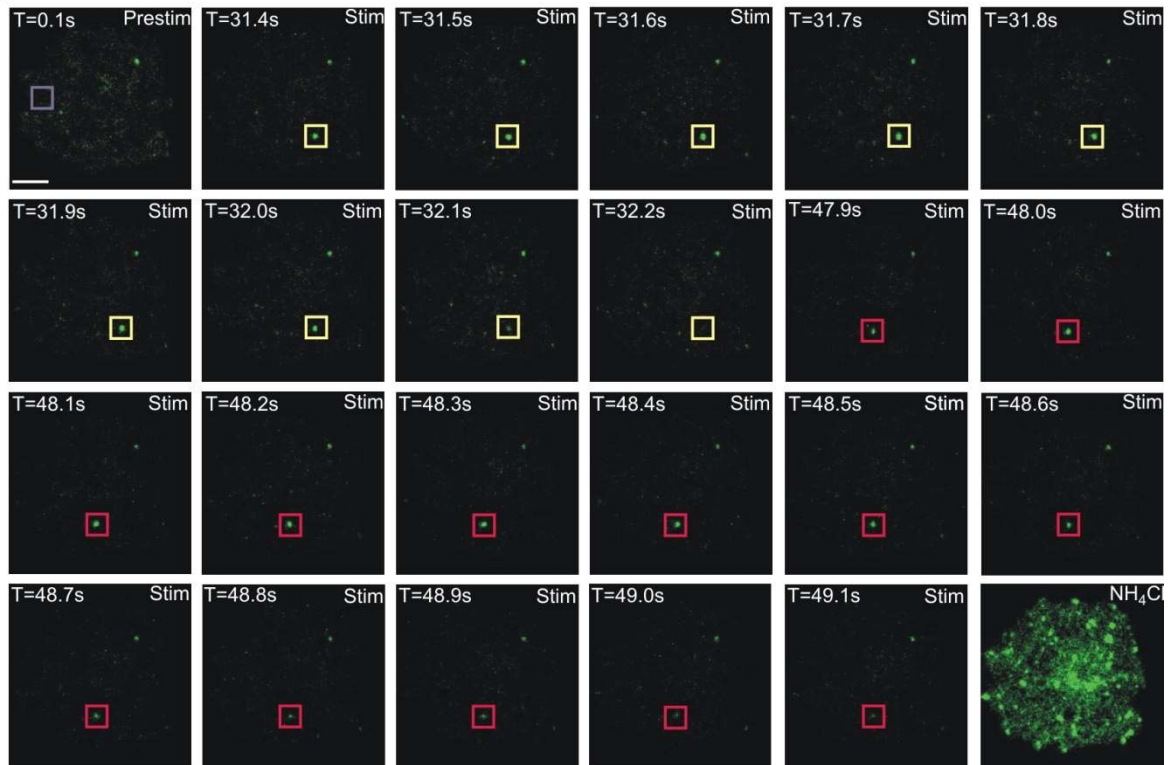


Fig. 9. Experimental strategy illustrates the principle of cargo discharge by using NPY-pHluorin: (A-B) Cartoon illustrating the principles of the NPY-pHluorin-based release assay. As a modified eGFP derivative, ecliptic pHluorin exhibits pH-dependent alterations in its emission spectrum (Miesenböck et al., 1998). When NPY-pHluorin resides in the vesicular lumen, at the luminal pH of 5.5 that is acidic, its fluorescence is quenched. After opening of the fusion pore during release, an aqueous junction between the vesicle lumen and the extracellular medium is

established that results a collapse in the vesicular $[H^+]$ gradient. Consequently, NPY-pHluorin is dequenched, and thereby is capable to report fusion pore opening, and cargo discharge. Thus release events can be monitored by a gain followed by a subsequent loss of fluorescence. That corresponds either to the discharge of the cargo molecule in the extracellular milieu or / and the successive re-acidification of the lumen ["Kiss-and-Run"]. (C) Schematic traces exhibiting the alteration in the fluorescence of pHluorin upon change in the luminal pH. Images adjacent to the trace (inset) show pictorial representation of a fusion event.

The infected cells were selected for imaging, based on their pHluorin's fluorescence (EGFP) intensity. Cells with excessively high expression of reporter molecules in the ER and Golgi network were excluded from further analysis. To maintain overproduction of proteins, these cells might exhibit a stress-driven energy crisis that in turn might induce erroneous cellular responses. Exocytotic events were elicited by the application of 10 μ M ionomycin, an ionophore known to increase the cytosolic calcium concentration. Successful exocytosis events were recognized by a rapid increase and a subsequent decay of fluorescence in the form of puncta at the fusion sites of the footprint area of the cell. Acquisition parameters (laser intensity, field-of-acquisition size and signal gain) were identical for all measurements. The experimental paradigm is illustrated schematically in Fig. 9, showing the pH-dependent dequenching of pHluorin upon a stimulation-evoked vesicle fusion event (Fig. 9 inset). An exemplary image series in Fig.10 A, shows a classical stimulus-evoked NPY-pHluorin event from the footprint of a mouse chromaffin cell with fluorescence appearance and its subsequent decay. Fusion events were recognized by visual inspection of brightening spots that appeared during stimulation, as also observed in earlier studies (Taraska et al., 2003; Taraska et al., 2004; Perrais et al., 2004; Zhu et al., 2007, An et al., 2010). For quantitative analysis, changes in fluorescence were measured over time within a defined region-of-interest (ROI; 8 pixels diameter, 1 pixel corresponding to 0.08 μ m) around identified fusion sites. The event frequency was determined by counting the number of brightening spots per stimulation period. Only events with the mean amplitude of 25 A.U., i.e. 5 times to the standard deviation of baseline noise or more, were analyzed for quantification. To overcome the problem of saturation in the fluorescent signals, extremely high amplitude events (≥ 150 AU) were excluded from the quantitative analysis (few events $\sim 2/158$ in wildtype cells).

A



B

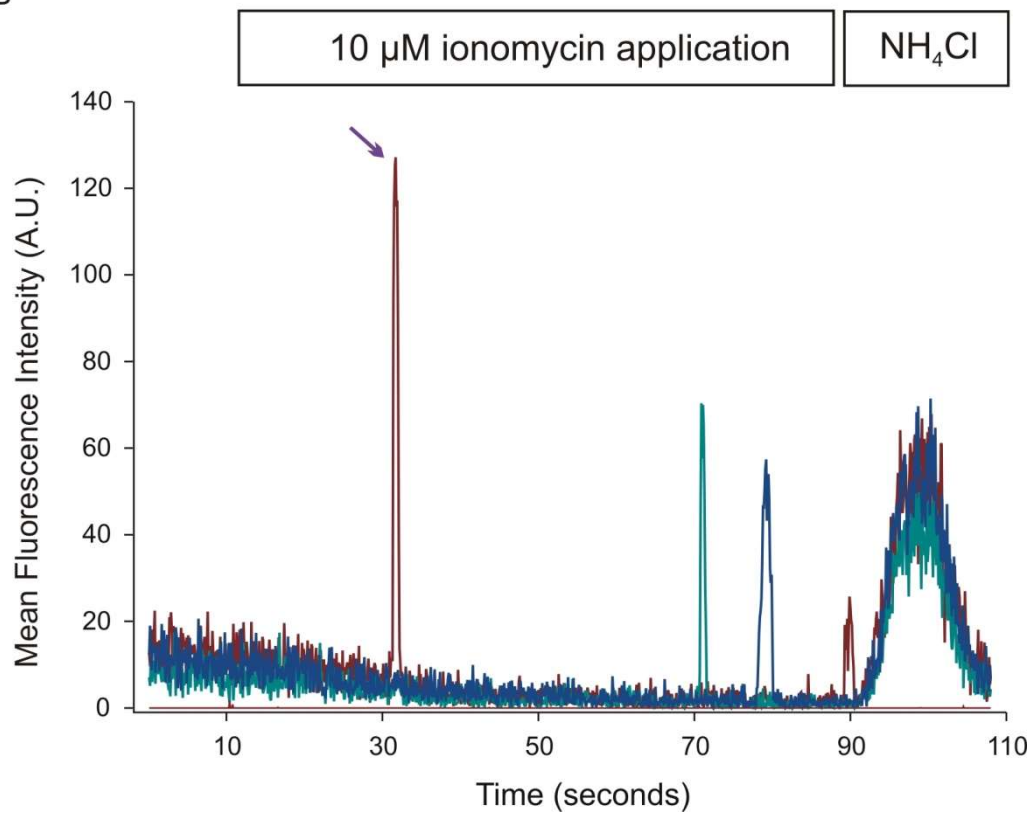


Fig. 10. Exemplary images and traces depict NPY release events: (A) Image series of the footprint area of a mouse chromaffin cell that was acquired at 10 Hz sampling rate. {Orientation left-to-right} the first image displays the cell in normal bath solution and the following nine images depict one stimulation-evoked vesicle release event that is marked by a yellow square. The next thirteen images represent a relatively long lasting vesicle (marked with a red square). The final image illustrates the residual NPY positive vesicles that have responded to ammonium chloride superfusion [Bar ~ 3 μm]. (B) Exemplary traces were obtained by tracking individual puncta over time-series of images with identical ROIs (8 pixels diameter ~ 0.64 μm). The maroon red trace illustrates the temporal profile of the events depicted within the yellow square in A.

Cells were routinely superfused with ammonium chloride (NH_4Cl) at the end of the experiment to visualize the residual NPY-pHluorin containing granules that have failed to undergo exocytosis. Ammonium chloride (NH_4Cl) neutralizes the intraluminal pH gradient as ammonia rapidly diffuses across the membranes and raises the intraluminal pH that in turn makes remaining secretory granules and/or re-internalized vesicles visible. Approximately, 30 discernable punctas/cell (most likely corresponding to vesicles) were seen upon treatment with NH_4Cl (Fig. 10A and B) within a footprint. Additionally, events with delayed onset of response were also excluded from further analysis, as kinetic response from this pool of events overlapped with the NH_4Cl -induced global increase of fluorescence that might also reflect re-internalized NPY-pHluorin containing granules. We observed that the ionomycin induces distinct dequenching and loss of signal events that occurred with an average frequency of 1.26 ± 0.22 events/cell (Cell, $N=123$; event, $n=156$). Thus, only a small fraction of membrane-proximal (docked) vesicles was released upon stimulation. The stimulation-induced fluorescence rise occurred due to the dequenching of luminal pHluorin molecule concomitant with the fusion pore opening. The signal decay might represent the discharge and subsequent diffusion of the cargo molecules from the fusion pore.

3.1.2 Stimulus-evoked NPY release events fulfill the hallmark of classical v-SNARE mediated and Ca^{2+} -regulated fusion process

To confirm that detected fluorescence signals correspond to classical SNARE-mediated fusion events of LDCVs, we analyzed whether NPY-pHluorin release is absent in the genetically null background of v-SNAREs (*synaptobrevinII^{-/-}*)

cellubrevin^{-/-}[SybII/Ceb] chromaffin cells. Previous studies have demonstrated that catecholamine release was almost abolished in these double knock out (doko) cell types (Borisovska et al., 2005; Kesavan et al., 2007). In agreement with these findings, we could not detect any release of NPY-pHluorin in the doko cells (Fig. 11 A). In contrast, the littermate control (Ceb^{-/-}) cells exhibited no alteration in the release frequency [1.77 ± 0.86 events/cell], when compared to our previous experiments with wildtype (C57/BL6) chromaffin cells [1.26 ± 0.22 events/cell] as shown in Fig. 11 A. Since, the lack of detectable fusion events in double v-SNARE deficient cells might also be due to the lack of NPY-pHluorin containing vesicles, we further analyzed the number of NPY containing vesicles at the cellular footprint area after application of NH₄Cl. An average of 33.66 ± 5.13 (n=303) NPY-pHluorin positive granules were observed in the doko chromaffin cells, which was similar to the littermate control (31.44 ± 4.73 , n=283) (Fig. 11 B). Thus, the de novo synthesis of NPY-containing granules is unaltered in SybII/Ceb double v-SNARE deficiency.

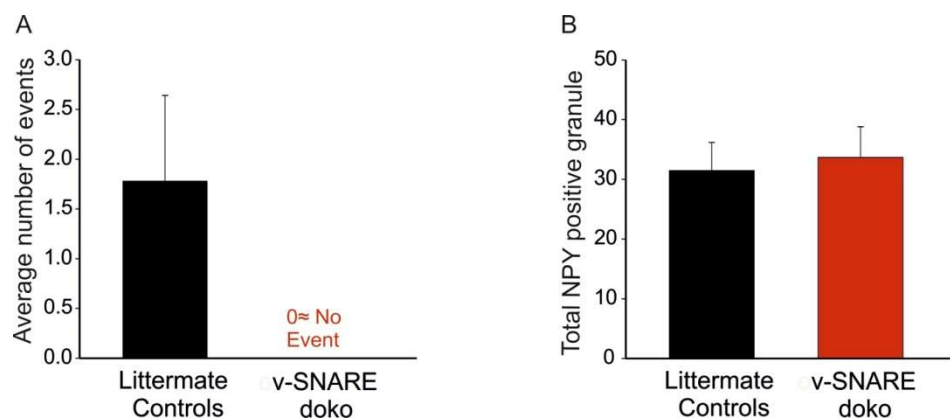


Fig. 11. v-SNARE deficiency leads to the abrogation of NPY-pHluorin release events: (A) No fusion events could be detected in SybII/Ceb double v-SNARE deficient cells. (B) Total number of NPY-positive puncta remained unaltered upon treatment with ammonium chloride solution. (Littermate control cells N=9, events n=16; v-SNARE doko cells (*doko*) N= 9, n=0). Error bars represent Standard Error of the Mean (SEM).

Altogether these experimental results show that cargo release from chromaffin granules can be successfully studied by using NPY-pHluorin as a reporter tool. They further demonstrate that the stimulation-evoked NPY-pHluorin fusion events were SNARE mediated release.

3.1.3 NPY-pHluorin release shows highly variable kinetics

We next analyzed the time-course of the transiently occurring fluorescent signals at the footprint of the chromaffin cell and observed high variability in event duration. In addition to very fast events with 'spike'-like traces, we found a pronounced fraction of events transiting through a 'plateau'-like phase before the fluorescence signal quickly dissipated (Fig. 12 A). To quantify this observation, the event half-width, i.e. the duration of an event at half of the peak amplitude was measured (Fig. 12 B). The signal amplitude of the events was scattered over a wide range, but the spike and plateau events did not vary in amplitude, therefore the frequency distribution displayed a unimodal right hand skewed distribution (Fig. 12 C). Alongside, we found that the median amplitude of the distribution was 54.92 A.U., the event amplitude should be proportional to the number of fluorescently labeled cargo molecules per vesicle the kinetic profile of the fluorescence signal may illustrate the retention of the cargo molecules and their subsequent release as demonstrated by loss of the fluorescence signal. An attractive explanation for spike and plateau events could be that they are due to the 'rapid' (near instantaneously) and the 'delayed' release of the cargo molecules, respectively.

Our quantitative analysis revealed a skewed distribution of event half-width with a major fraction of events belonging to the range of 100-400 ms and the rest of the events were found in the tail and the median value for the half-width was 0.59 s (590ms) (CellsN=56, events n=158), implying that the event half-width scattered over a very wide range. Close analysis of the frequency distribution revealed a slight 'shoulder' (Fig. 12D, see arrow) in the half-width distribution and a corresponding 'kink' in the cumulative distribution, which led us to interpret that there were two underlying event sub-populations, one with a maximum standing below 400 ms [40% of the total events], and another with a maximum around 900 ms. This might imply that there is a differential mode of cargo release.

Nevertheless, the duration of the plateau phase might also be continuously regulated and the delayed dilation of the fusion pore might be a cardinal regulatory factor. The event amplitude did not provide any clear correlation with the event half-width (Fig. 12 E), suggesting that the amount of cargo present in the vesicles was not responsible for influencing the variable time course of the NPY-pHluorin events. The decay

of the fluorescence is generally interpreted as discharge and dispersion of the fluorescently labeled cargo into the extracellular milieu. Alternatively, the decay phase could also be driven by the reacidification of the retrieved vesicular event (addressed in section 3.4).

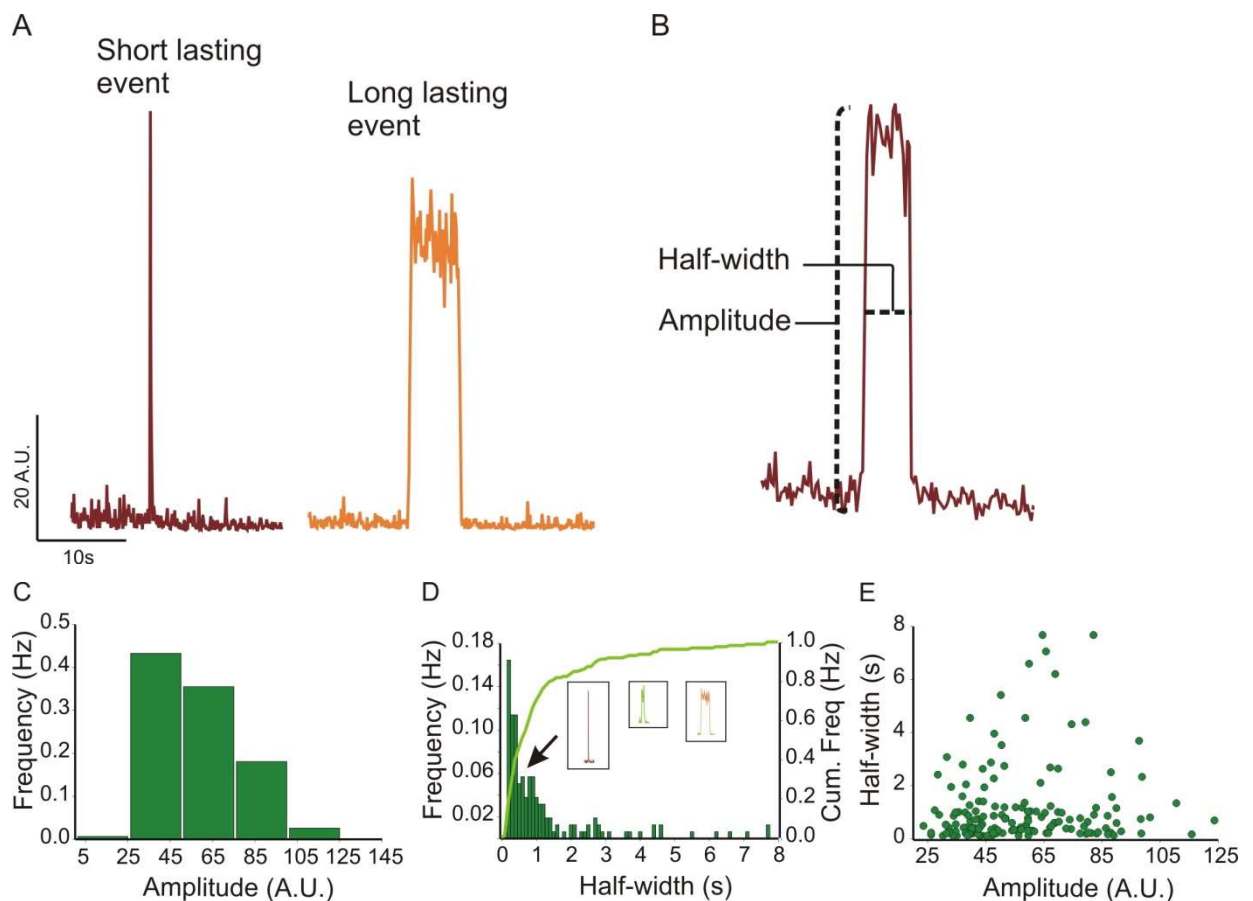


Fig. 12. NPY release reveals a high level of heterogeneity in the discharge properties of single vesicles: (A) Exemplary traces of NPY-pHluorin show discrete types of NPY-pHluorin release, i.e. short lasting spike-like and long lasting plateau-like events. To illustrate the results more profoundly, the events are depicted at the same time scale. (B) A cartoon to depict analyzable kinetic parameters of NPY-pHluorin events, such as event amplitude and half-width. Event parameters were measured with a custom written routine in IGOR. (C) Frequency distribution of the event amplitude plotted with a bin of 25 A.U., exhibiting a positive skewed distribution. (D) Based on the event half-width, the frequency distribution was plotted with a bin of 0.1 s or 100 ms. Spike-like events are located in the left hand side of the distribution and the highly variable long-lasting plateau-like events are on the right hand side of the distribution. However, segregation of these two sub-populations was possible only by the presence of a shoulder (see arrow) at the 400-ms range,

inferring that this is a variable distribution of bi-modal release events. (N=56; event n=158). (E)
Plotting the correlation of the amplitude and the duration of an event, i.e. half-width.

Given the previous data set, which depicted that the signal time course was mainly governed by the discharge of the cargo molecule, hence in turn, this might also be regulated by several factors, such as biophysical properties of the NPY molecule (dimension, diffusion constant), mobilization from the vesicle core and the geometry of a restricting fusion pore. Furthermore, spatial location of the contact-patch in the vesicle membrane at the fusion site might also influence the two-dimensional mobility of released material in the focal plane. In spite of having kinetic differences, spike and plateau events exhibited a similar decay. In order to address this more comprehensively, we derived the time constant for decay (τ) by fitting the decay phase of the signal time-course of a detected event with a mono-exponential function as follows:

$$F = F_b + Ae^{-\frac{t}{\tau}} \dots\dots\dots(1)$$

Where A represents the maximum amplitude and F_B indicates the baseline fluorescence. In case of the spike-like events, the fit interval started at the maximum and extended for 2 seconds (Fig. 13 A). For the plateau-like events, the left border of the fit was placed at the transition point of the plateau phase and the decay phase (Fig. 13 B). Quantitatively, we found a positively skewed distribution with a maximum in the range of 100-200 ms and a median of 0.093 s (Fig. 13 C). Interestingly, we noticed that the decay constant (τ) covered a narrow range in the distribution, when compared to the widely distributed half-width. Importantly, we did not observe a clear correlation between event half-width and decay time (τ) (Fig. 13 E). This indicated that the stationary phase (plateau) is mechanistically distinct from the processes that shape the decay phase. They also suggest that both event types are terminated by cargo release proceeding with similar speed. Furthermore, no direct correlation could be established between event amplitude and tau (τ) confirming further that the time taken by the molecule to be discharged was independent of the vesicular cargo content (Fig. 13 D).

Previous reports demonstrated that the initial fusion pore diameter was not larger than that of an ion channel (~ 2 nm) (Lindau et al., 1995; Lindau et al., 2003), whereas the molecular dimensions of NPY and EGFP were $\{4.3 \times 1.9 \times 1.4\}$ nm and $\{4.6 \times 3.2 \times 3.1\}$ nm, respectively (Tsuboi et al., 2004). Thus, it is conceivable that this narrow fusion pore can restrict the expulsion of the bulkier cargo, such as NPY-pHluorin, until the fusion pore is completely dilated. Such a scenario can lead to 'plateau'-like events with a stationary phase constantly demonstrating an unquenched fluorescent cargo. On the other hand, spike events rapidly crossed this barrier of initial pore opening, thus resulting in an instantaneous loss of fluorescent signal from the vesicles. Collectively, this data set showed that NPY release followed a high degree of variability in duration but showed similarity in decay.

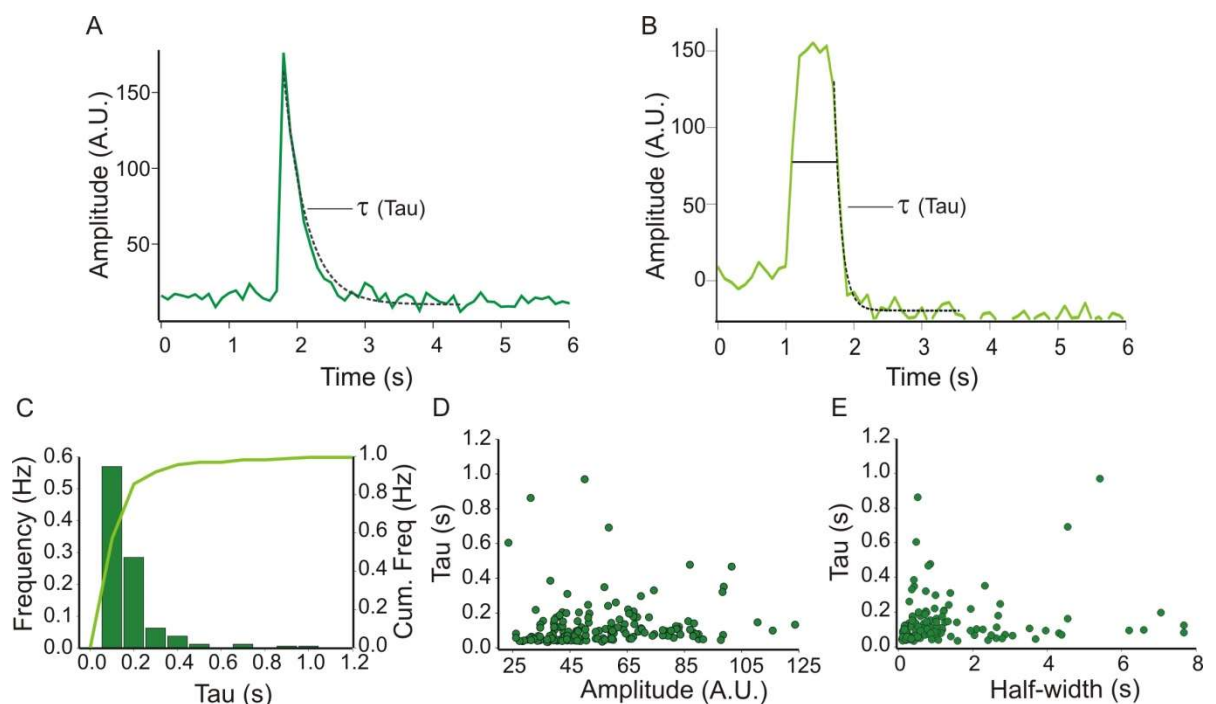


Fig. 13. Quantitative analyses depict uniformity in the decay pattern of NPY release events, in spite of variability in the duration: (A) Schematic representation of the mono-exponential time constant of decay (τ) of an exemplary 'spike' event, which was derived after fitting decay phase with a mono-exponential function. (B) Graphical illustration of the tau (τ) of a 'plateau' event. (C) Event frequency of tau with a bin width of 100 ms predominantly exhibits a positively right-handed skewed distribution. (D) Scattered plot demonstrating no correlation between event amplitude and event tau. (E) The variability in the event duration did not follow a steady correlation with event tau. (N=56; event n=158).

Taken together, the spike-like events reflect discharge of the cargo molecule from the vesicle through a fully dilated fusion pore and plateau events (plateau) illustrate temporarily hindered release of cargo due to a narrow, undilated fusion pore. In contrast, the time course of complete signal loss is similar to both event types and may represent the diffusion of cargo molecules in the extracellular space, as expected upon rapid fusion pore dilation and complete merger of the vesicle with the plasma membrane.

3.1.4 Reacidification does not influence the kinetics of the NPY-pHluorin time course

From the previous set of experiments we could establish that the fluorescence loss might be occurring due to the discharge of the NPY molecule. Alternatively, one might speculate whether reacidification of re-internalized NPY-pHluorin molecule may also contribute in the loss of signal. To test for the role of reacidification on the signal time course, we studied the aforementioned NPY-pHluorin release experiments in the presence of 1 μM bafilomycin (Baf) in the cell bath. Baf is a reversible blocker for vacuolar-type H^+ -ATPase (v-ATPase pump) that inhibits the $\text{H}^+/\text{Ca}^{2+}$ antiporter system in the vesicles, thus abrogating the change in the intravesicular pH of internalized vesicles (Dröse et.al 1993; Zhang et al., 1994). This change in the pH occurs when vesicles are retrieved back into the intracellular side of the cell membrane, upon premature closure of the fusion pore (Sankaranarayanan et al., 2000; Burrone et al., 2006). In the case that the signal loss occurred due to the retrieval and subsequent reacidification of vesicular lumen, Baf treatment should alter the kinetics of signal time course of single event. Here our data set demonstrated that on average bafilomycin induced no significant change in the kinetic parameters of the single event. Firstly, we found no alteration in the event amplitude in Baf-treated cells, which was 58.65 ± 5.93 A.U. compared to the control cells with an amplitude of 60.64 ± 2.69 A.U. (Fig. 14 A). Furthermore in the presence of Baf, the mean half-width of NPY-pHluorin event was 1.42 ± 0.387 s, whereas events from control cells exhibited a mean half-width of 1.25 ± 0.173 s (Fig. 14 B). We also observed a slightly but not significantly faster time constant of decay after treatment with bafilomycin (mean tau (τ) in control cells 0.195

± 0.059 s, bafilomycin-treated 0.094 ± 0.017 s; N11, n=21) that cannot be the result of diminished reacidification and may reflect variabilities due to the small samples size ($P=0.064$; Figure 14C).

Therefore, our data provide evidence that the time course of NPY-pHluorin signal is insensitive to Baf treatment. Henceforth, the results suggest that the decay of the signal time course of NPY-pHluorin was mainly governed by the discharge of NPY molecule from the core of the vesicles rather than by the reacidification of re-internalized vesicle.

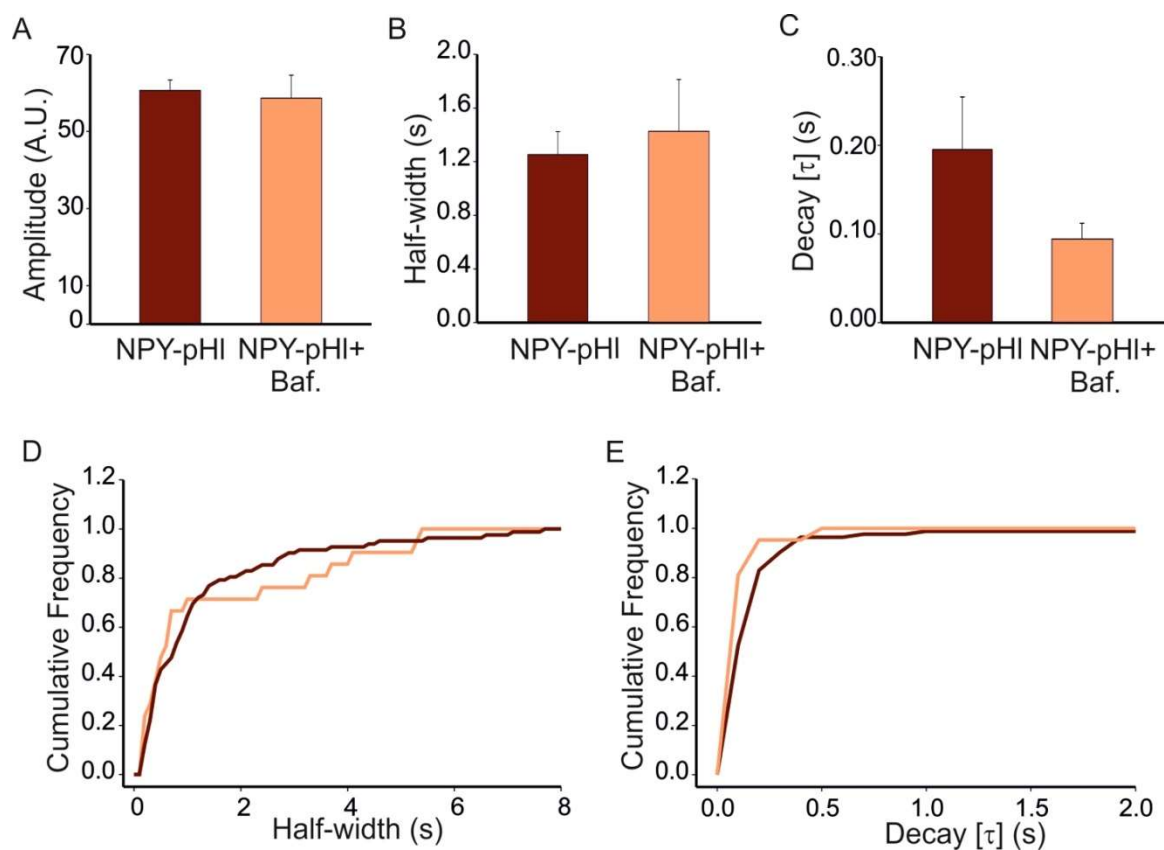


Fig. 14. Bafilomycin induces no change in the kinetics of the NPY-pHluorin signal time-course: Cell weighed analysis of (A) signal amplitude (B) half-width (C) decay tau (τ) ($P=0.064$). (D) Cumulative frequency of events (E) mono-exponential tau (τ) between baf treated (orange) and baf untreated groups (maroon). Baf untreated control cells (N=28), events (n= 82); Baf treated cells (N=11), events (n=21). Error bars represent standard error of mean (SEM).

3.1.5 Radial dispersion of NPY molecules from the fusion site

To substantiate that the fluorescence decay is due to the loss of NPY molecule, we performed line scan analyses of individual fusion events. To detect the radial dispersion of the cargo molecules with reasonable fidelity, we confined our analyses to events with minimum amplitude of 70 A.U., as vesicles with higher number of cargo molecules make radial dispersion more readily detectable. Fluorescence dissipation of an event was measured with a multiple-lines scan covering an area of 2 μm X 0.48 μm that comprised the geometrical center of the event and the surrounding regions (Fig. 15 A).

The spatial profiles were obtained for two successive time points of the decay ($\delta t = 100$ ms), i.e. first frame and second frame of decay. The peaks of the line-scan were manually aligned to the mid-point of the line and traces were fitted with Gaussian function as follows:

$$F = F_b + Ae \left[-\left(\frac{d - d_0}{SD} \right)^2 \right] \dots\dots\dots 2$$

Where A = Amplitude of the Gaussian Bell; $d - d_0$ = mid-point of the Gaussian bell and SD (Standard deviation) = Width of the Gaussian. Firstly, our results revealed a Gaussian profile of fluorescence signal over the distance of 2 μm centered at 1 μm , which was almost diminished in the next frame taken at an interval of 100 ms. Most likely, rapid diffusion of cargo molecule away from the fusion site, as also shown in exemplary traces from a spike event (Fig. 15 B) is responsible for the signal loss within 100 ms. This scenario was also found for plateau events, as demonstrated by exemplary traces in Fig. 15 C.

On average the line-scan traces of NPY-pHluorin events resulted in a Gaussian distribution of the fluorescence signal plotted over distance at the moment of their first detection. The subsequent detecting frame (100 ms later) exhibits approximately 30% of the peak amplitude of the first frame demonstrating an extensive loss of signal over a single frame (Fig. 16 A, B).

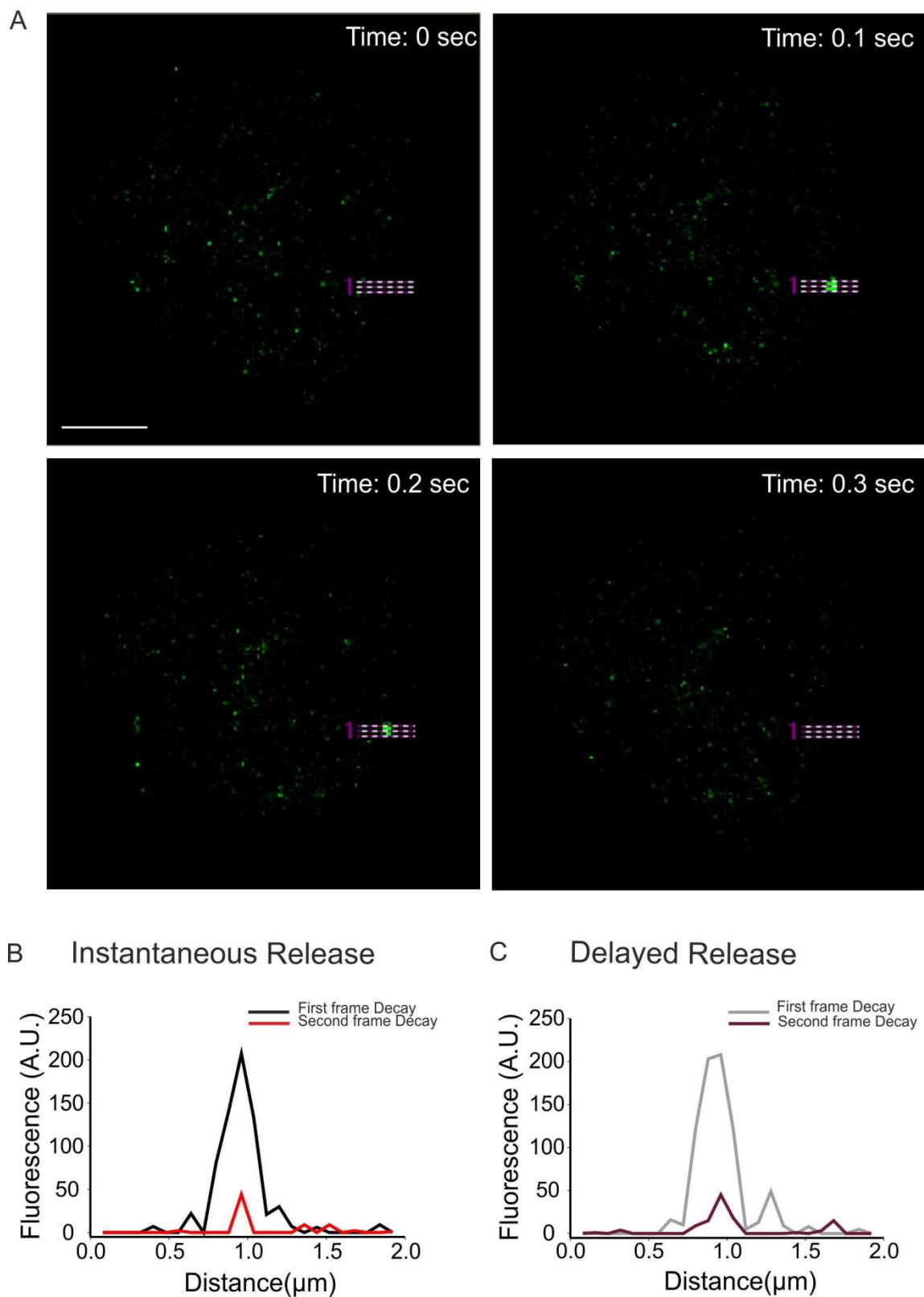


Fig. 15. NPY dispersion occurs instantaneously from fusion site: (A) Exemplary images illustrating the line-scan analysis of a chromaffin cells with a rectangular ROI [24 pixels x 6 Pixels].

(B) Representative traces in black and red represent consecutive time point of decay from a Spike-like event, resulting in a drastic loss of signal. (C) The exemplary traces from plateau-like events in grey and maroon represent subsequent time points of decay, which replicates the behavior of the above-mentioned 'spike'-like event [Bar $\sim 3 \mu\text{m}$].

Notably, normalization of the subsequent traces did not reveal any discernable broadening of the spatial profile as it is expected if the amplitude reduction is due to diffusion of cargo molecules away from the fusion site. Instead these results rather suggest that discharge of NPY molecules is the rate-limiting factor for the observed amplitude reduction. Given the rapid diffusion of NPY-pHluorin [Diffusion coefficient (D) $\sim 8 \mu\text{m}^2/\text{sec}$ (Swaminathan et al., 1997)] in aqueous solution, it is possible that the majority of NPY-pHluorin molecules escape their detection field of $2 \mu\text{m}$ within the time period of 100 ms.

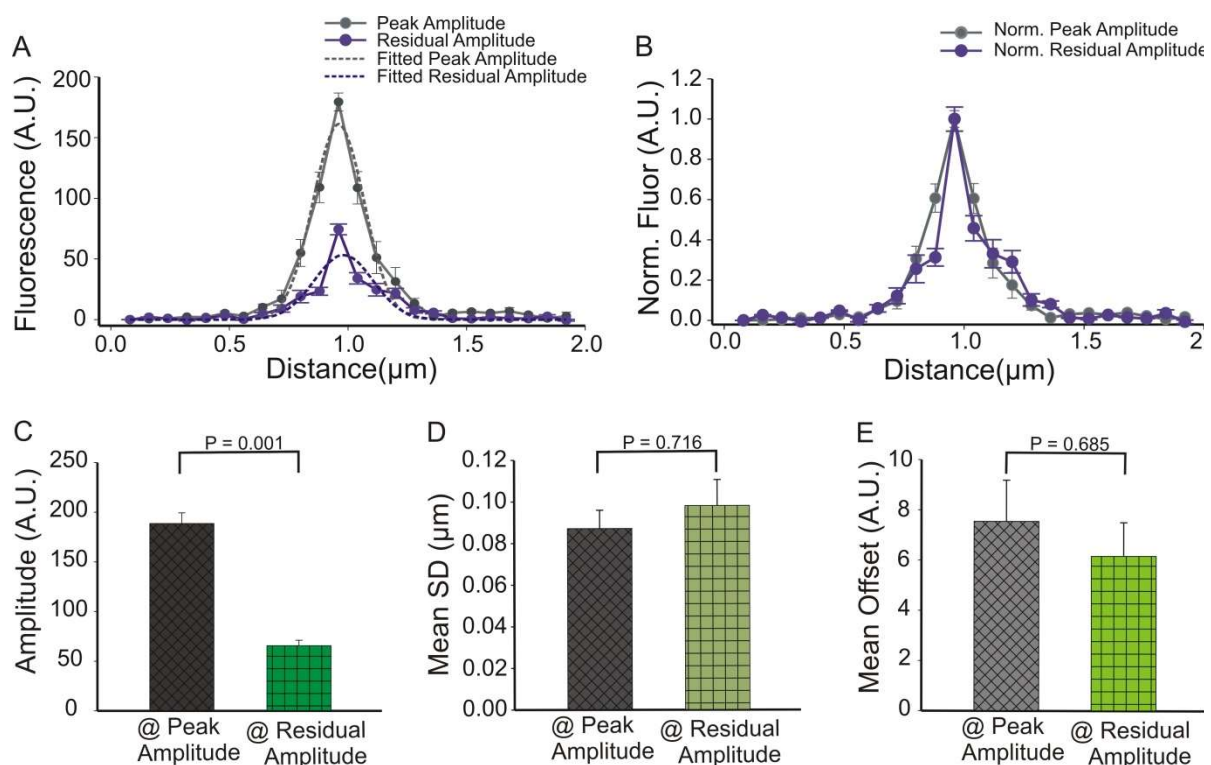


Fig. 16. NPY-pHluorin release events at weight-scale exhibited no radial dispersion: (A) Traces show an average spatial profile of NPY-pHluorin release events at two subsequent time point of decay (Grey and purple), resulting neither an increase in spatial broadening nor in signal offset. (B) Average traces normalized to the peak value did not illustrate any spatial broadening and/or a rise in signal offset. (C) The mean amplitude exhibited almost 4-fold fluorescence drop

at the subsequent decay time ($P=0.001$, Rank-sum test). (Wild type, events: $n=22$). (D) Mean SD obtained from the Gaussian fitting from the pool of events depicts no alteration in the SD, following amplitude drop. (E) Mean signal offset was also unchanged over the decrease in the signal amplitude over time. Error bars represent standard error of the mean (SEM). (For detail see Table 4)

However, in a few cases we could observe two alternative scenarios, where accumulation of the cargo was detected within the measurement region ($2 \mu\text{m} \times 0.48 \mu\text{m}$), resulting in an increase in the signal offset (Fig 17 A, A#) and an increase in the SD of the Gaussian profile (Fig 17 B, B#) accompanying the amplitude drop. Both phenotypes were observed for spike and also for plateau events. Such post-release detection of diffusing cargo molecules in the vicinity of the fusion site may provide an indication for close approximation of plasma membrane and coverslip plane, thereby generating a narrow cleft that hindered the normal dispersion rate of NPY-pHluorin. Consequently, the lower rate of removal of cargo molecules can lead to this accumulation in the vicinity of the fusion site.

Tab. 4: Individual parameters of Gaussian fittings of NPY-pHluorin events:

Info.	Ampli-Peak	SD-Peak	Mid-Peak	Offset-Peak	Ampli-Residual	SD-Res.	Mid-Res.	Offset-Res.
1	159.86	0.08	0.94	23.63	33.04	0.13	0.90	22.36
2	197.79	0.12	1.07	15.06	39.62	0.16	1.16	8.22
3	128.83	0.07	0.92	6.55	38.47	0.08	0.90	7.09
4	237.76	0.09	0.95	5.34	79.80	0.05	1.00	13.44
5	135.94	0.11	0.97	2.23	61.04	0.05	0.96	NA
6	148.59	0.14	1.03	12.57	45.91	0.17	1.06	6.09
7	225.06	0.10	0.92	3.89	43.41	0.06	0.96	1.48
8	233.20	0.04	0.92	5.46	59.11	0.04	0.97	5.00
9	113.64	0.08	1.02	1.88	76.53	0.07	0.99	1.61
10	240.36	0.09	0.95	2.48	78.97	0.13	0.96	2.60
11	103.60	0.07	0.95	21.98	44.21	0.06	0.95	16.12
12	207.76	0.04	0.96	2.19	83.58	0.06	0.94	0.07
13	198.90	0.09	0.95	3.17	40.34	0.01	0.96	1.20
14	139.45	0.05	0.93	9.84	43.83	0.04	0.93	7.40
15	199.35	0.10	1.00	12.84	107.49	0.22	0.93	7.40

16	157.84	0.01	0.95	18.05		77.06	0.09	0.96	NA
17	229.96	0.09	0.95	1.07		66.00	0.02	0.99	NA
18	174.37	0.06	0.94	7.37		73.49	0.12	1.05	-0.34
19	266.11	0.09	0.91	-1.10		87.64	0.19	1.01	1.86
20	260.79	0.13	1.06	1.20		140.85	0.16	0.97	7.92
21	251.02	0.21	0.97	-5.57		72.87	0.15	1.08	3.74
22	137.83	0.05	0.96	15.75		49.23	0.10	1.05	3.82
Avg	188.55	0.09	0.96	7.54		65.57	0.10	0.99	6.16

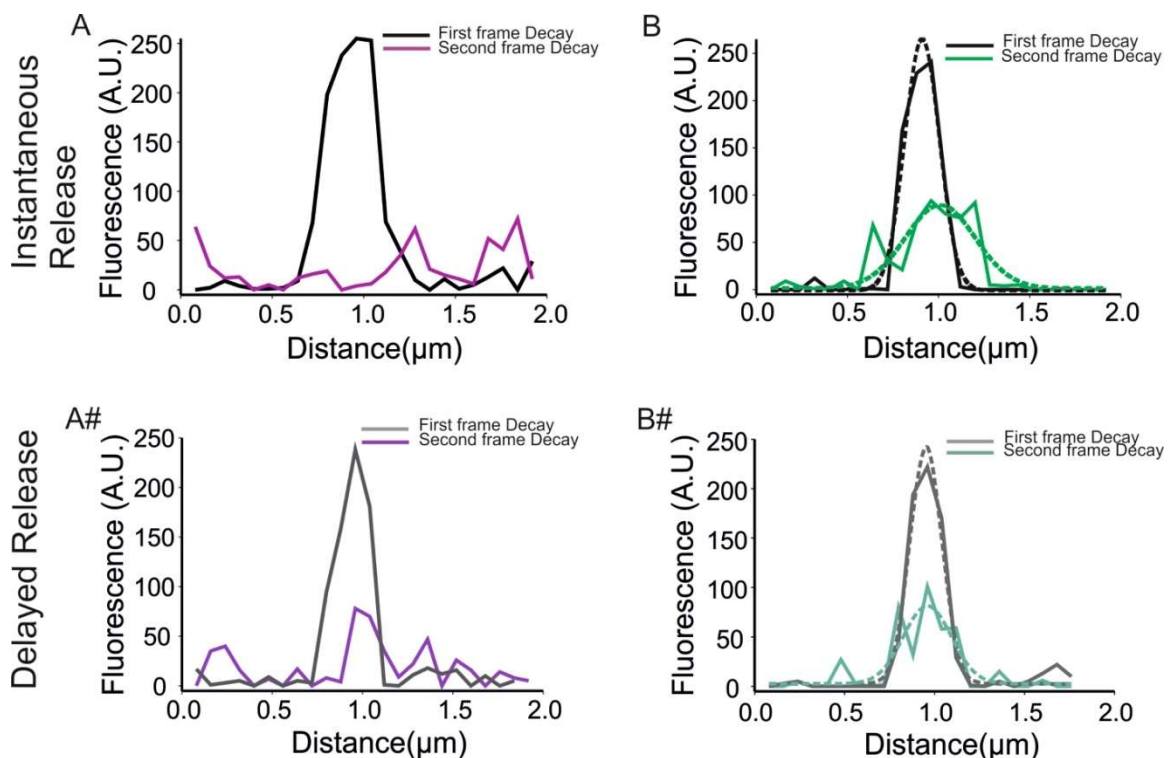


Fig. 17. Diffusion based dispersion of cargo material observed in some NPY-pHluorin events: (A) Traces representing the subsequent decay time from a spike event, providing evidences for a rise in the signal offset. (A#) Another set of representative traces demonstrating a rise in the signal offset for a plateau event. (B) The radial dispersion from a spike-like event was exhibited in the form of a spatial broadening with subsequent fluorescence loss. Gaussian fitted traces (broken line) depicting an increase in the width / SD of the fitted traces, complementing amplitude drop. (B#) Standard traces represent a 'plateau' event exhibiting broadening of the signal at subsequent time points complementing the amplitude drop.

Considering the rate-limiting role of cargo efflux in the diffusion, we next tried to visualize the release of NPY-pHluorin cargo molecules using total internal reflection microscopy (TIRF).

3.1.6 TIRF images acquired with 20 Hz sampling rate confirm rapid discharge of cargo

Due to the temporal limitation in our detection method with the 10 Hz sampling rate in LSM, we opted for a 2-fold faster acquisition microscopic method that is TIRF. We again performed line-scan analysis of NPY fluorescence similar to diffusional discharge to the cargo molecule to provide supporting evidences for the aforesaid differential diffusion. After background subtraction, fluorescence distribution was measured with a rectangular ROI covering a dimension of $3.12\ \mu\text{m} \times 0.78\ \mu\text{m}$. The aforementioned parameters of the line-scan measurement were similarly followed. With 2-fold higher acquisition rate, i.e. 20 Hz (50 ms/ frame) in TIRF, we were not able to detect diffusing cargo molecules in the fusion site and also in the encompassing region of the fusion site. Exemplary and the normalized average traces are shown in Figure 18 (A, B), on average, loss of the signal amplitude was not accompanied with a significant alteration in the SD of the spatial profile (SD for first frame 2.4697 ± 0.138 pixels and SD for second frame was 2.4408 ± 0.277 pixels).

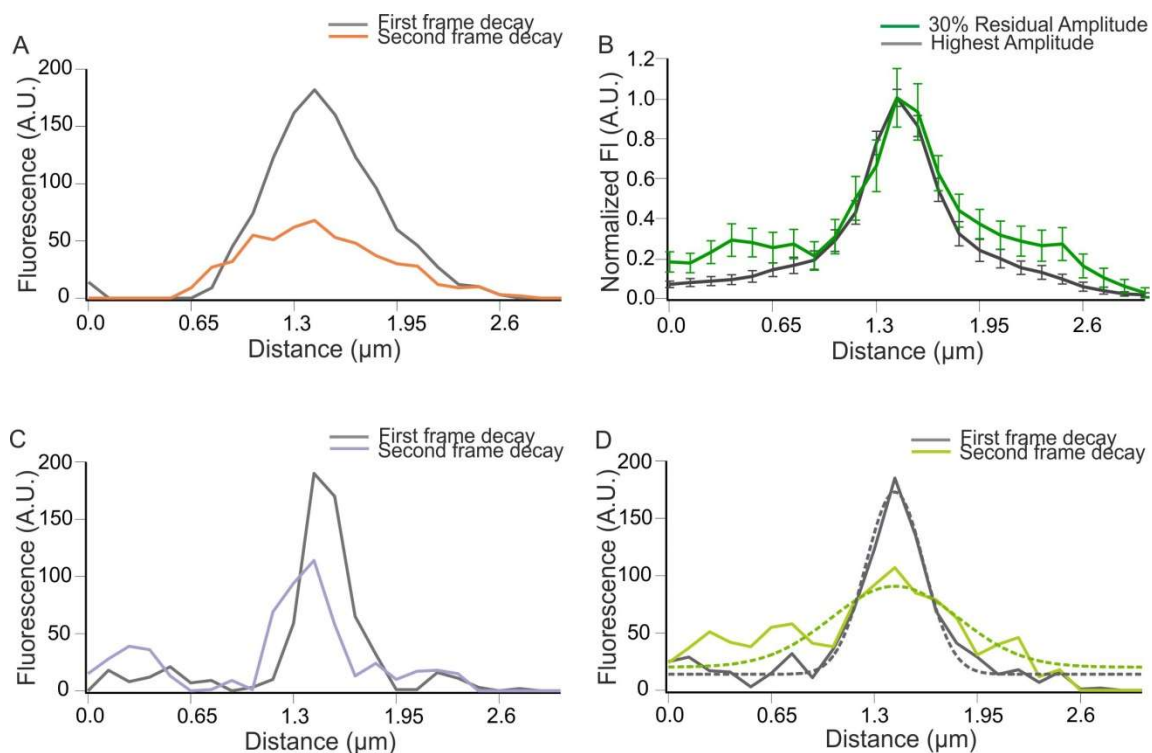


Fig. 18. Differential diffusion mode of NPY discharge in higher sampling TIRF microscopy: (A) Exemplary traces of NPY release events showing rapid diffusion-based radial dispersion. (B) Average traces normalized to peak amplitude and 30% residual amplitude, subsequently aligned to the peak that is set to the mid-point or center of the event. (Wild type event, n=27). [Error bars represent standard error of the mean (SEM)]. (C) Representative traces showing an event, illustrating an increase in the signal offset at the subsequent time point with a time interval of 50 ms. (D) Exemplary traces from of NPY release events, showing an increase in the Gaussian SD at the consecutive decay time, illustrating the accumulation of diffusing cargo material in the vicinity of fusion site.

Furthermore, in line with our previous LSM recordings, we could rarely observed fusion scenarios that are indicative for the accumulation of diffusing cargo molecules in the vicinity of fusion site, as illustrated by an increase in the signal offset (Fig. 18 C) and an increase in the Gaussian SD (Fig. 18 D).

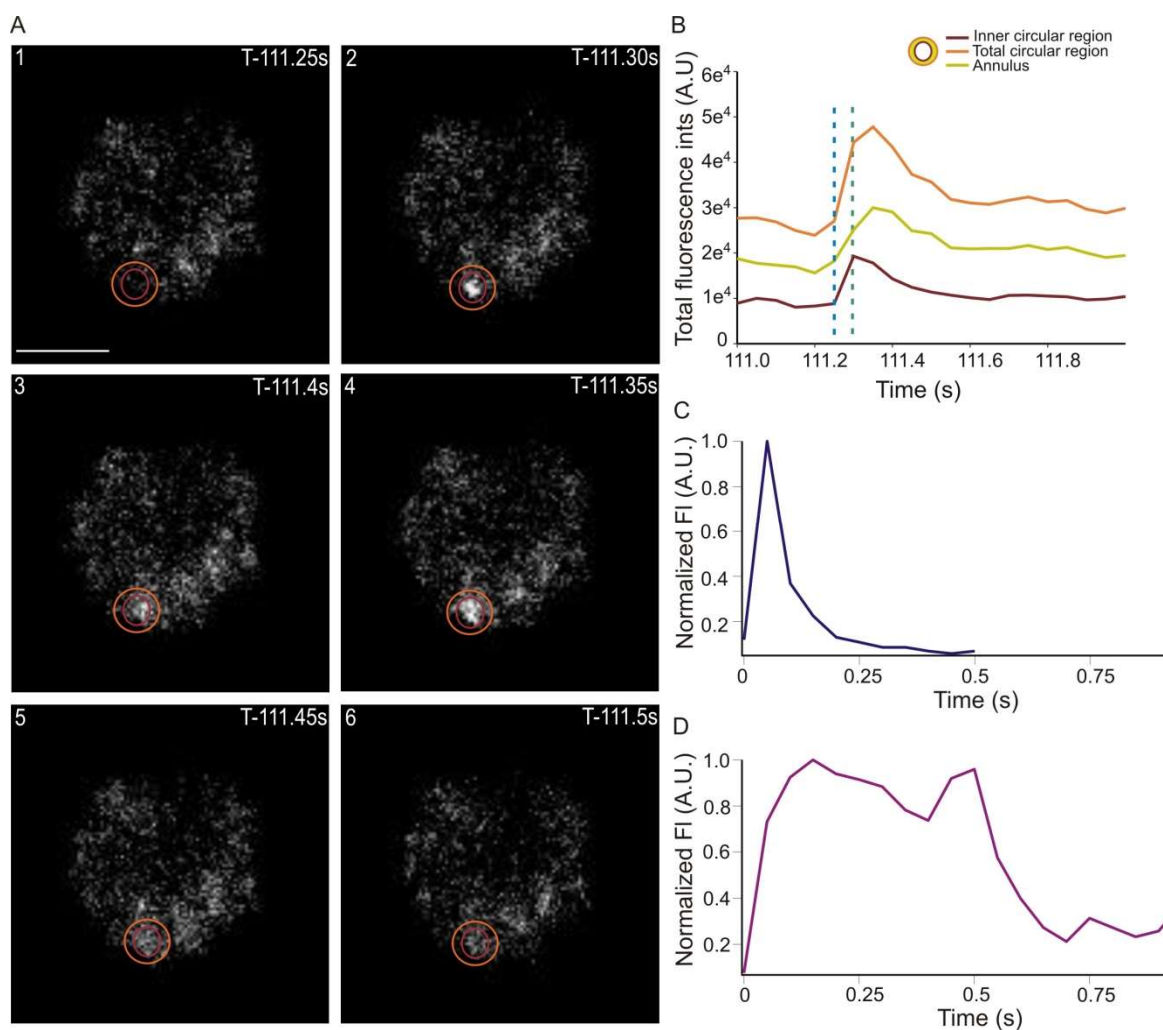


Fig. 19. Exemplary images and traces depicting a NPY release event at the evanescent field, alongside deciphering variability in event time course: (A) Exemplary images of the footprint of a chromaffin cell depicting a stimulation-evoked NPY release event. The image frames were acquired at 50 ms time interval. (Bar $\sim 5 \mu\text{m}$). (B) Two representative traces each depicting the integrated fluorescence intensity of the same fluorescent puncta defined by two circles having different diameters: $0.65 \mu\text{m}$ (maroon) and $1.3 \mu\text{m}$ (orange). The green trace illustrates the fluorescence of the annulus, derived by subtracting the fluorescence of the inner circle from the outer circle. (C & D) two exemplary traces of the normalized time profile of NPY release events, exhibiting 'spike' (purple trace) and 'plateau' (magenta) –like events, respectively.

Fig. 19 A illustrates the temporal profile of such a NPY release event captured at the cell footprint by acquiring images at 20 Hz in TIRF microscopy. Seeking further for signs of diffusional broadening, we also analyzed the integrated fluorescence of two concentric circles around fusion site. Integrated fluorescence of the annulus was attained by subtracting values of the inner region (width 5 pixels) from the outer region (width 10 pixels) (Fig. 19 B). As shown in Fig. 19 B cargo diffusion from the inner circle was initiated at 111.3 seconds as its fluorescence values started dropping down. At that very moment, the fluorescence values were still increasing in annulus and outer circle. Indeed a right hand shift in the temporal fluorescence profile of the annulus compared with the inner region was observed. This behavior illustrates cargo diffusion from the center of the fusion site (inner circle) into the event-surrounding region (annulus) (Fig. 19 B), providing strong evidence for diffusional dispersion of these cargo molecules.

Additionally, faster TIRF experiments also preserved the high variability of event time course similar to the LSM recordings that included the co-existence of both 'spike' (Fig. 19 C) and 'plateau' (Fig. 19 D), clearly showing that the observed heterogeneity in the time course is not a product of detection method. Moreover, similar cloud-like dispersion of cargo was observed for some 'plateau' like events (data not shown).

Taken together, based on kinetic parameters, such as signal upstroke and decay (that are illustrated as fusion pore opening and cargo release), our findings regarding the NPY-pHluorin time-course are consistent with previously reported findings of NPY release from large dense core vesicles of neuroendocrine cells (Steyer et al., 1997; Taraska et al., 2003; Zhu et al., 2007).

3.1.7 NPY-like molecule with high diffusion coefficient demonstrates 'point-source' dispersion

The process by which matter is transported from one part of a system to another part is known as diffusion. It can also be experimentally demonstrated by pouring water in a tall cylindrical vessel, which is half-filled with iodine solution. With the course of time, the distinctive initial boundary between colored iodine solution and transparent water gradually becomes less pronounced. After which this boundary completely disappears and results a uniform but less intense iodine solution throughout the cylinder. This uniform dispersion of iodine is generated as a result of random molecular motion. The motion of a single molecule can be described in terms of the familiar 'random walk' picture and the travelled distance can be calculated by the mean-square distance travelled at a given time interval. [Mathematics of Diffusion, J Crank, 2nd edition, oxford press, 1975]. General solutions of the diffusion equation can be obtained for a variety of initial status and boundary conditions provided that the diffusion coefficient (D) is constant. Crank's principle of diffusion of mass transport in one-dimensional plane from a point source can be recreated from the following equations. [Mathematics of Diffusion, J Crank, 2nd edition, oxford press, 1975]

From a plane source,

$$C = \frac{A}{\sqrt{t}} \exp\left(-\frac{x^2}{4Dt}\right) \dots\dots (i)$$

Where A is an arbitrary constant, is a solution of

$$\frac{\partial C}{\partial t} = D \frac{\partial^2 C}{\partial x^2} \dots\dots (ii)$$

This equation describes for diffusion in one dimension where D is constant and C denotes concentration, x and t represent distance and time, respectively. The expression is symmetrical with respect to $x = 0$, tends to zero as x approaches infinity positively or negatively for $t > 0$, and for $t = 0$ it vanishes everywhere except at $x = 0$, where it becomes infinite. The total amount of substance M diffusing in a cylinder of infinite length and unit cross-section is given by

$$M = \int_{-\infty}^{\infty} C dx \dots\dots (iii)$$

And if the concentration distribution is that of expression (i) we see, on writing

$$x^2 / 4Dt = \xi^2 \quad dx = 2(Dt)^{\frac{1}{2}} d\xi \quad \dots\dots (iv)$$

$$M = 2AD^{\frac{1}{2}} \int_{-\infty}^{\infty} \exp(-\xi^2) d\xi = 2A(\pi D)^{\frac{1}{2}} \dots\dots (v)$$

[{i-v} *Mathematics of Diffusion*, J Crank, 2nd edition, oxford press, 1975]

In one-dimensional, instantaneous point source, and when diffusion will occur at infinite medium i.e. without definitive boundary,

M (mass) is released at **t** (time) =0 and **X** (distance) = 0.

Initial condition, **C(x) = Mδ(x)**

$$C(x,t) = \frac{M}{\sqrt{4\pi Dt}} \exp\left(-\frac{x^2}{4Dt}\right) = [M/L] \dots\dots\dots (3)$$

Assuming instantaneous release we simulated lateral dispersion of NPY-pHluorin at different time intervals. For this, we calculated the distance travelled by a molecule with 8 μm²/sec diffusion coefficient within a field, which is comparable to the ROI lengths used in our line-scan analysis. As shown in Figure 20 A and B, we could show that NPY-pHluorin's radial dispersion occurs over a distance of 2 μm (covering 1 μm on both side from the center) and on a distance of 0.64 μm (0.32 μm radius) that denotes the circular ROI of the kinetic measurement. Traces represented by navy blue to indigo cover the time interval from 0.1 sec to 0.6 sec (sampling rate 0.1 sec / frame). The traces depicted a 3-fold loss of fluorescence within the first 0.1 sec, illustrating that the majority of the molecules are moving out of the selected ROI distance, i.e. 2 μm within a time interval of 0.1 s. The detected signal further deteriorated at circular ROI (0.32 μm radius) at the same time interval of 0.1 s, as materials traverse out of the field of measurement in a quick fashion. This set of data agrees well with our

experimental results, shown in figures 15 B and 15 C, given us no evidence for a detectable accumulation of NPY molecules close to fusion site.

To further confirm the limitation in the temporal resolution in our experiments, we simulated dispersion with a 10-fold higher temporal resolution, i.e. 100 Hz. This simulation resulted a detectable lateral dispersion from the point source that accompanied the drop in concentration (Fig 20 C - dotted line). However, this 100 Hz temporal resolution was unattainable by our experimental setup.

Moreover, our simulation study also depicted that only with 100 Hz acquisition rate we could monitor an exponential relation between standard deviation (SD) or width and the amplitude at different time intervals, the hallmark for detectable diffusion from a point source (Fig 20 E). Nonetheless, even with the superior temporal resolution of 100 Hz, mobility of the material could not be detected in real time within a distance, resembling the circular ROI (Fig 20 D - dotted line).

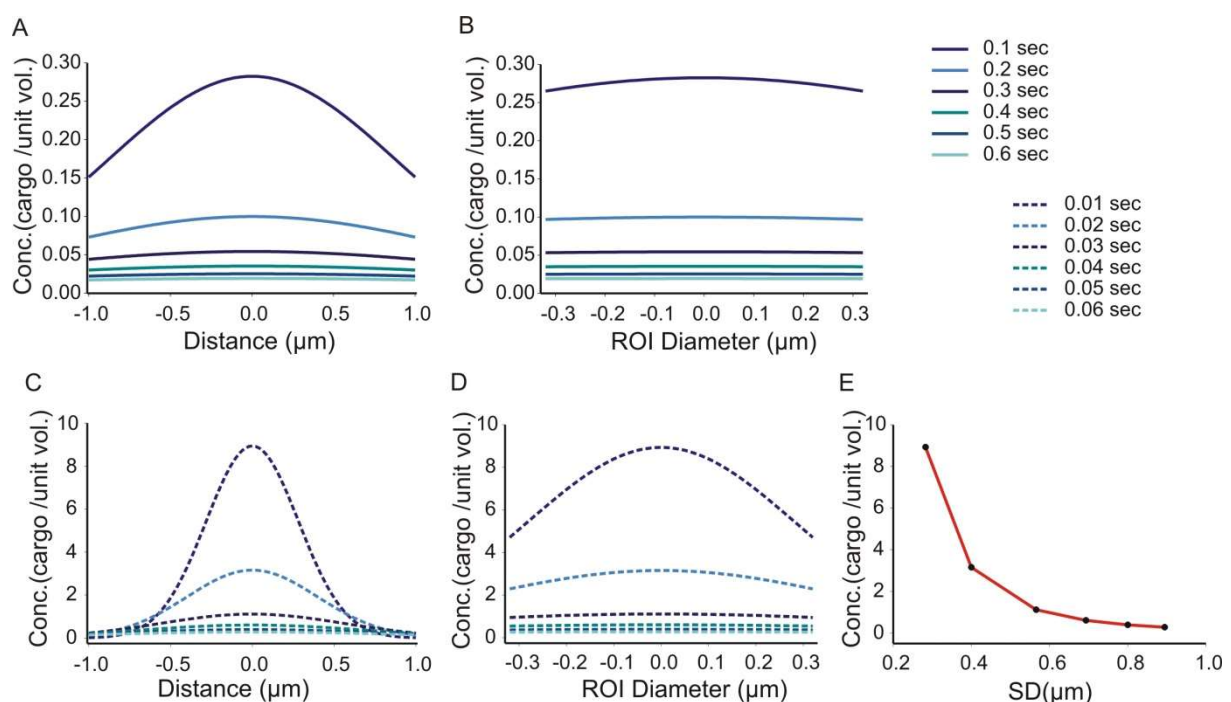


Fig. 20. Calculation of radial concentration profiles of cargo molecules around the release site at different time points: (A) Traces (lines) depicting diffusion and distribution of NPY likewise material within a distance of 2 μm from the center, at a time interval 0.1-0.6 sec, (blue 0.1 sec-indigo 0.6 sec). (B) Traces represent diffusion of material within a distance of 0.64 μm , resembling circular ROI (0.32 μm radius) in our kinetic measurements. (C) Traces in the dotted line illustrate mobility of the same materials at 100 Hz temporal rate, i.e. (dotted blue to 0.01 sec- dotted indigo

0.06 sec). (D) Spatial profiles for circular ROI distance were depicted that were extracted from C within a distance of 0.64 μm . (E) SD or width of each Gaussian distribution [from plot D] at every time profile depicts an exponential relation.

Therefore, the limiting temporal resolution of our microscopic detection methods prevented the detection of rapidly diffusing cargo molecules, such as NPY-pHluorin. To circumvent the problem of rapidly diffusing molecules and to acquire a read-out for dispersion with this sampling rate, we comparatively analyzed also a slowly diffusible molecule in later sections, i.e. the membrane bound SynaptopHluorin (Syb-pHluorin) in stimulation-evoked release [See section 3.2.1].

3.1.8 NPY-pHluorin release time course is unaffected by the mode of stimulation

Previous reports suggested that the mode of stimulation regulates the expulsion of the cargo molecule (Fulop et al., 2006; Fulop et al., 2007). Additionally, earlier reports have shown that exocytosis of chromaffin granules can be elicited by depolarizing cells either with high potassium solution [90 mM K^+] (Borisovska et al., 2005) or by the application of 10 μM ionomycin (Schütz et al., 2005). Both protocols induce an elevation of $[\text{Ca}^{2+}]_i$ via calcium influx thus triggering secretion. Membrane depolarization by the extra-cellular application of 90 mM K^+ , leads to opening of voltage-gated calcium channels (CaV). As CaV is inactivated during prolonged depolarization, Ca^{2+} -influx will be transient and persist for a few seconds.

Alternatively, ionomycin, a calcium selective ionophore, incorporates into membranes and allows for a direct entry of Ca^{2+} -ion that is unregulated and predominantly limited by the stability of the ionophore. Thus, ionomycin should generate a Ca^{2+} increase that is prolonged and consistent to stimulate release, unless the activity of ionomycin reaches a saturation point. Since release of peptidergic cargo molecules requires a complete dilation of the fusion pore, hence we thought that the alteration in the stimulation paradigm might also alter the release properties from the pore.

In contrary to our notion, the event frequency for high 90 mM K^+ was found to be 1.68 ± 0.444 events/ cell [N (cells) = 29; n (events) = 49], which was comparable to the 10 μM ionomycin-evoked event frequency of 1.26 ± 0.22 events /cell.

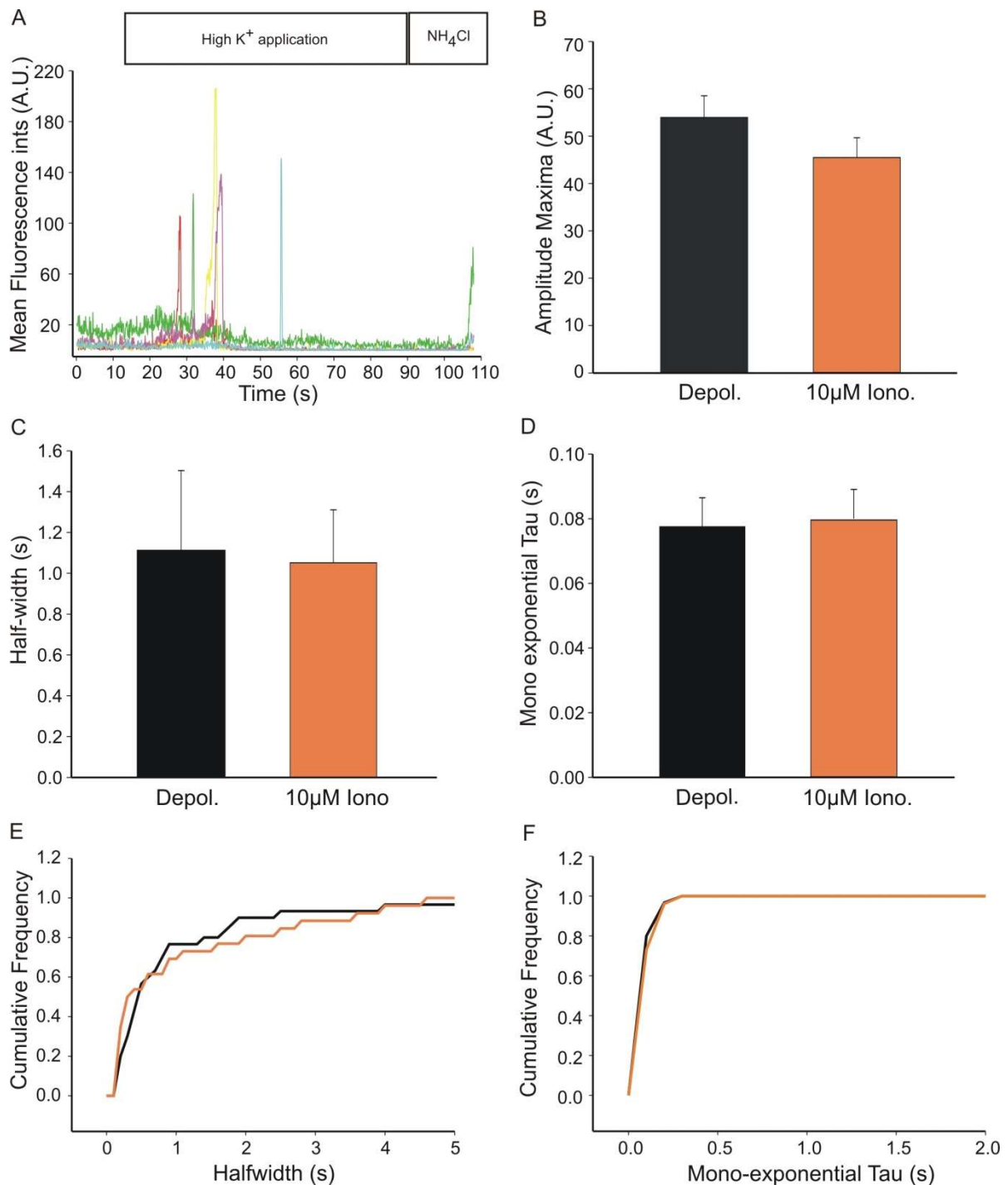


Fig. 21. Kinetic properties of NPY-pHluorin release events are unchanged with depolarization-induced stimulation: (A) Exemplary traces depict depolarization-induced NPY-pHluorin events. (B) Mean amplitude maxima of the signal between high K^+ -solution and 10 μ M lonomycin (C) Mean half-width between high K^+ -solution and 10 μ M lonomycin (D) Mean tau (τ) in cells stimulated by application of high K^+ -solution ($n=17$) or by application of 10 μ M lonomycin ($n=12$) (E) Cumulative distribution of event half-width observed under both stimulation conditions.

Events were distributed using a bin width of 0.1s. (F) Event tau (τ) of both the stimulation conditions. Events were distributed using a bin width of 0.1 s. Error bars represent standard error of the mean (SEM).

Furthermore, our results demonstrate that the shape and kinetic properties of single events induced by both the stimulation paradigms are indistinguishable (Fig. 21 A) [See also Fig. 10B -- ionomycin evoked response]. The cell-weighted average amplitude was 53.93 ± 4.59 A.U. for high K^+ -response and 45.46 ± 4.19 A.U for ionomycin evoked response (Fig. 21 B). Furthermore, average event half-width and tau (τ) were found to be 1.05 ± 0.025 and 0.079 ± 0.009 seconds, respectively for ionomycin-induced response (Fig. 21 C, D). For the high K^+ -response, the average half-width and tau (τ) were 1.11 ± 0.38 and 0.077 ± 0.008 seconds, respectively (Fig. 21 C, D).

Thus, we did neither observe alterations in the distribution of events half-width nor in tau (τ) (Fig. 21 E, F) giving us no evidence for any shift in the mode of exocytosis with NPY-pHluorin release.

3.1.9 Main calcium sensors play a fundamental role in the facilitation of the NPY-pHluorin release

The functional redundancy between the two Synaptotagmin isoforms namely Synaptotagmin 1 and 7 (SytI and SytVII) as Ca^{2+} sensors for exocytosis in adrenal chromaffin cells has been illustrated previously (Schonn et al., 2008). Furthermore, functional overlap of the Synaptotagmin isoforms 1 and 9 (SytI and SytIX) in LDCV secretion has also reported in PC12 cells (Zhu et al., 2007). To elucidate the role of calcium sensors for peptidergic release, we performed NPY-pHluorin release experiments with chromaffin cells that are deficient in the calcium sensors SytI and SytVII. Genetic ablation of SytI and SytVII strongly reduced secretion 0.13 ± 0.07 release events/cell. In contrast to corresponding littermate control, cells from SytVII single knock out mice, exhibited no alterations in the frequency of release events [1.17 ± 0.46 events/cell] (Fig. 22 A), when compared with chromaffin cells from wildtype (C57/BL6) control mice [1.26 ± 0.22 events /cell].

To rule out the possibility of reduced vesicle number at cellular footprint that might also be responsible for the reduction in the event frequency, we counted NPY positive granules after neutralization of intraluminal pH with NH_4Cl . Interestingly, we found that the number of residual NPY-granules was unaltered in the SytI/SytVII double knock out cells, when compared to the littermate controls (SytVII ko). The SytI/SytVII deficient cells on an average exhibited 32.77 ± 3.57 NPY positive punctae at the cellular footprint similar to the littermate control cells which on an average exhibited 30.13 ± 3.07 NPY punctae (Fig. 22 B).

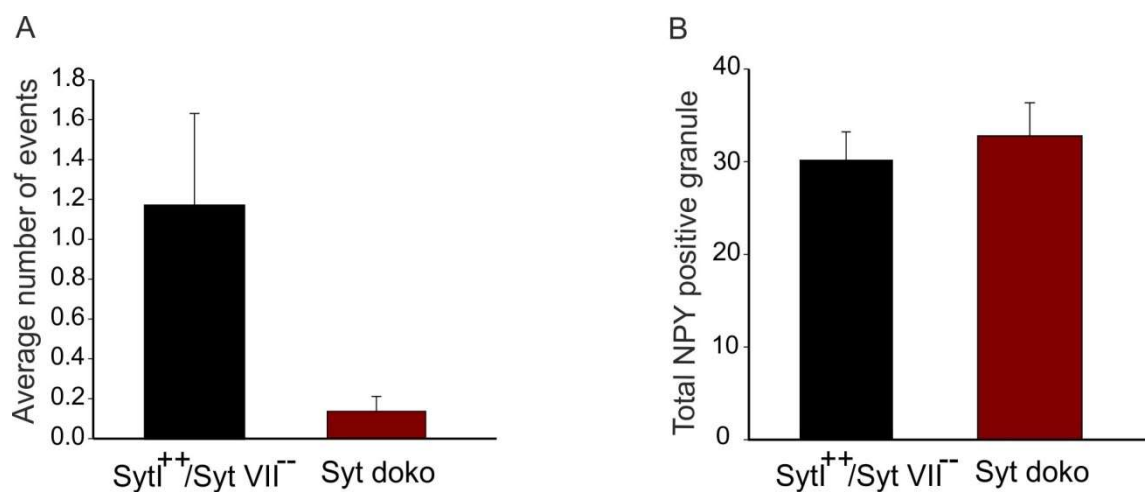


Fig. 22. Loss of both SytI and SytVII leads to a reduction in NPY-pHluorin release from LDCVs: (A) quantitative analysis of event frequency depicts a drastic reduction in the SytI/SytVII double knockouts when compared to littermate controls (SytVII ko). (B) The total number of NPY-positive punctas remains unaltered upon alkalization of intraluminal structure. (Littermate SytVII^{-/-} control cells n= 23, SytI^{+/+}/SytVII^{-/-} cells n= 22). Error bars represent Standard Error of Mean (SEM).

Therefore, we can conclude that Synaptotagmins are the main calcium sensors for NPY release from chromaffin granules in good agreement with previous measurement of membrane capacitance (Schonn et al., 2008) or amperometric analysis of catecholamine secretion (Dhara et al., 2014).

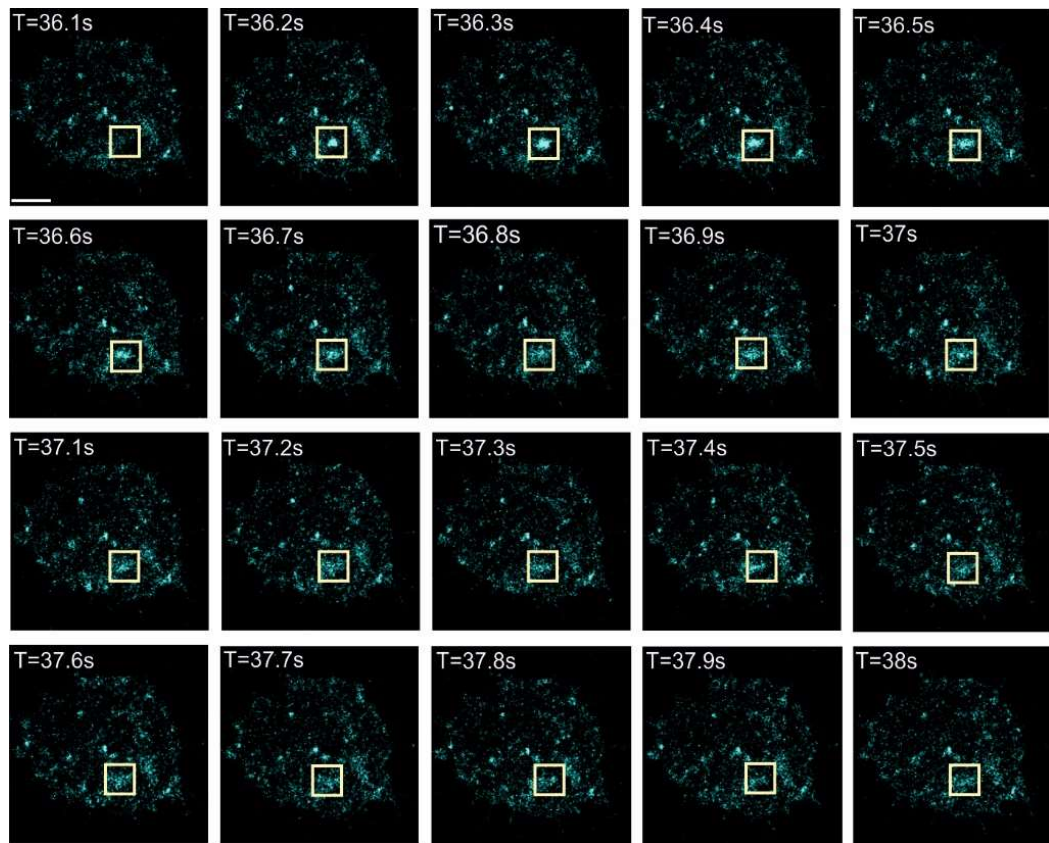
Collectively, our results on NPY-pHluorin release have shown that this cargo molecule is a faithful reporter to monitor stimulus-evoked vesicular exocytosis. The rapid fluorescence uprise of NPY-pHluorin signal upon fusion pore opening occurred due to

the dequenching of pHluorin molecule, as expected for a pH-sensitive variant of GFP. Furthermore, fluorescence decay most likely reports the discharge of the cargo molecule from the core of fusion pore. The stationary plateau phase of NPY-pHluorin time course that occurred exactly before the decay was due to the restricting fusion pore diameters, which hindered the release of the cargo molecule from the vesicle. On the other hand, transiently occurring spike-like events represented a different type of vesicular exocytosis, where fusion pore dilated rapidly after its initial opening leading to expulsion of the cargo molecules without any temporal delay. Our experimental results further provided evidences that the release of NPY-pHluorin molecules from the LDCVs depends not only on v-SNARE proteins but also dependent on the calcium sensing proteins, such as SynaptotagminI and SynaptotagminVII, consistent with previous reports demonstrating the functional importance of these Synaptotagmin isoforms in granular exocytosis. (Schonn et al., 2008; Dhara et al., 2014). In addition, our results showed that reacidification of re-internalized vesicles has no role in the time course of NPY-pHluorin. Lastly, cargo efflux from the vesicle core was found to be rate limiting for the time course of the detected NPY-pHluorin release events. Nonetheless, acquisition speed restricts the visualization rapidly diffusing cargo molecule in real time. To resolve with the detection problem, in the next section we tried to extend our analyses to a membrane bound fluorescently tagged molecule that is VAMP_{II}-pHluorin [SynaptopHluorin (Syb-pHluorin)], where the pHluorin molecule was tagged to the luminal part of the membrane anchored synaptobrevinII [See section 3.2.1].

3.2.1 Stimulation evoked rise in $[Ca^{2+}]_i$ leads to the dissipation of vesicle membrane-bound VAMP_{II}-pHluorin signal

Keeping the temporal limitation in the detection method in mind, we intended to use a slowly diffusible molecule to study the fate of secretory vesicles at post fusion state. The facilitatory role of VAMP_{II} or SybII in the initiation of vesicular exocytosis is well established. Syb-pHluorin, a pHluorin variant of SybII fused to its C-terminus, where the pHluorin molecule resides in the vesicular lumen (Miesenböck et al., 1998; Sankaranarayanan et al., 2000; Sankaranarayanan et al., 2001; Burrone et al., 2006). Similar to NPY-pHluorin events, we acutely overexpressed Syb-pHluorin on DIV-2 or 3 chromaffin cells and imaged them after 5 hrs of infection.

A



B

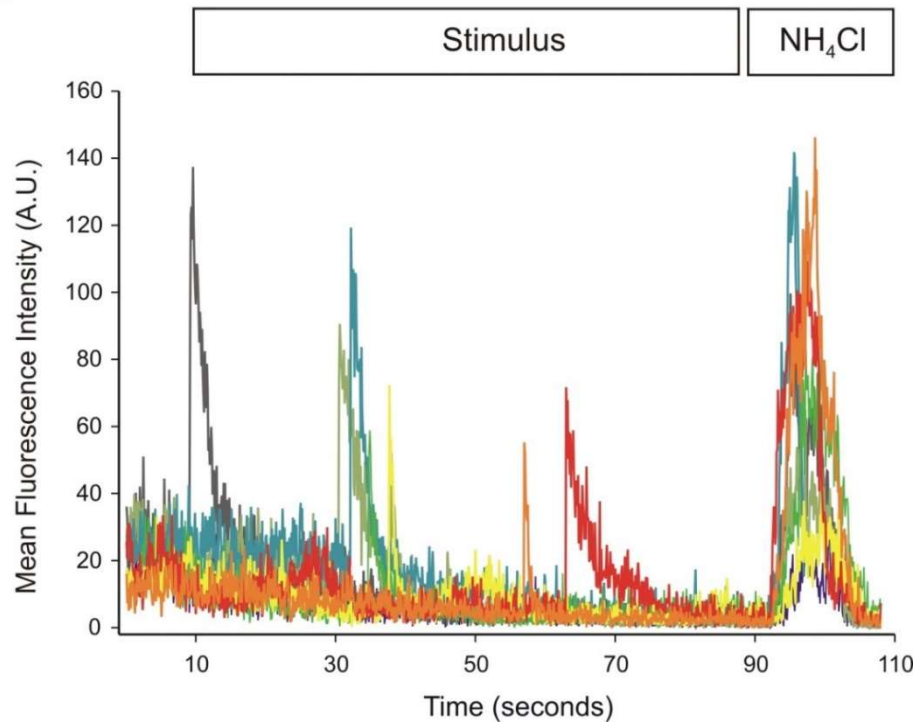


Fig. 23. Exemplary images and traces depicting SynaptopHluorin (Syb-pHluorin) signal dissipation upon stimulation: (A) Live time-lapse images of Syb-pHluorin at the footprint of a mouse chromaffin cell depicting the onset of a fluorescence signal that gradually dissipates over time. (B) Exemplary traces were obtained by tracking individual puncta through the entire stack with defined ROIs that were 8 pixels in diameter corresponding to 640 nm. (Bar ~ 5 μ m).

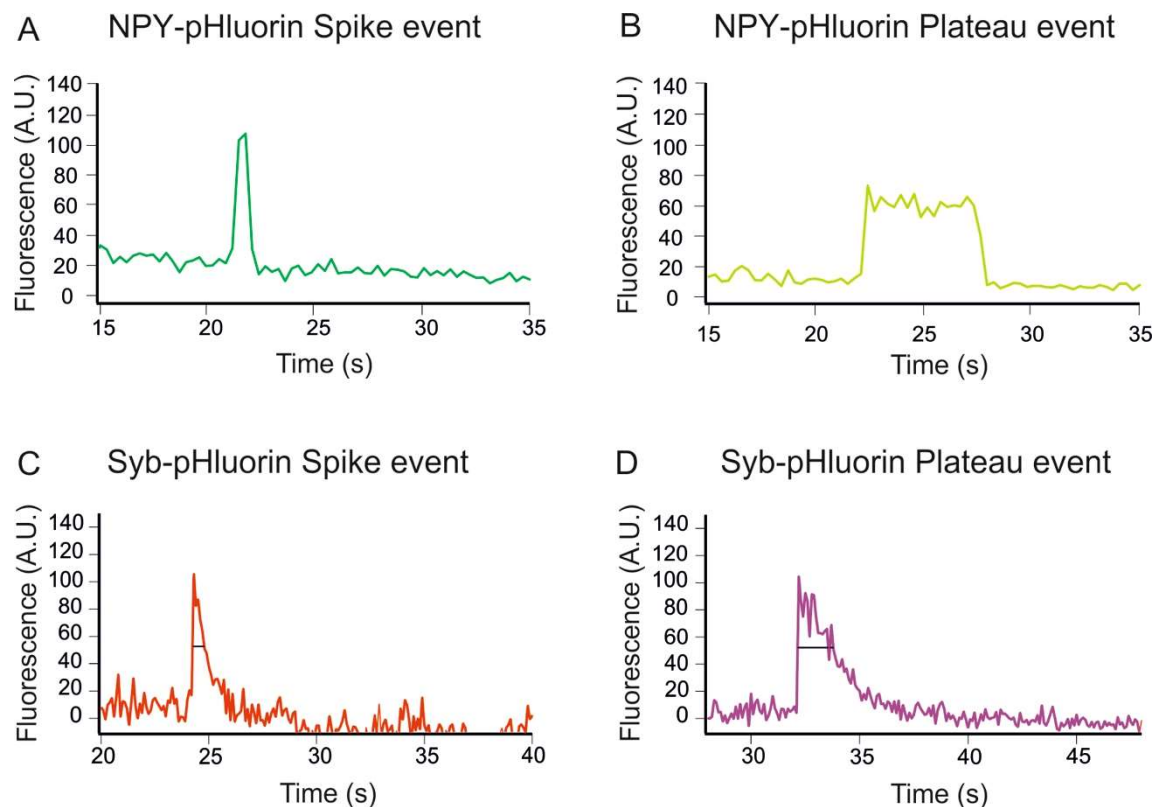


Fig. 24. Representative traces of classical stimulation-evoked NPY-pHluorin and SynaptopHluorin (Syb-pHluorin) signal time course: (A) An exemplary trace showing classical NPY-pHluorin spike-like or instantaneous release event. (B) A classical NPY-pHluorin trace illustrating a stimulation-induced plateau-like or delayed release event on a comparable time scale to NPY-pHluorin event, (C) an exemplary trace showing a short lasting or spike-like time course Syb-pHluorin event. (D) An exemplary Syb-pHluorin plateau or long lasting events, showing similar up-rise in the signal time course but a prolonged decay.

To elicit and monitor vesicular exocytosis, cells were stimulated with 10 μ M ionomycin and simultaneously imaged at the footprint at 10 Hz (100 ms/ frame) sampling rate on the stage of LSM microscope. As shown in Fig. 23 A, a classical stimulation-induced Syb-pHluorin event is illustrated by the sudden appearance of a fluorescence spot at

the cell footprint, which gradually disappears over time. The time course of Syb-pHluorin events was obtained by measuring the mean fluorescence with circular ROIs having a diameter of 8 pixels [0.64 μm] through the time series of images. The behavior of Syb-pHluorin events, with respect to the rapid signal uprise and gradual decay could be well demonstrated in the temporal profiles (Fig. 23 B).

Again the rapid uprise of the signal occurred due to the dequenching of pHluorin molecules that are bound to the luminal part of the SybII. Therefore, similar to NPY-pHluorin the rise time of the signal could not be well resolved with our detection method. Furthermore, close observation of the individual traces revealed a high degree of heterogeneity among Syb-pHluorin events. The heterogeneity in the event duration appears to be similarly prominent as often NPY-pHluorin events, as illustrated in the highly scattered event types shown in Fig. 25 (A, B). In Fig. 24 we depicted two exemplary NPY-pHluorin (A, B) and 2 classical Syb-pHluorin events (C, D), to show the difference in their time course. The direct comparison of the temporal profiles of both event types, confirmed that the decay of Syb-pHluorin was much slower than NPY-pHluorin. This was not surprising because Syb-pHluorin is a membrane bound molecule, unlike NPY-pHluorin. The slower decay may correspond either to the radial dispersion of SybII within membrane or is due to retrieval (endocytosis) of the vesicles following vesicular fusion or/and subsequent reacidification of the secretory vesicles. The kinetic differences between Syb-pHluorin events and NPY-pHluorin events are consistent with the notion that NPY cargo release is expected to be faster than lateral dispersion of membrane bound molecules in the plasma membrane. Yet, despite kinetic differences in the decay phase of Syb-pHluorin events report similar fusion scenarios as observed with NPY release ranging from short lasting spike-like to long-lasting plateau-like events. It shows that independent to the nature of the reporting molecule distinct types or modes of fusion can be detected. For better understanding of these kinetically divergent scenarios, further quantitative analyses of Syb-pHluorin' kinetic profiles were performed.

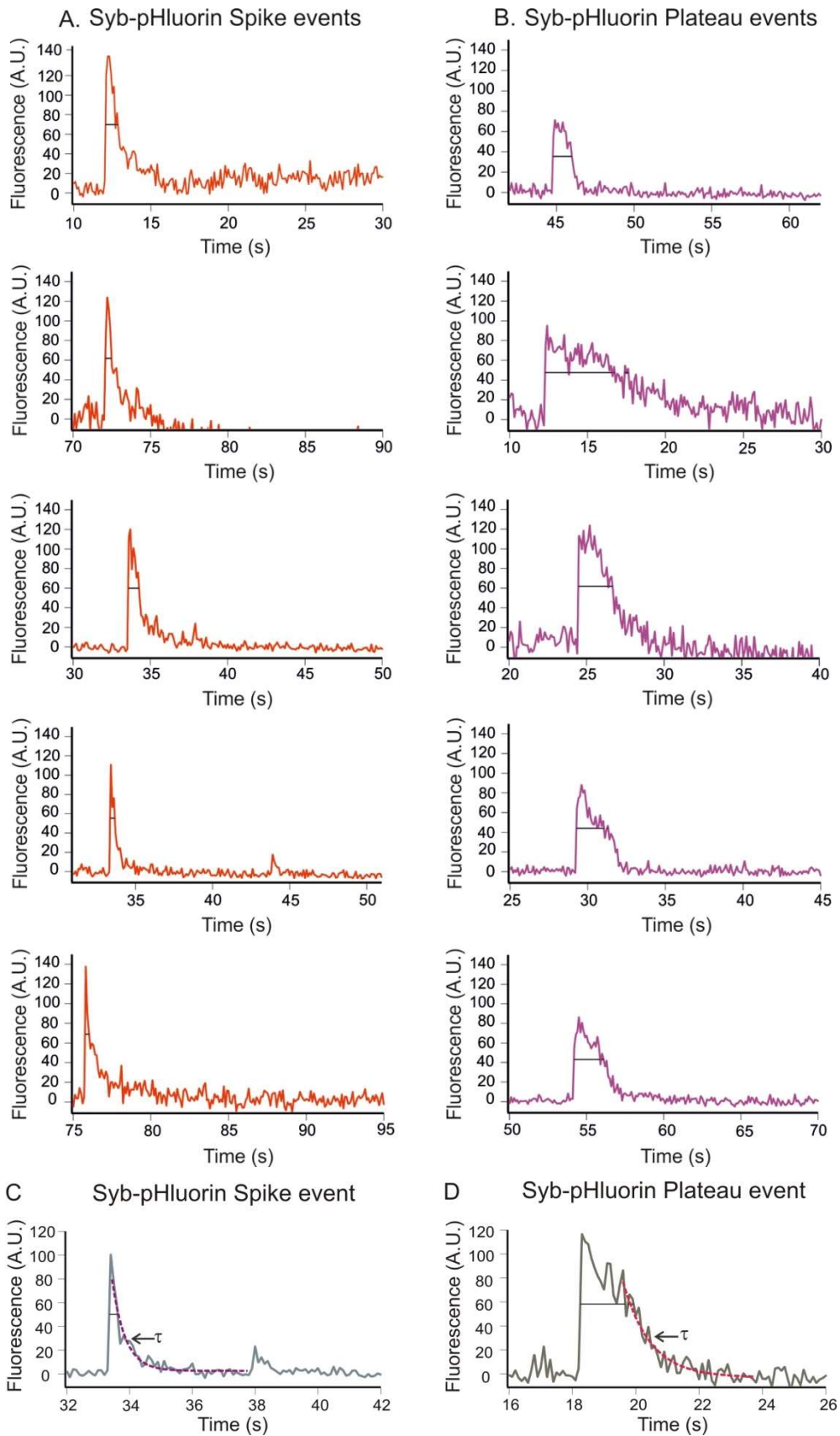


Fig. 25. Graphical presentation of heterogeneous SynaptopHluorin events: (A) Exemplary traces of short-lasting Syb-pHluorin or 'spike'-like events, exhibiting moderate variability in the kinetic profiles plotted on a similar time-scale. [Top to bottom] (B) Representative traces of long lasting or 'plateau'-like events, illustrating even higher variability in the kinetic profile of this event type, in comparison to 'spike' events [Top to bottom]. (C) and (D) demonstrate exemplary traces obtained from a 'spike' and a 'plateau' events. Furthermore, fitted traces were shown in dashed line to provide an illustration of the fitting function.

3.2.2 Kinetics of Syb-pHluorin time course is highly heterogeneous

For quantitative analysis, only events with a mean fluorescence ≥ 30 A.U. (5 times SD of baseline noise) were analyzed. To avoid saturation problems, extremely high amplitude events were barred from the cell weighted average analysis. Event amplitude exhibited a skewed unimodal distribution with a median of 66.60 A.U. (Fig 26 A). The median half-width of the events was 0.90 s (cells N=36, events n=134), and is thereby about two folded longer than the half-width of NPY release measured before. Yet, the frequency distribution of event tau (τ) revealed scattered and right-handed skewed distributions with median of 0.87 s (Cells N=36, events n=134), which is nearly 10-fold larger than the decay time course observed with NPY fusion events. Given these kinetic differences it is important to note that the half-width

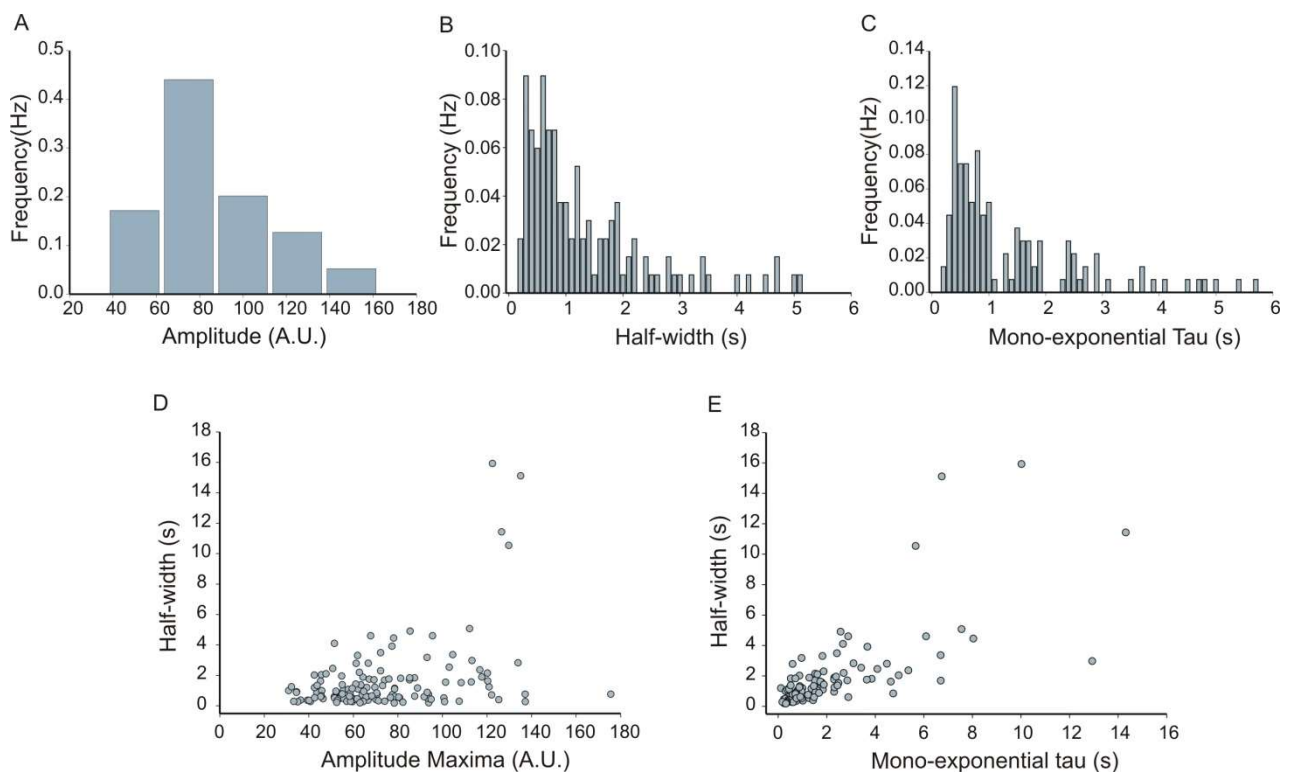


Fig. 26. High-level heterogeneity was observed in the stimulation-evoked kinetics of Syb-pHluorin signal time-course: (A) Frequency distribution of event amplitude with a bin of 25 A.U. depicts unimodal positive skewed distribution. (B) Event half-width exhibited a highly variable positive skewed distribution, after binning events with 100 ms. (C) For event tau (τ) a highly variable positively skewed distribution with multiple over-hang is observed when events were binned at 100 ms. (D) Scatter plot between amplitude and half-width did not reveal any positive correlation, thus indicating that cargo content has no effect in the kinetics. (E) Scatter plot between event half-width and tau (τ) showed a correlation, depicting that event decay is influenced by event duration. [No. of cells (N)=36, No. of event (n)=134].

of pHluorin dependent events comprises both the latency until fusion pore widening as well as the time course of cargo dispersion. In contrast, the time constant of signal decay should depend on cargo dispersion. Additionally, signal decay from Syb-pHluorin might also correspond to the vesicular retrieval/endocytosis from the fusion site and subsequent reacidification of the vesicular lumen, as will be tested below. Furthermore, no direct correlation is observed between event amplitude and half-width, indicating again that the amount of pHluorin molecules does not play a regulatory role in kinetic profiling (Fig. 26 D). Nevertheless, due to the interdependence of event half-width and tau (τ) we could see a correlation between these parameters.

Collectively, our results using Syb-pHluorin as an alternative reporter for exocytosis confirmed the view that variability in the kinetic profile of fusion events resulted from a variable delay or latency for fusion pore widening. Moreover, it became clear that kinetic differences between both event types in the decay time course are best explained by quick release of freely diffusible cargo NPY-pHluorin molecules versus the lateral dispersion of membrane bound Syb-pHluorin molecules. In order to get a better understanding of the mechanisms influencing the variable kinetics, in the next section we have studied the spatial distribution of SybII within the plasma membrane.

3.2.3 Spatial distribution of vesicular synaptobrevin in the fusion site accompanying vesicular exocytosis

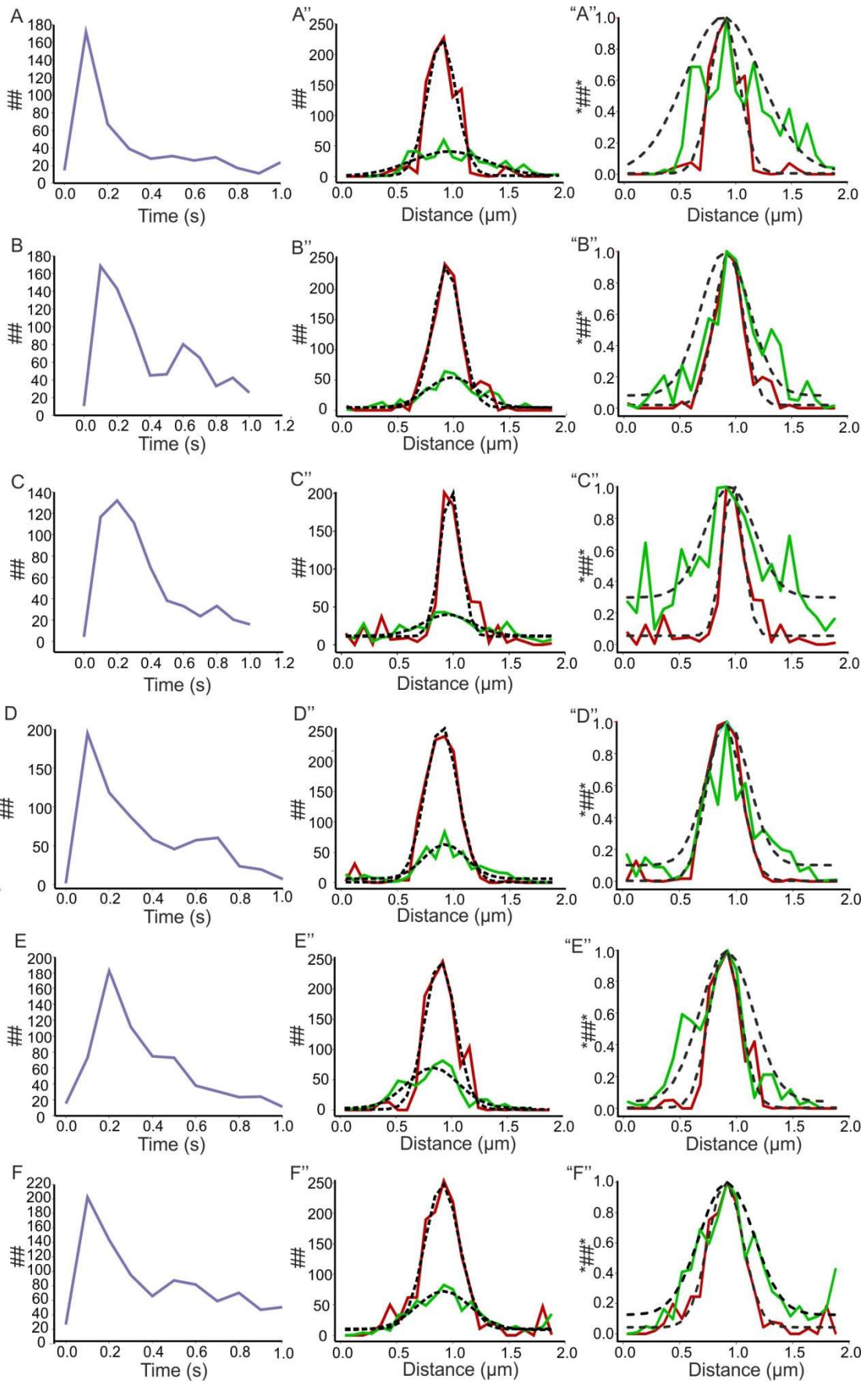
The experimental line scan measurement of Syb-pHluorin was performed within an area of 2 μm X 0.48 μm . Based on the kinetic analysis, events were pre-selected

for spatial analysis. Extremely high amplitude events were barred from spatial analysis because the peak fluorescence from these events were reaching saturation point. Hence for the spatial analysis, the mean grey scale values for individual events were obtained for 5 pixels from the center of the ROI line, i.e. core of the fusion site and plotted to recreate the temporal profiles of the center region of the line (Fig. 27 A-F; Fig. 28 A-E), which were comparable to the kinetic profiles of those events (data not shown).

Moreover, we approximately estimated the time frame at which the signal drops down to 30% of the peak. Spatial profiles for the peak and 30% residual amplitude (Avg. of 5 frames) were plotted over 2 μm distance centered at 1 μm (Fig. 27 A"-F"; Fig. 28 A"-E"). The spatial profile of the peak and the 30% residual amplitude were fitted with Gaussian function described in equation no. 2. In order to appreciate the diffusional broadening of the fluorophore in form of an increase in Gaussian SD in the measurement area, we normalized all traces to the highest value (Fig. 27 "A"-“F”; Fig. 28 "A"-“E”). From these spatial profiles, we observed that the Gaussian SD at peak amplitude was $\geq 0.1 \mu\text{m}$ that broadened over amplitude drop in the course of time (Fig. 27 A"-F"), which is further substantiated from normalized plots and an increase in ΔSD [SD at residual amplitude – SD at peak] (Fig. 27 "A"-“F”). We also observed that this increase in ΔSD primarily restricted to short lasting or spike-like events (Fig. 27 A-F). An attractive explanation for this observation could be that SybII only slowly distributes within the plasma membrane and might be further hindered during its passage through the neck of the fusion pore.

An attractive explanation for this observation could be that SybII only slowly distributes within the plasma membrane and might be further hindered during its passage through the neck of the fusion pore.

Altogether, based on the spatial and the temporal data set we can conclude that these Syb-pHluorin events should represent vesicles do completely merge with the plasma membrane and thereby allow for dispersion of the membrane bound EGFP-tagged SybII molecules.



[## Mean Fluorescence]

[*##* Normalized Fluorescence]

Fig. 27. Exemplary temporal profile of the core of the fusion site and spatial profile of short-lasting Syb-pHluorin event: (A-H) Average of 5 centered pixels over time-stack exhibits development and decay of fluorescence in a temporal profile from an individual event. (A"-H") Red traces from individual events illustrate spatial profile of a single frame that shows peak amplitude from individual events, depicted in A-H. Furthermore, green traces on the same plots portray mean fluorescence of 6 time-points of the traces, where amplitude of centered region drops down to 30% of the peak amplitude. Fitted traces (black dashed line) with a Gaussian function resulted in a visible and numerical increase in SD/width of the traces over distance, following amplitude drop from peak to 30% residual fluorescence. Notably, events with quicker amplitude drop from peak, are more prone to show increase SD. {See Time scale}. ("A"-“H”) Average traces were normalized to highest value.

Hence for the spatial analysis, the mean grey scale values for individual events were obtained for 5 pixels from the center of the ROI line, i.e. core of the fusion site and plotted to recreate the temporal profiles of the center region of the line (Fig. 27 A-F; Fig. 28 A-E), which were comparable to the kinetic profiles of those events (data not shown).

Moreover, we approximately estimated the time frame at which the signal drops down to 30% of the peak. Spatial profiles for the peak and 30% residual amplitude (Avg. of 5 frames) were plotted over 2 μm distance centered at 1 μm (Fig. 27 A"-F"; Fig. 28 A"-E"). The spatial profile of the peak and the 30% residual amplitude were fitted with Gaussian function described in equation no. 2. In order to appreciate the diffusional broadening of the fluorophore in form of an increase in Gaussian SD in the measurement area, we normalized all traces to the highest value (Fig. 27 "A"-“F”; Fig. 28 "A"-“E”). From these spatial profiles, we observed that the Gaussian SD at peak amplitude was $\geq 0.1 \mu\text{m}$ that broadened over amplitude drop in the course of time (Fig. 27 A"-F"), which is further substantiated from normalized plots and an increase in ΔSD [SD at residual amplitude – SD at peak] (Fig. 27 "A"-“F”). We also observed that this increase in ΔSD primarily restricted to short lasting or spike-like events (Fig. 27 A-F). An attractive explanation for this observation could be that SybII only slowly distributes within the plasma membrane and might be further hindered during its passage through the neck of the fusion pore.

An attractive explanation for this observation could be that SybII only slowly distributes within the plasma membrane and might be further hindered during its passage through the neck of the fusion pore.

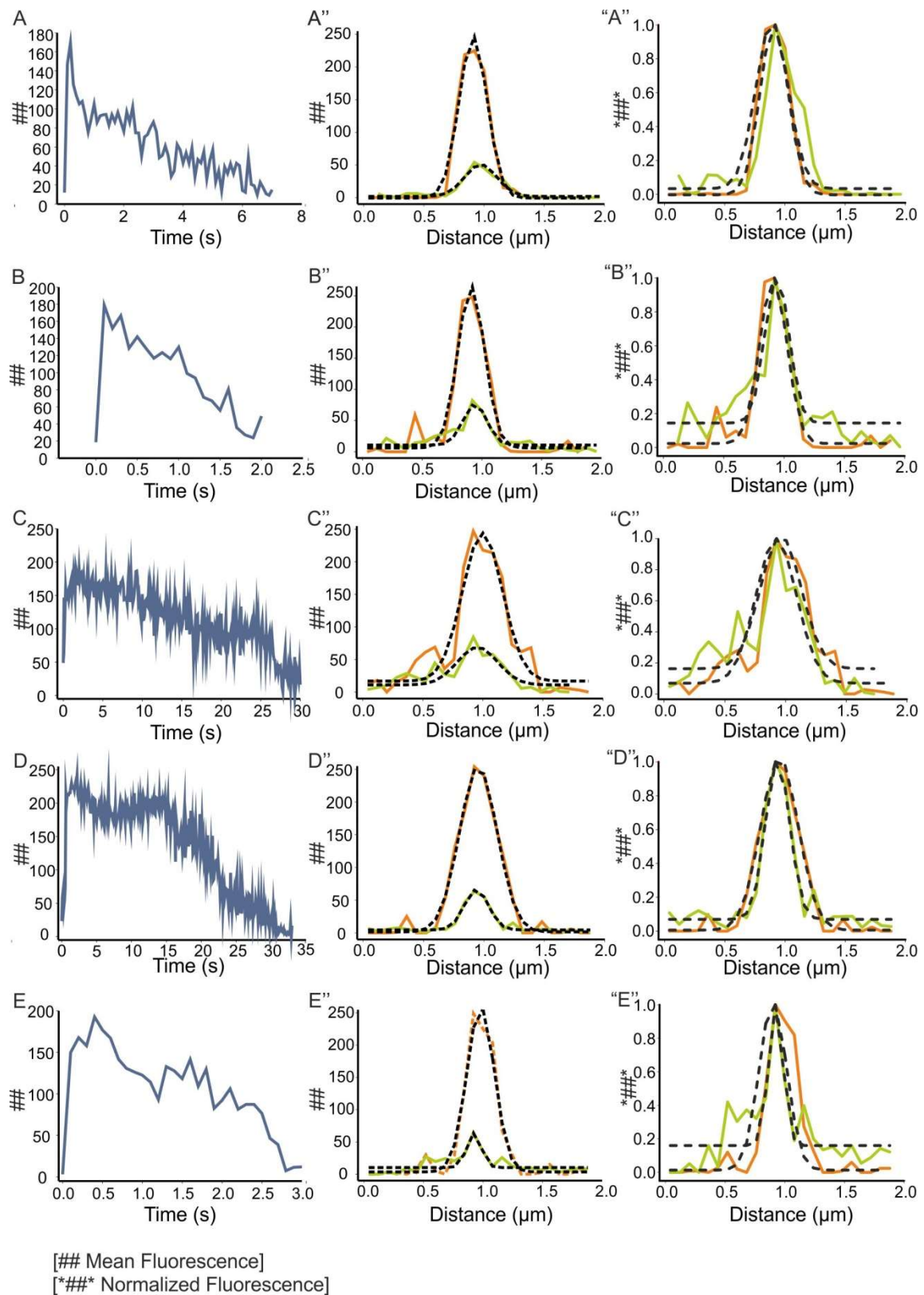


Fig. 28. Representative traces showing the temporal profile and spatial profile of Syb-pHluorin long-lasting events at fusion site and surrounding region: (A-E) Average

fluorescence of 5 centered pixels over the time-series exhibited development and decay of fluorescence over time. (A"-E") In the corresponding plot, orange traces from an individual event illustrate the spatial profile of peak amplitude from the same events depicted in A-E. Green traces on the same plots portray average of 6 time-points of the traces, where the amplitude of centered region drops down to 30% of the peak amplitude [fluorescence values in grey scale. Fitted traces (black dashed line) with a Gaussian function resulted in neither a visible nor numerical increase in SD/width of the traces over distance, following amplitude drop. ("A"-“E”) Average traces were normalized to highest value.

Altogether, based on the spatial and the temporal data set we can conclude that these Syb-pHluorin events should represent vesicles do completely merge with the plasma membrane and thereby allow for dispersion of the membrane bound EGFP-tagged SybII molecules.

In extension, line-scan analyses from long-lasting plateau-like Syb-pHluorin events revealed that these events mostly yielded a very sharp SD at peak amplitude, which was mostly $< 0.1 \mu\text{m}$ (Fig. 28 A-E; Fig. 28 A"-E"). This narrow SD did not broaden further when the amplitude drops. Henceforth, no significant \square SD could be determined for the subsequent frames (Fig. 28 "A"-“E”). Interestingly, after scrutinizing the kinetics of the same events, this population also exhibited a high degree of heterogeneity in the decay ranging from a monophasic time course (Fig. 28 A, B) to a clearly biphasic decay (Fig. 28 C, D, E).

Thus, it is possible that different physiological mechanisms contribute to the termination of the fluorescence signal. Indeed, the loss of the fluorescence signal might represent an undocking of vesicles from the plasma membrane after membrane fission or rapid reacidification leading to re-quinching of Syb-pHluorin in the retrieved vesicles.

3.2.4 Reacidification of the internalized vesicular lumen contributes in the kinetics of Syb-pHluorin signal time course

Beside diffusional dispersion of SybII molecule in the plasma membrane, endocytosis of SybII followed by removal of the vesicle and/or its reacidification may also contribute to the decay of the Syb-pHluorin signal. To test the potential role of reacidification in this process, we used again Bafilomycin A1 (Baf) (Dröse et.al 1993; Zhang et al., 1994) that abolishes the change in the intravesicular pH of the vesicles after

internalization. Thus, we comparatively analyzed the aforementioned parameters of the time-course of Syb-pHluorin signals in the presence and the absence of 1 μ M Baf in the extracellular medium.

Our results demonstrated that the number of fluorescent puncta were unchanged upon Baf treatment without stimulation indicating that inhibition of H⁺ transport does not prematurely lead to alkalization of the LDCV lumen (Fig. 29 A) nor does it change the mean signal amplitude of Syb-pHluorin (Fig. 29 B).

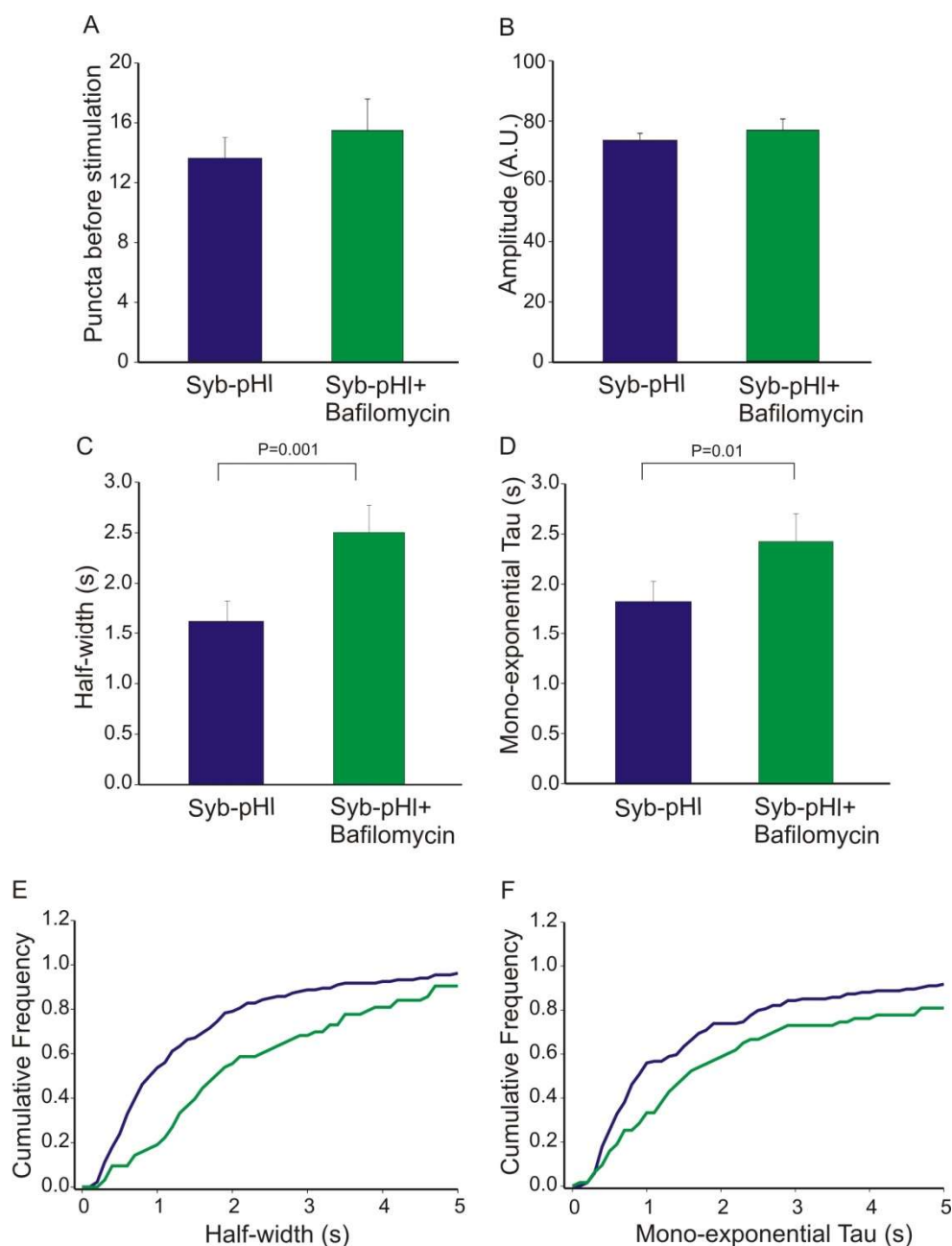


Fig. 29. Bafilomycin induced alteration in the kinetics of Syb-pHluorin time course: (A) Average pHluorin-positive puncta at *ab-initio* level is unchanged in presence of bafilomycin. (B) Mean signal amplitude was also unaffected with bafilomycin treatment implying that sorting of SybII in the vesicle membrane is unaltered in the presence of Baf. (C) In the presence of Baf, mean half-width was significantly increased, compared to control events. (D) Cell-weighted average of tau [τ] was also increased upon treatment with Baf. (E) Cumulative frequency of Syb-pHluorin events plotted on a 100-ms bin for event half-width, where a right hand shift to higher values in the distribution was observed upon bafilomycin treatment. (F) The same trend was followed by the event frequency in the tau (τ) value, providing consecutive evidence for prolonged event duration. *** $P < 0.001$; ** $P < 0.01$, Rank-sum test. Error bars represent SEM. [Number of cells (control) N-36; event n-134]; [(With bafilomycin treatment cells, N- 20; event n-63)].

Importantly, in the presence of Baf the kinetics of the Syb-pHluorin events are prolonged (Fig. 29 E, F). The cell-weighted average of the half-width was found to be 2.5 ± 0.26 seconds (Fig. 29 C), whereas in control cells the mean half-width was 1.62 ± 0.2 s. [$P < 0.001$]. We also observed a significant increase in the cell-weighted average tau (τ). Baf treated cells exhibited a mean tau (τ) of 2.42 ± 0.27 s, whereas in control events average tau (τ) was 1.82 ± 0.20 s, [$P < 0.01$] (Fig. 29 D). Henceforth, this data suggested that the time-course of Syb-pHluorin is also governed by the reacidification of internalized vesicles.

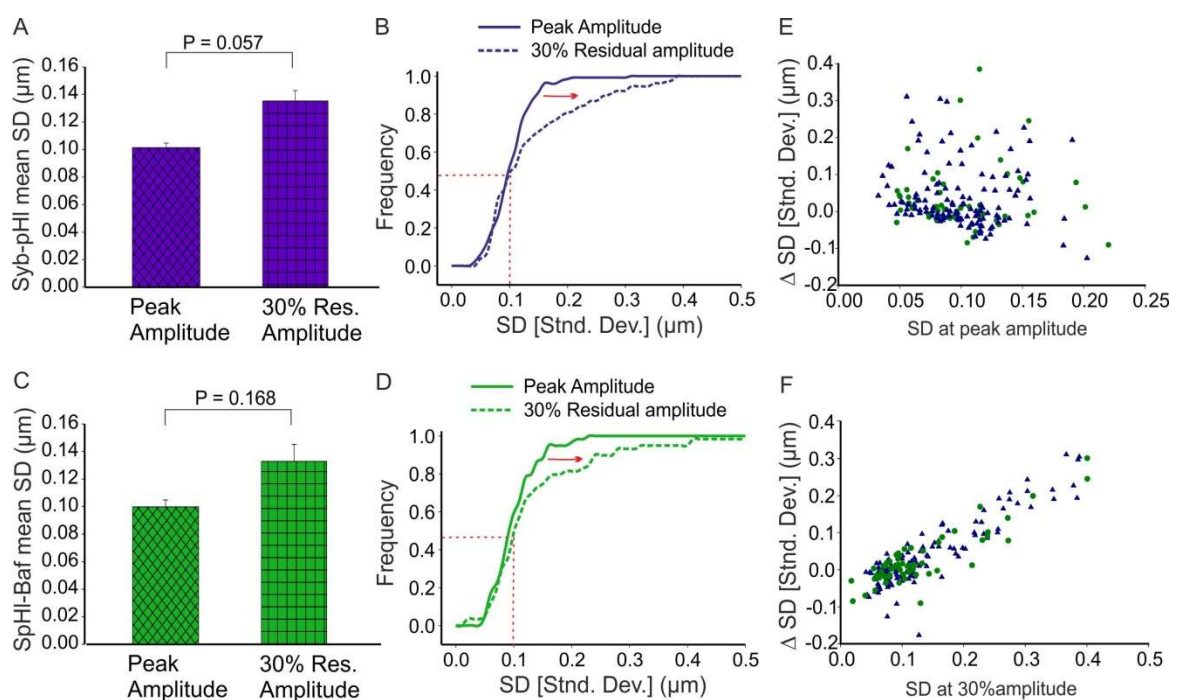


Fig. 30. Lateral diffusion of synaptobrevin in the course of exocytosis: (A) Cell weighted average analysis depicting an increase in SD at 30% residual amplitude in Syb-pHluorin control events. (B) Average SD from Baf-treated Syb-pHluorin events, illustrated a similar increase over amplitude drop, as in control events in Fig. A. (C) Cumulative frequency of Syb-pHluorin control events on absolute SD values at peak and 30% residual amplitude (D) Frequency distribution of Baf-treated eventson absolute SD values for peak and residual amplitude, both plots were generated after binning event SD at 0.001 μm .

Taken together, our experiments show that Baf treatment slowed the time course of the Syb-pHluorin whereas the kinetics of the NPY-pHluorin signal time course were insensitive to Baf treatment (Section 3.1.4). Overall, the analyses of these pHluorin variants make it possible to determine the kinetics of various processes in the pathway of exocytosis like cargo discharge, lateral dispersion of membrane bound molecules or endocytosis followed by reacidification.

Our analyses have established that spike and plateau events are often accompanied with stronger ($\text{SD} > 0.1 \mu\text{m}$) or lesser ($\text{SD} < 0.1 \mu\text{m}$) lateral dispersion of the Syb-pHluorin signal, respectively. These results point to the possibility that spike-like fusion events lead to complete membrane merger whereas plateau events may reflect fusion where the vesicle's integrity is preserved. Closer analysis of the corresponding frequency distributions of control Syb-pHluorin events revealed a kink in the curve for the SD values of the 30% amplitude distribution (Fig. 30b). In good agreement with our previous observations, events with an initial SD value of less than 0.1 μm showed no tendency for lateral spreading of the SybII signal that parallels the amplitude reduction. In contrast, the other population with SD values larger than 0.1 μm showed clearly increased lateral spreading that parallels the amplitude reduction.

We next asked the question whether fusion types that differ regarding the spatial distribution of SybII-pHluorin also differ regarding their sensitivity towards Bafilomycin. Importantly, similar lateral dispersions (SD) for the peak amplitude and for the 30 % amplitude were observed in the absence and presence of Bafilomycin (Fig. 30) indicating that this drug has no off target effects that may interfere with the mobility the SybII molecules.

To correlate the spatial and kinetic characteristics, we generated scatter plots for parameters such as event half-width and tau (τ) with absolute SD at peak amplitude and residual 30% amplitude. Furthermore, we also analyzed the relation between the

Δ SD and kinetic parameters, such as half-width and tau (τ). While Bafilomycin reproducibly increases the half width of the events (Fig. 31B and Fig. 31D, compare purple triangle versus green circles) it did not preferentially affect events either with low SD ($<0.1 \mu\text{m}$) or with high SD ($>0.1 \mu\text{m}$).

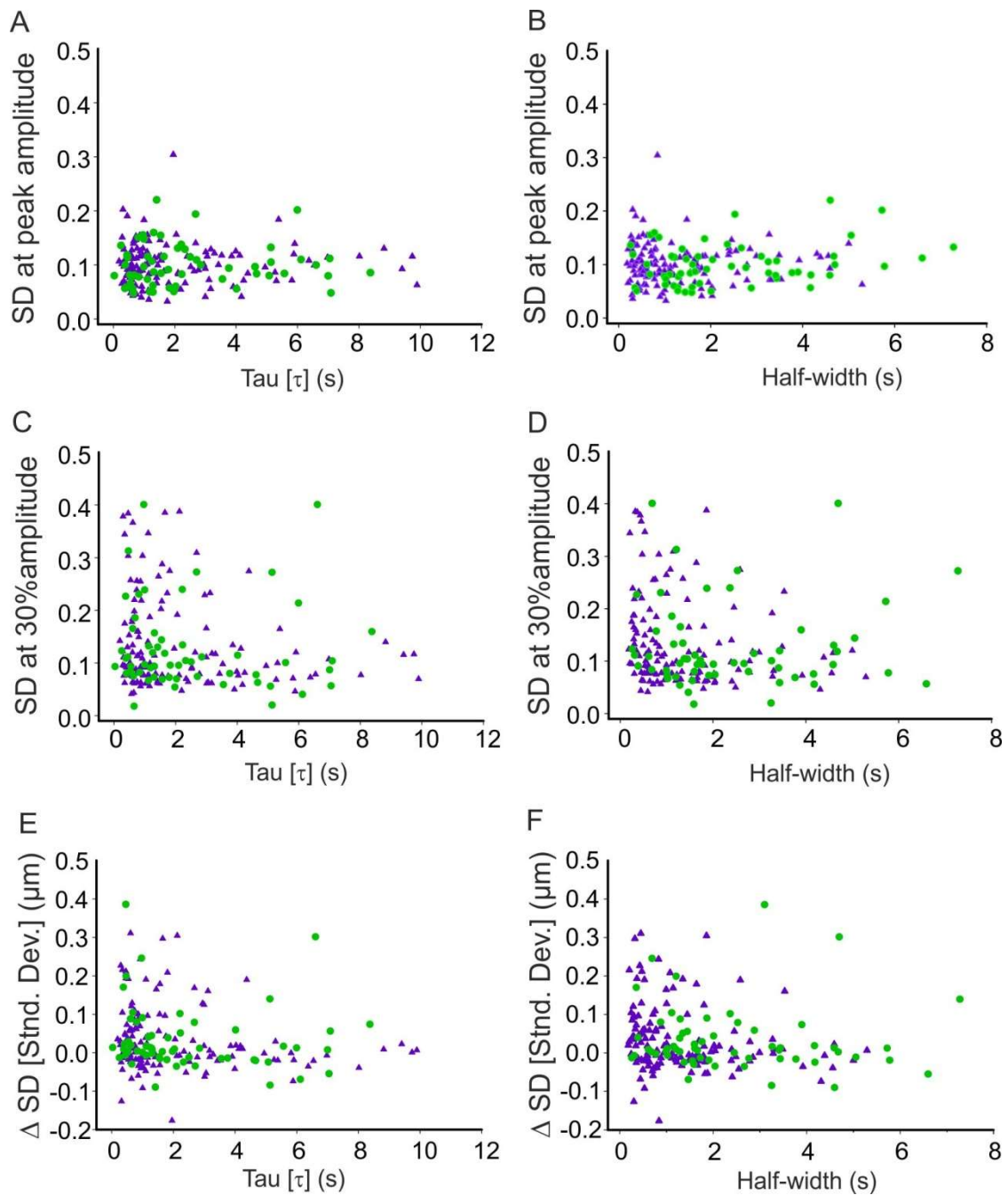


Fig. 31. Spike and plateau events are kinetically distinctive and Baf primarily affects plateau events: (A) Scatter plot illustrate no correlation between SD at peak amplitude and τ . (B) Another scatter plot between event half-width and SD at peak amplitude depicted no correlation but presence of clusters in both groups, demonstrating events with relatively shorter half-width and faster τ more prone to show lateral dispersion. (C) Scatter plot illustrating correlation between Δ SD at peak amplitude and τ . (D) Scatter plot illustrating correlation and event half-width and the residual 30% amplitude. Both plots were showing events with faster τ and shorter half-width showed a cluster in control group above and below 1 sec half-width range, whereas Baf-treated events are more scattered. (E) and (F) scatter plot between Δ SD, and half-width and τ replicated the same phenomenon that the cluster present in the control cells in the range of negative Δ SD was obliterated in presence of Baf [Bafilomycin treated cells N = 20; event n=59 {Spike 10 / Plateau 49}]. *** P<0.001; ** P<0.01, performed on Rank-sum test. Error bars represent SEM.

A similar conclusion was reached if we compared lateral spreading with the time constant of decay (Fig. 31 A, C, E). Taken together, these results suggest that blocking reacidification affects both event types irrespective of whether they encompass more or less lateral spreading of the SybII molecules in the plasma membrane. This results also agrees with the observation that Bafilomycin shifts the entire frequency distribution for halfwidth to higher values without affecting specifically short (spike-like events) or long-lasting events (plateau-like events).

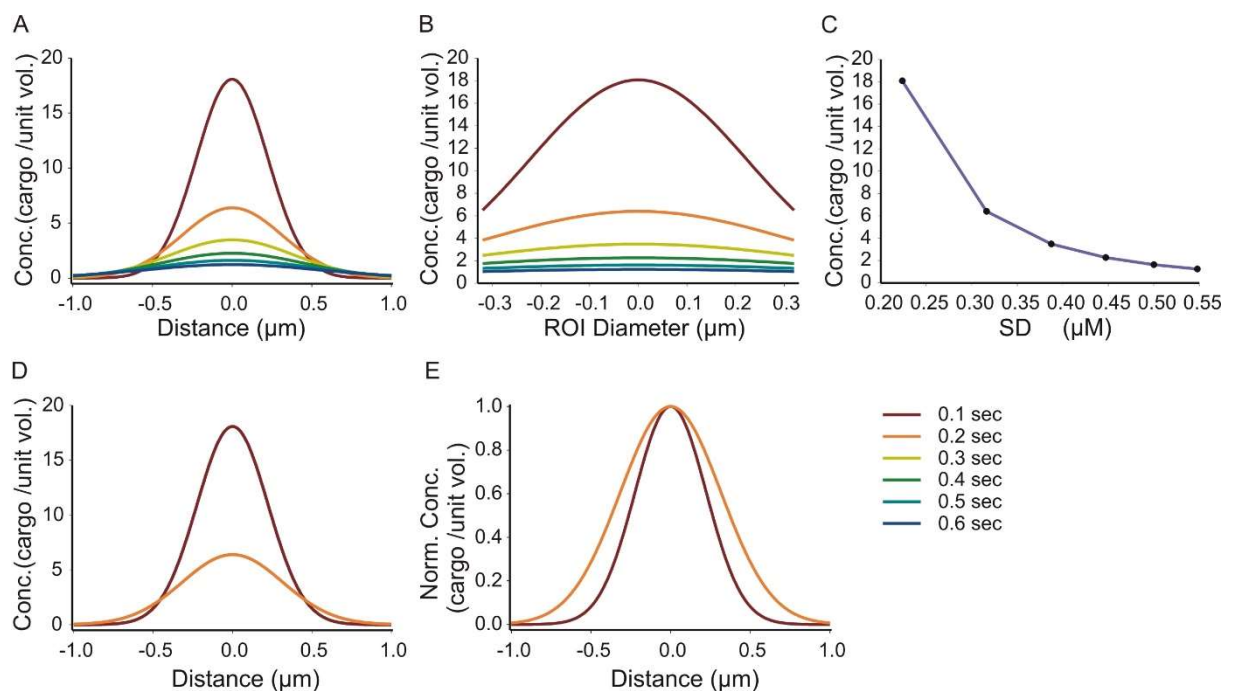


Fig. 32: Simulated function with Crank's equation revealed lateral dispersion of a molecule with a diffusion coefficient of $0.5 \mu\text{m}^2/\text{sec}$ from an instantaneous point source: (A) Traces depicting lateral diffusion of Syb-pHluorin molecules with a diffusion coefficient [D] of $0.5 \mu\text{m}^2/\text{s}$ over a distance of $2 \mu\text{m}$. (B) In particular with the circular ROI (Radius= $0.32 \mu\text{m}$), simulation traces define the dispersion of material within an interval of 100 ms. (C) The SD of the Gaussian curve fitted for each temporal profile plotted over amplitude drop. (D) First two time-points of the material diffusion were extracted to depict 70% loss of the material over a time interval of 0.1 s, depicting complementary spatial broadening of the signal over time. (E) Traces in Fig. D normalized to its peak amplitude.

Last but not least we also simulated using Crank's equation the lateral dispersion of Syb-pHluorin after complete membrane merger [diffusion coefficient (D) $\sim 0.5 \mu\text{m}^2/\text{s}$, (Gaffield et al., 2009)] within a 2-dimensional plane mimicking the plasma membrane. After instantaneous exposure of the molecules ($t=0\text{s}$) the concentration profile drops in amplitude and progressively broadens with increasing time (Fig. 32 A, B). The reduction in amplitude was clearly accompanied by a broadening of the concentration profile, as it can also be appreciated after normalization of the traces (Fig. 32 D, E). The systematic analysis for different time intervals (0.1s, 0.2s, 0.3s, 0.4s, 0.5s and 0.6s) revealed an inverse relationship between the amplitude of the concentration profile and its width, as quantified by changes in the standard deviation (SD) of the Gaussian fit approximating the data (Fig. 32 C). Thus, assuming a 16-fold slower diffusion coefficient of Syb-pHluorin compared with that for NPY-pHluorin, our simulation results revealed that diffusional dispersion of released sybII molecules within the plasma membrane should be clearly detectable at a time resolution of 0.1 s/frame.

Altogether, our experimental and theoretical analyses show the different pHluorin variants are suitable to determine the kinetics of various processes in the pathway of exocytosis, such as cargo discharge from vesicular lumen, complete merger of vesicles accompanied with lateral dispersion of membrane bound v-SNARE molecules as well as rapid endocytosis of vesicles followed by reacidification also contribute to the signal decay of Syb-pHluorin events.

3.3.1 ComplexinII (Cpx) is the only isoform that expresses in murine chromaffin cells

Previous reports have implicated Complexin (Cpx) in the regulation of the exocytotic fusion pore (Archer et al., 2002; An et al., 2010; Dhara et al. 2014). Therefore, we intended to study its effects on NPY-pHluorin fusion events. Given that multiple isoforms of complexin (at least CpxI and CpxII in neurons and neuroendocrine cells) exists, we first tested which isoform is indeed expressed in chromaffin cells. Earlier investigations suggested that the complexin (Cpx) isoform present in adrenal chromaffin cells is ComplexinII (CpxII) (Cai et al., 2008). To verify this finding, we checked expression profiles of different Cpx isoforms (CpxI and CpxII) and other SNARE proteins in brain and adrenal glands with an antibody that recognizes both isoforms with similar affinity [Synaptic system product no.122102], as it recognizes SNARE-binding domain of complexin isoforms that is conserved between CpxI and CpxII. As shown in Fig. 33A the immunoblot revealed two bands one for CpxII and another one for CpxI in the blot from brain homogenate as well as from adrenal glands (Fig. 33 A). One possible explanation could be that the CpxI band in the adrenal gland resulted from pre-ganglionic nerve fibers innervating chromaffin cells.

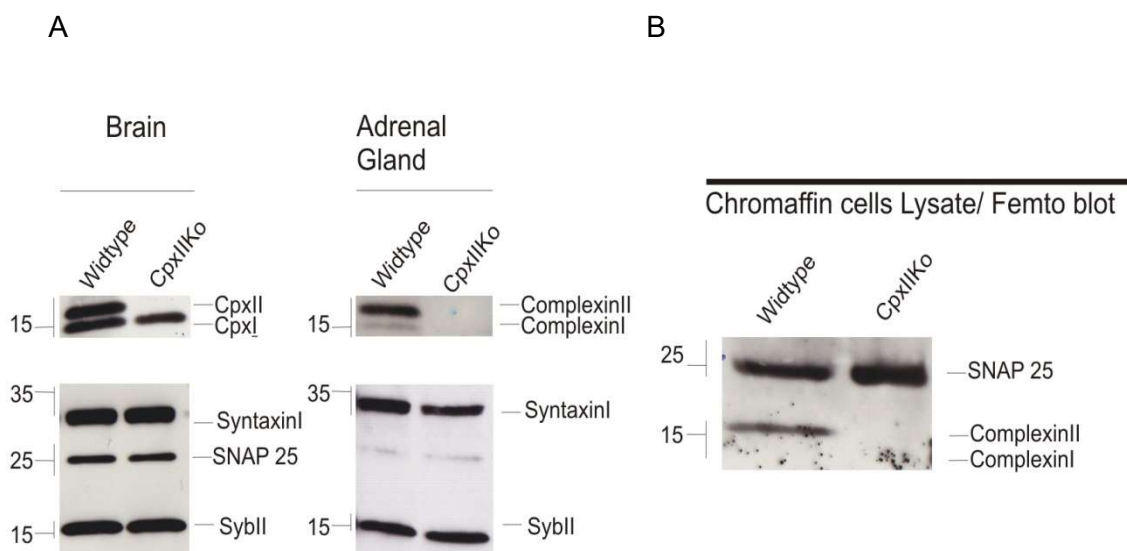


Fig. 33. CpxII expression in brain, adrenal gland and chromaffin cells: (A) Western blot analyses performed on brain lysate, adrenal gland lysate and chromaffin cell lysate. (Left panel). 10 μ g protein samples were loaded for brain, 30 μ g samples loaded for adrenal gland lysate. [SynaptobrevinII 69.1: mouse monoclonal {Ssys Cat no.104211}]; [SNAP 25 71.2:

mouse monoclonal {Ssys Cat no.1111111}}; [Syntaxin1 78.2: mouse monoclonal {Ssys Cat no.110001}}; [CpxI, II: Poly clonal, Recognizes SNARE binding domain of protein {Ssys Cat no.122102}}. (Right panel). (B) Cell lysate was prepared from plated cells with 2X lammelli buffer, and loaded into the gel and subsequently probed on femto-blot, probing Cpx(I, II) ,and SNAP 25 as loading control.

To circumvent this problem, we extracted proteins from the cultured chromaffin cells that should be devoid of any pre-ganglionic structure. To deal with the problem of low yield of extracted protein material from seeded chromaffin cells, we directly harvested the cells in 30 μ l of sample buffer and loaded them on PAGE gel for electrophoresis. Subsequently a highly sensitive detection method, i.e. Femto-blot was used (see method section 2.2.3.4), which is capable to detect very low amounts of protein, [lower limit of detection \geq few femtograms of proteins]. As shown in Fig. 33B only one immunopositive band could be found in the blot directly prepared from cultured cells indicating that CpxII is indeed the only one isoform expressed in these cells (Fig. 33 B). Moreover, the data also demonstrate that loss of CpxII does not lead to compensatory changes in the expression level of either Syntaxin, SNAP-25 or Synaptobrevin, a notion that was also important for the interpretation of our previous physiological findings (Fig. 33 A, B; Dhara et al., 2014).

3.3.2 ComplexinII ablation leads to a marginal increase in the event frequency and it also increases the spike-to-plateau ratio

We next intended to elucidate the kinetic profile of the NPY-pHluorin signal time course in CpxII deficient chromaffin cells. To do that, we overexpressed NPY-pHluorin molecule in CpxII knockout cells (CpxKO) and stimulated them with 10 μ m ionomycin to monitor vesicular exocytosis. Primarily, our data revealed a slight increase in the event frequency in absence of CpxII. The cell-weighted average of Cpx deficient cells showed 1.54 ± 0.356 events/cell, whereas littermate control cells exhibited 1.162 ± 0.288 events/cell ($P = 0.618$) (Fig.34 A). This marginal increase in the event frequency in CpxKO cells might be parallel to the previously reported finding from our group (Dhara et al., 2014), which demonstrated an increase in the tonic release of catecholamine in CpxKO cells due to unclamping of SNARE complex by Cpx. Additionally, our result did not demonstrate any alteration in the number of NPY-

positive granules at the vesicle footprint. Hence, we concluded that Cpx deficiency did not lead to any alteration in vesicle biogenesis (Fig. 34 B). In extension, considering our aforesaid data [section 3.3 (Fig. 12D)] we manually segregated these groups of NPY-pHluorin events into two different classes, i.e. spike-like events (duration < 400 ms) and plateau-like events (duration > 400 ms).

Based on this segregation, our data revealed an increase in the ratio of Spike /Plateau events in CpxKO cells. For instance, in CpxKO cells 32 spike events was found out of 69 events and the rest 37 events were plateau events of variable duration, revealing a Spike/ Plateau ratio of 0.864 (Fig. 34 C), whereas in littermate cells 16 spike events and 29 plateau events were observed in 45 release events, revealing a Spike-to-Plateau ratio of 0.551.

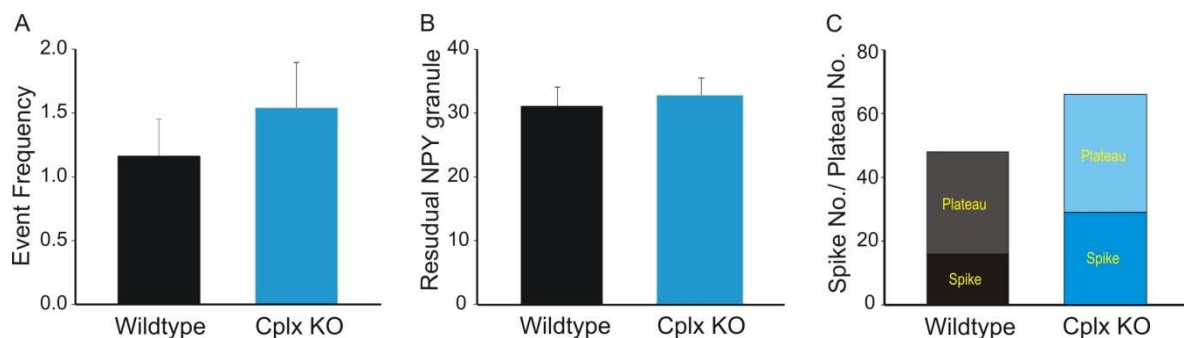


Fig. 34. CpxII ablation marginal influence in the frequency of NPY release event but facilitates an alteration in the plateau to spike ratio: (A) Event frequencies were calculated by manually counting the total number of events over the number of effectively recorded cells. (B) Total number of NPY-positive granules that appear upon ammonium chloride treatment in CpxII deficient and in littermate control cells. Error bars represent Standard error of mean (Control cells N=38, Knockout cells N=49). (C) The ratio between spike and plateau event were calculated for both groups, with the 400-ms threshold of segregation (Fig. 12D). Based on this categorization, 32 out of 69 events falls into the category of spike event, whereas in control cells 16 out of 45 events were found to be spike event, yielding more spike events in Cpx deficient cells.

Taken together, these data suggest that there is an increase in the event frequency in the deficiency of Cpx. In extension to our previous finding (Dhara et al., 2014), the unclamping of SNARE complex by the loss of CpxII might contribute to the release of more events that might also be changing the ratio of spike and plateau events in

vesicle exocytosis. Moreover, this surplus of spike events might be analogous to the excess release events of catecholamine that is represented as tonic release events occurring in CpxKO (Dhara et al., 2014). To address this affect in a profound manner, we extended our next analyses to the kinetic parameters of the signal time course.

3.3.3 ComplexinII deficiency does not influence the kinetics of NPY-pHluorin signal time course

To find a correlation between the aforementioned catecholamine tonic release (Dhara et al., 2014) and the spike events in NPY-pHluorin release, we further extended our analyses to address the kinetic profile of NPY-pHluorin release in Cpx deficient cells, by measuring single event kinetic parameters, such as amplitude, half-width and time constant for decay (τ) for individual events.

Our results demonstrated that Cpx ablation leads to no significant change in the signal amplitude of the events. The mean and median amplitude CpxII deficient cells was found to be 76.84 ± 2.96 A.U and 75.09 A.U. respectively. In littermate control cells the mean and median amplitude was found to be 63.40 ± 2.95 A.U. and 61.03 A.U. (Fig. 35 A). Thereby, it confirms that the deficiency of Cpx does not significantly influence the amount of cargo uptake in the vesicles. This result corroborates with catecholamine release events in CpxKO cells, where amperometric event amplitude was found to be unaltered in Cpx loss (Dhara et al., 2014). As shown in Fig. 35 B, the average half-width was found to be 1.00 ± 0.22 seconds for wildtype littermates and 0.95 ± 0.17 seconds in CpxKO cells, implying a minor change as reflected in frequency distribution, as half-width of CpxKO events are starting from lower values (Fig. 33 E). In addition, the average tau (τ) for wildtype littermate and CpxKO cells was calculated to be 0.138 ± 0.022 seconds and 0.163 ± 0.033 seconds respectively (Fig. 35 C). In line with this finding, the frequency distribution exhibited no shift in the event population (Fig. 35 F).

Overall, these observations with analyzing peptide release have substantiated our previous result, which demonstrated that Cpx deficiency did not alter kinetic properties of the single amperometric events for catecholamine release [charge, amplitude, rise time, half width, pre-spike duration and pre-spike charge] (Dhara et al., 2014). Our data also suggested that CpxII deficiency did not induce premature

closure of the fusion pore.

In summary, the combined set of data from NPY-pHluorin depicted in the previous section and Syb-pHluorin data set from this section provides new information regarding the process of membrane fusion in chromaffin cells. For our studies, we took the advantage of pH-dependent quenching-dequenching phenomenon of pHluorin's fluorescence that is tagged with vesicular cargo NPY.

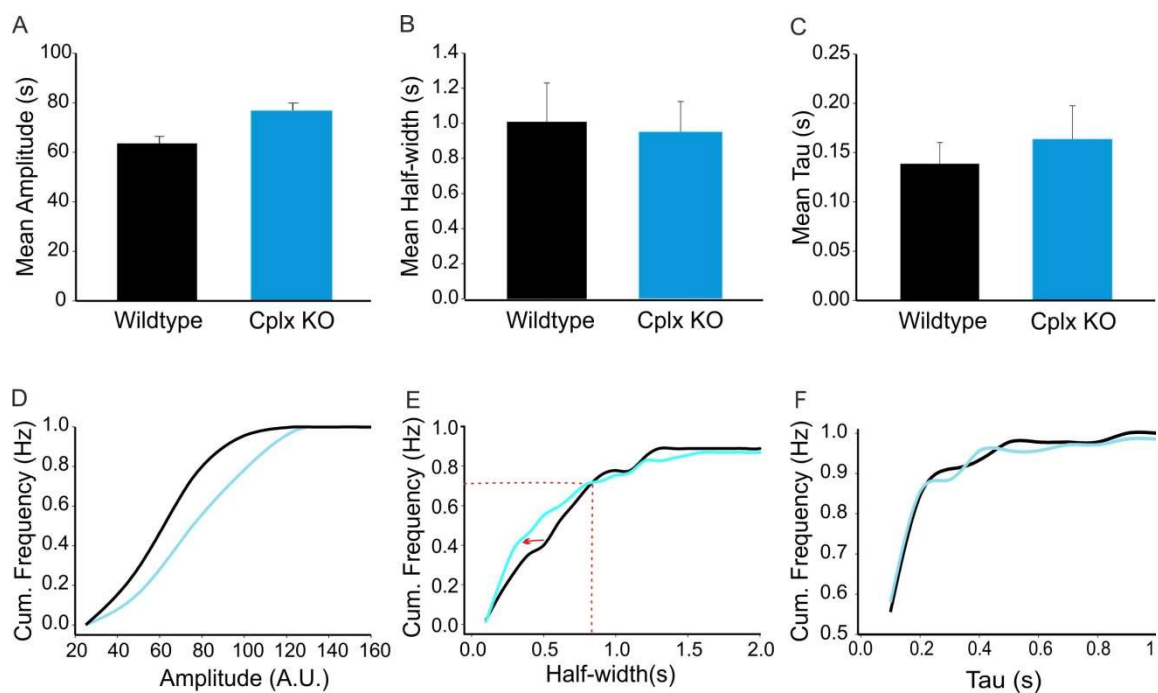


Fig. 35: CplxII does not control the kinetics of single fusion event for NPY release. Weight-scale analyses presented for (A) Mean amplitude, depicting no significant alteration. Kinetic property, such as (B) mean half-width was also found to be unchanged between control and Cpx KO cells. (C) Time constant for Decay [τ], was also found to be unaffected in the deficiency of Cpx. Cumulative frequency for (D) amplitude exhibited a right-hand positive shift, when plotted with a bin of 25 A.U. Frequency distribution of (E) Half-width and (F) Tau [τ], both were unaltered, when they were plotted at 0.1-second bin. Error bars represent Standard error of mean (Control cells N=16, Knockout cells N=21; Control event n= 45, Knockout event n= 69).

Given the respective dimensions of 4.6 x 3.2 x 3.1 nm and 4.3 x 1.9 x 1.4 nm, our data revealed that NPY-pHluorin can be used as a reporter to monitor stimulus-evoked vesicular exocytosis by the gain and subsequent loss of fluorescence signal. The rapid uprise in the fluorescence of NPY-pHluorin on local superfusion of exocytosis-inducing agents, such as 10 μ M ionomycin or depolarizing high K^+ solution reports fusion pore opening. The subsequent loss in the signal occurred

due to the discharge of the NPY cargo molecules from the vesicle. However, the stationary plateau phase of some NPY-pHluorin events after signal uprise illustrated hindrance in the release of the cargo molecule. Given molecular dimension of NPY-pHluorin cargo and diameter of initial fusion pore (1-2 nm), the cargo may not be able to pass through the initial fusion pore unless pore dilates to certain diameters allowing the passage of bulkier molecules. Consequently, this temporal delay resulted into plateau-like phases. Spike-like events, however, illustrated a different type of membrane fusion that releases cargo rapidly without any temporal delay, as the fusion pore most likely reaches a maximal dilated state. Additionally, we found that these events [both spike and plateau events] were classical v-SNARE mediated, Ca^{2+} -regulated vesicular exocytosis. Besides, our results demonstrated that the NPY-pHluorin release from LDCVs strongly depends on the calcium sensing proteins, SytI and SytVII. Moreover, we found that reacidification has no role in the signal time course of NPY-pHluorin but that cargo efflux represented the rate limiting step for the decaying signal. We also studied differential kinetics and spatial behaviors of membrane bound slowly diffusing SynaptopHluorin (Syb-pHluorin) molecules, with dimensions of $4.6 * 3.2 * 3.1$ nm, $10-15 * 1.3 * 1.1$ nm for pHluorin and Syb, respectively. For spike-like Syb-pHluorin events experimental data and simulation results showed lateral spreading of the v-SNARE protein indicating complete merger with the plasma membrane. For plateau-like events, instead, no signs for diffusional spreading could be found suggesting that the vesicle's integrity is preserved in the course of exocytosis. In general, the release time course of Syb-pHluorin events was significantly slower than that of NPY-pHluorin and also sensitive to the v-ATPase blocker bafilomycin. This shows that reacidification of the vesicles clearly contributes to the decay of these fluorescence signals.

4. Discussion

Trafficking of cellular organelles has been extensively studied in *in-vitro* cell free systems and in diverse physiological processes in cellular systems. Majority of the information on vesicular exocytosis and its molecular mechanisms have been determined mostly from the studies of synaptic transmission and the transport of different cargo molecules (neurotransmitter, hormones). In addition, the cardinal role of SNARE and other accessory proteins in exocytosis has been proven beyond reasonable doubts. Synchronized actions of these proteins facilitate the release of cargo molecule through the fusion pore (Jahn and Scheller, 2006; Verhage and Sorensen 2008; Südhof and Rothman, 2009; Südhof and Rizo, 2011; Fasshauer and Jahn 2012; Jahn and Fasshauer, 2012). The cardinal role of the fusion pore in exocytosis has already been discussed in sections 1.2.4 and 1.5. Previously, information on fusion pore was primarily obtained from amperometric recordings of oxidizable molecules such as catecholamines (e.g., epinephrine, norepinephrine or dopamine) (Chow et al., 1992; Ureña et al., 1994; Schroeder et al., 1996; Pothos et al., 1998; Wang et al. 2001; Wang et al. 2003; Bruns, 2004; Staal et al., 2004; Borisovska et al., 2005; Kesavan et al., 2007) and indolamines (e.g., serotonin) (Bruns et al., 1995, Bruns et al., 2000). Catecholamines and dopamines are very small molecules ($M_w \sim$ few daltons) and release of these molecules occurs at a time scale of 1-50 ms (Bruns et al., 1995, Bruns et al., 2000; Borisovska et al., 2005; Kesavan et al., 2007). Thus, amperometric recordings provide a readout of cargo release for a short time domain after initiation of exocytosis. Peptidergic molecules are bulkier in size than biogenic amines, Neuropeptides (NPY) and tissue plasminogen activator (tPA) in chromaffin cells and insulin in β -pancreatic cells have a longer time course of release [ranging from 100-ms to a few seconds] (Taraska et al., 2003; Tsuboi et al., 2003; Taraska et al., 2004; Zhu et al., 2007). Furthermore, they are often known to co-exist with epinephrine / norepinephrine in LDCVs of chromaffin cells (Fulop et al., 2006) and are known to co-release with catecholamine upon elevation of $[Ca^{2+}]_i$ (Perrais et al., 2004). Given the efficacy of new imaging methods, we were interested to explore the time domain of peptidergic release that is 10-fold longer than the time domain measured in amperometry. By this, we intended to provide new insight of regulated vesicular exocytosis from cargo discharge to the post-fusion state.

Consistent with this idea, experiments with pHluorin variant provided a direct read-out for fusion pore opening as monitored by dequenching of the luminal pHluorin molecule in the form of fluorescence uprise. Subsequent stationary phases of NPY- or SybII-pHluorin events provided an estimate on the duration of a semi-stable fusion pore that hinders the exchange of fluorescently labeled molecules with the extra-cellular space or the plasma membrane. Last but not least, the decay of this signal is expected to be informative regarding the kinetics of cargo release and of endocytotic processes encompassing reacidification.

4.1 Stimulus evoked NPY release from chromaffin granule

Imaging techniques are advantageous over other techniques in monitoring the behavior of single vesicle exocytosis, as vesicles can be specifically labeled with fluorescent markers. Here we made use of a pHluorin-based probe fused with NPY to monitor the fusion of LDCVs similar to the previously reported work on LDCV fusion from PC12 cells (Taraska et al., 2003; Zhu et al., 2007).

In earlier studies, the superfusion of high potassium [K^+] was extensively used as a stimulation paradigm for the elicitation of exocytosis. The elevated [K^+] made the plasma membrane potential less negative, causing the opening of voltage-gated calcium channels, leading to Ca^{+2} influx inside cell. The subsequent NPY release from chromaffin granules could be detected due to the presence of fluorescent tags, such as EGFP, pHluorin and mCherry as reported by Taraska et al., 2003; Zhu et al., 2007 and Hugo et al., 2013, respectively. Alternatively, the Ca^{2+} ionophore ionomycin can be used as an agent to increase intracellular calcium influx and to elicit exocytosis from SSVs and LDCVs at serotonergic neurons (Bruns et al., 2000) or catecholamine release from neuroendocrine LDCVs (Schütz et al., 2005). Both release events were readily detectable by amperometry. Here, we successfully implemented the ionomycin stimulation protocol to evoke peptidergic release from vesicles (Fig.10) (Fig. 23).

Null mutation of the synaptobrevin or VAMP 2 exhibited a strong inhibition of action potential-evoked transmitter release at synapses (Deitcher et al., 1998; Schoch et al., 2001). VAMP3/cellubrevin, a structural homologue of synaptobrevin, has been also reported to have functional contribution in the catecholamine release (Borisovska et al., 2005). Furthermore, co-sorting of synaptobrevin and cellubrevin

was also observed in the secretory vesicles of neuroendocrine systems of PC12 and chromaffin cells (Chilcote et al., 1995; Borisovska et al. 2013), leading to functional redundancy of the v-SNARE proteins (VAMP-2 and VAMP-3) (Borisovska et al., 2005). Particularly, this study encouraged us to check the v-SNARE dependency of this NPY release event. Here our results revealed a clear phenotype of v-SNARE dependency in *Syb^{-/-}/Ceb^{-/-}* (doko) chromaffin cells, as NPY release events were found to be abrogated in this cell type. However, no alteration was observed in the vesicle biogenesis from late endosome and in recruitment of these vesicles in the vicinity of cell membrane (Fig. 11). Our finding, together with the previous observations further substantiates v-SNARE dependency of LDCV exocytosis.

Intracellular calcium signal primarily modulates the Sub-millisecond temporal precision of the neurotransmitter release. Firstly, SynaptotagminI (SytI) was identified as a major calcium sensor in the central synapses (Perin et al., 1990; Geppert et al., 1991; Geppert et al., 1994). Subsequently, other Syt isoforms were identified as a vesicular Ca^{2+} -sensor for fast exocytosis in forebrain and chromaffin cells (Maximov et al., 2005; Fernandez-Chacon et al., 2001; Voets et al., 2001; Sorensen et al., 2003). Deletion of SytI led to a significant reduction in the readily releasable pool (RRP) of vesicles in chromaffin cells, but the slowly releasable pool (SRP) and release property of the vesicles during sustained phase of release were unaltered (Voets et al., 2001; Dhara et al., 2014). Moreover, SytVII was identified as a functionally overlapping Ca^{2+} -sensor for secretory vesicular exocytosis in chromaffin cells (Schonn et al., 2008). Indeed, in absence of both isoforms, RRP was abolished, alongside SRP and sustained component were also significantly reduced (Schonn et al., 2008). In close correlation, we found that NPY-release was significantly reduced in SytI/SytVII deficient cells (Fig. 22) without changing the biogenesis of LDCVs as judged from the unaltered number of NPY-positive vesicles. In summary, our measurements of NPY-pHluorin signal time course fulfill hallmarks of regulated vesicular exocytosis that have been monitored also with other techniques.

4.2 Variable kinetics of cargo release are due to variability in the opening of the fusion pore

In analyzing the signal time course of NPY-pHluorin, we found that the rise-time of fluorescence signals was extremely rapid (< 0.1 sec). This is due to the small molecular dimensions of hydrated proton [H_3O^+ ($M_w \approx 19\text{g/mol}$)], as they are rapidly and efficiently transported through initial fusion pore facilitating the dequenching step of pHluorin. Thus, the up-stroke of the signal marks first opening of the fusion pore (Fig. 24). The time course of NPY-pHluorin signals can be separated into three cardinal phases, such as rise-time, duration and decay.

Rise-time – The molecular dimension of hydrated Proton is (H_3O^+) [0.1 (O-H) * 0.2 (H-H) * 0.2 (H-H)] nm, while the diameter of initial fusion pore is < 3 nm (Lindau et al., 1995; Lindau et al., 2003). Therefore, hydrated protons diffuse nearly instantaneously to the vesicular lumen, giving rise to the signal upstroke. Since all our experimental fluorophores are pHluorin variant (NPY-pHluorin and Syb-pHluorin), hence the rise-time of signal is similar for all fluorophores.

Duration – NPY-pHluorin fusion events are characterized by variable kinetics ranging from short-lasting spike to long-lasting plateau events. In contrast to tiny hydrated proton, large sized cargo molecules can often not escape the vesicle because of restricting fusion pore diameters. According to this the resulted exocytotic fusion pore must temporarily exhibit a diameter of smaller than 3 nm that hinders the efflux of molecules like NPY and EGFP (see Table).

Protein	Molecular mass <i>kDa</i>	Residues	Volume <i>nm³</i>	Dimensions <i>xyz</i> <i>nm</i>
EGFP	26.9	238	32.6	$4.6 \times 3.2 \times 3.1$
NPY	4.3	36	5.2	$4.3 \times 1.9 \times 1.4$

[Taken from Tsuboi et al., 2004 J. Biol. Chem.]

Decay–Once the signal decay has started, it is similarly rapid in spike and also in plateau events reaching on average the resolution limit of the recording system ($\tau=0.097$ s). This quick expulsion of cargo should lead to a cloud of freely diffusible molecules around the fusion site. But in contrast to this expectation, diffusion of NPY

in the extracellular space is even more rapid. Thus, the majority of the fusion events do not exhibit any detectable accumulation of fluorescent molecules in the direct vicinity of the fusion site. Hence, it appears that dispersion of liberated molecules is even faster than their discharge from the vesicle.

To test this hypothesis, we have simulated such a scenario with the Crank's equation assuming instantaneous discharge and calculated the dissipation of the spatial concentration gradients over time. Indeed these simulations reveal that diffusional dispersion is so fast that often in one frame (interval 100 ms) the majority of molecules has quickly dispersed and left the region of interest. Some fusion events however, provide positive evidence for cargo accumulation around the fusion site and may reflect the rare situation of the narrowing lateral clefts between the plasma membrane and the coverslip. This may provide enough diffusional hindrance to allow for a detectable accumulation of the released cargo molecules. Hence, the signal decay indeed represents discharge and the diffusion of the cargo molecule in the extracellular milieu from the vesicle (Fig. 13). Furthermore, we could conclude that kinetics of the NPY-pHluorin time course is not influenced by the amount cargo (Fig. 13).

Previously, Perrais et al., 2004 reported NPY-EGFP release from chromaffin cells that illustrated two categories of event types, i.e. one population represented classical discharge events and the other one interpreted as retention of the cargo in the vesicle (Perrais et al., 2004). In addition, they also showed that the delayed release of tPA-EGFP occurred due to the incomplete dilation of the fusion pore. These results also agree with electrical measurements of the fusion pore, where mast cells and chromaffin cells have exhibited a semi-stable state of fusion pore with diameter ranging from 0.5 – 2 μm (Spruce et al., 1990; Curran et al., 1993; Albillos et al., 1997). Complementary to these findings, our NPY-pHluorin results also depicted a diverse release kinetics ranging from spike-like to plateau-like scenarios that may very well be due to rapid and delayed fusion pore dilation, respectively (Fig. 12).

On the other hand, the plateau-events should be distinguished from short-lasting flickering of foot signal in amperometry, known as pre-spike-foot (PSF). The latter event resulted from the initial opening of the fusion pore followed by the subsequent rapid expansion of the pore coinciding with complete expulsion of the cargo (Lindau

et al., 1995; Zhou et al., 1996; Bruns 2004; Borisovska et al., 2005; Kesavan et al., 2007). Initial fusion pore diameters (< 3 nm) prevent NPY-discharge entirely, whereas they only reduce release of catecholamines (Lindau et al., 1995, Lindau et al., 2003). In any case, both assays, NPY discharge and amperometry, provide evidence for temporal variability in the complete dilation of the exocytotic fusion pore that can be converted into variable kinetics of the signal time course.

Altogether, our experiments provided evidence that NPY-pHluorin can be used as a new tool to monitor consecutive stages of vesicular exocytosis from fusion pore opening to cargo discharge and its subsequent dissipation. This could not be monitored with other NPY-bound fluorophore, such as NPY-EGFP and NPY-mRFP due to their limited sensitivity to pH change prevents the detection of the initial opening of the fusion pore (Taraska et al., 2003).

In addition, the fundamental role of reacidification in the kinetics of pHluorin molecules has been well evident while measuring the time course of Syb-pHluorin in synaptic boutons (Sankaranarayanan et al., 2001; Burrone et al., 2006). Complementary to this, we intended to elucidate the role of reacidification, if any, in the decay of NPY-pHluorin over time. As we expected, here our data revealed that the kinetics of NPY-pHluorin time course is independent of the reacidification of the endocytosed vesicles (Fig. 14), i.e. Baf did not influence the NPY-pHluorin time course, such as half-width and time constant for decay (τ); hence we could rule out the possibility that the reacidification of vesicular lumen plays any role in governing the time-course of NPY-pHluorin. Therefore, the decay phase of NPY-pHluorin' time course is mainly governed by the discharge of the cargo molecules from the fusion site.

On further dissection of the NPY-pHluorin time course, while complementing earlier investigations that reported the modulatory role of Complexin (Cpx) in the regulation of the exocytotic fusion pore (Archer et al., 2002; An et al., 2010; Dhara et al. 2014), we intended to address its implications on NPY-pHluorin fusion events. In particular, Dhara et al., 2014 demonstrated that for catecholamine release CpxII ablation is ineffective on the fusion pore expansion at higher intracellular calcium, rather it prolongs the fusion pore expansion at low $[Ca]_i$. In accordance to these findings our peptide release results demonstrated that CpxII ablation leads to no alteration in the kinetics of NPY-pHluorin signal time course. Besides, previous findings showed that

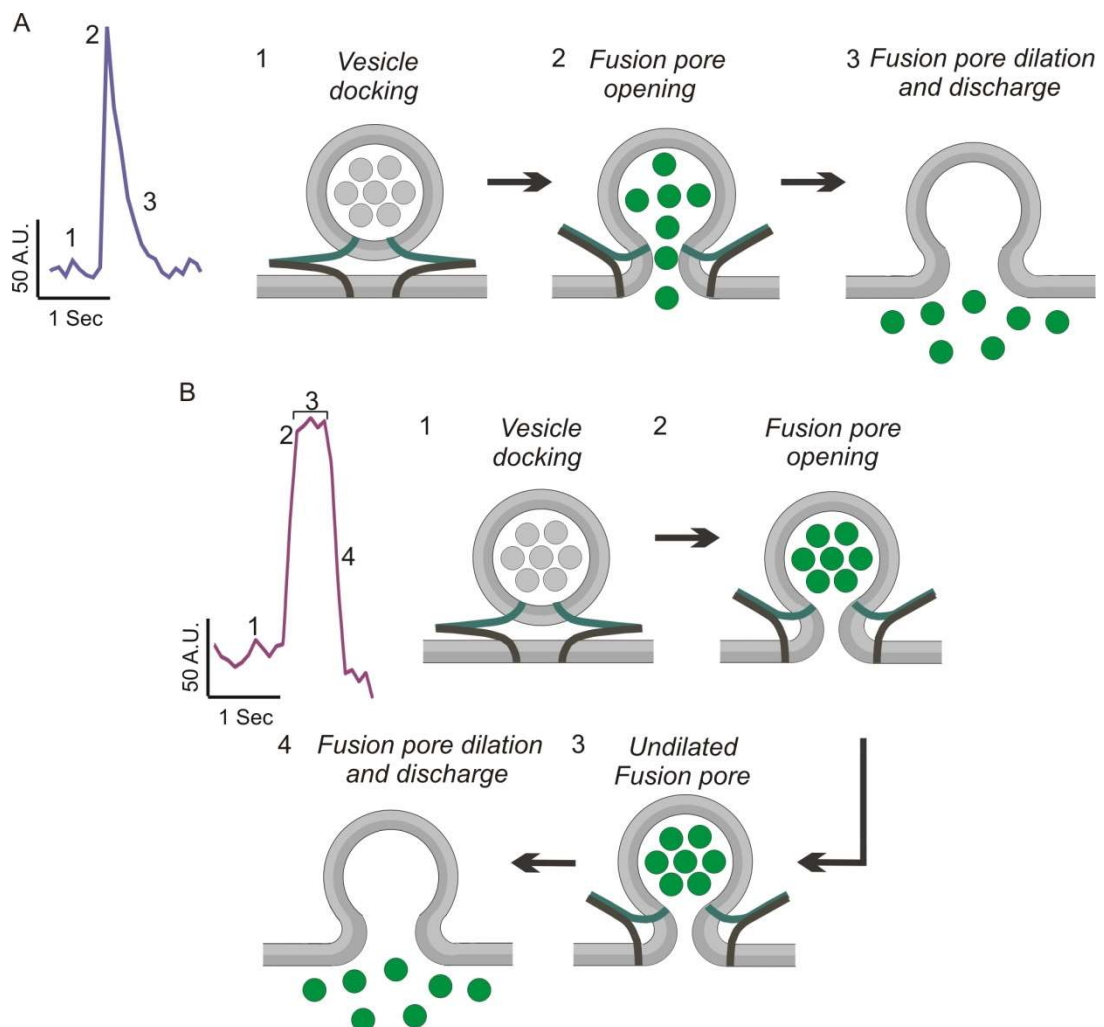
the loss of CpxII resulted in premature exocytosis at sub-micromolar $[Ca]_i$, due to the unclamping of SNARE complex (Dhara et al., 2014). In line with these findings, our CpxII deficiency induced alteration in the spike/plateau ratio, i.e. more spike events were released for NPY-pHluorin (Fig 34, 35). This surplus of spike events may result from reduced clamping in the absence of CpxII, enabling an unhindered pull of SNAREs on their TMDs (Trans-membrane domain) to complete membrane merger (Dhara et al., 2014).

4.3 Efflux of the cargo molecules and its discharge-based diffusion are the main rate-limiting steps of NPY release

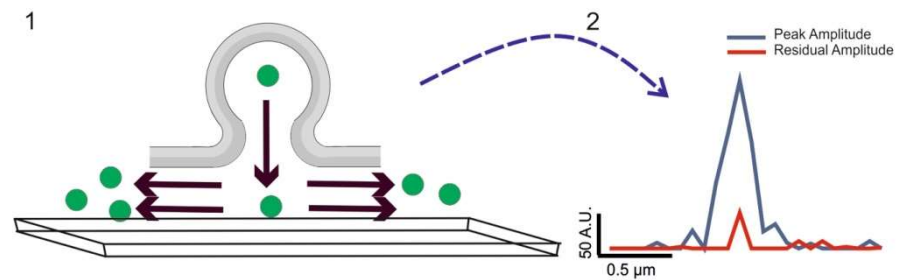
The simulation data (Fig. 20) together with the experimental results on release (Fig. 12-13) of NPY and its spatial distribution (Fig. 15-20) reproducibly demonstrated that the dispersion of diffusing cargo molecule could not be monitored at real time, irrespective of the available detection methods, i.e. 10 Hz sampling in LSM (Fig. 15, 16) or 20 Hz sampling in TIRF (Fig. 18 A, B). This is because NPY-pHluorin might be released into a void/unrestricted space in between plasma membrane and coverslip surface. This lack of environmental restriction enables NPY-pHluorin to disperse at its normal diffusion rate. Nonetheless, other consequences of diffusing cargo molecules, such as increased signal offset and increased Gaussian SD (Fig. 17, 18) could also be observed in spike as well as in plateau events. These two diffusion phenotypes led us to conclude that sometimes accumulation of cargo molecules occur at variable range, as narrow clefts are generated between the vesicle and plasma membrane due to membrane invaginations. This inhibits diffusion of NPY-pHluorin molecules to follow its normal dispersion rate in the 2-dimensional planes (Fig. 36). With TIRF recordings of NPY-pHluorin that have provided visual evidence of cloud-like dispersion of diffusing cargo molecules (Fig. 19 A, B), we can further demonstrate that the signal decay indeed corresponds to the discharge and subsequent diffusion of the cargo molecules from the fusion site. This visual observation corroborates with the previous study by Zhu et al., 2007 that demonstrated NPY-pHluorin release from PC12 cells. After acute expression of NPY-pHluorin in PC12 cells, the stimulus-evoked release events resulted in three fusion modes, such as 'kiss-and-run', 'kiss-and-stay' and full fusion, which were primarily regulated by the coordinated action of SytI and SytIX. Additionally, our data

indicated that the efflux of cargo from the fusion site might be a rate-limiting step in defining the kinetics of NPY-pHluorin release.

Taken together, our measurements with NPY-pHluorin provided a new avenue in the investigation of cargo release from LDCVs in the perspective of fusion and post-fusion stage of vesicular cargo discharge. Our finding provided new information on fusion pore opening and post-fusional diffusion of cargo extending previously reported investigations on single vesicle fusion properties, such as retention and expulsion time-course of vesicular cargo, like NPY release from neuroendocrine system, especially in form of NPY- mRFP and EGFP release from PC12 cells, (Taraska et al., 2003, Perrais et al., 2004; An et al., 2010).



C. Non-detectable dispersion of NPY-pHluorin molecules



D. Detectable dispersion of NPY-pHluorin molecules

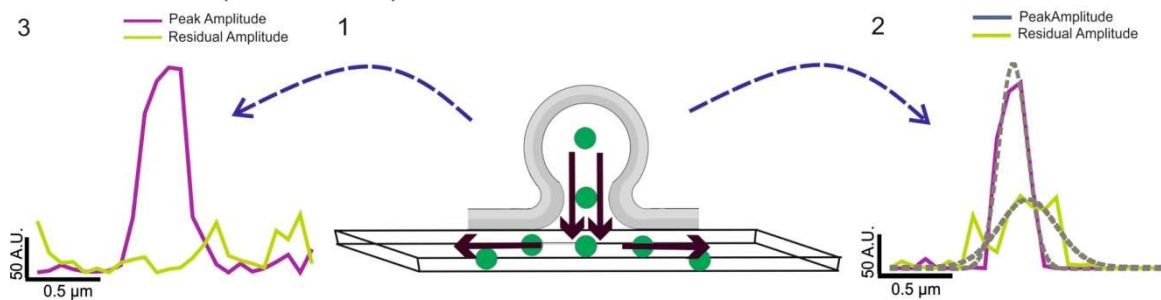


Fig. 36: Schematic model illustrating stimulation-evoked NPY-pHluorin release events from chromaffin cells LDCVs: A. Stages of *instantaneous release event*. (1) Vesicles are docked in the close proximity of plasma membrane. (2) Dequenching of pHluorin molecule, after opening of the fusion pore. (3) Discharge of NPY-pHluorin in the extracellular milieu. B. Stages of *delayed release event*. (1) Docking of vesicle in the vicinity of plasma membrane. (2) Opening of the fusion pore, leading to the dequenching of pHluorin molecule. (3) Restricted dilation in the fusion pore that inhibits deliverance of cargo, generating variable retention time of the cargo in the vesicular lumen. (4) Delayed discharge of the cargo molecule. C. Schematic presentation (1) illustrates probable physiological context of a release event, where diffusing cargo molecules from the fusion site could not be detected that is demonstrated by the extensive loss of signal within an interval of 100 ms (2) This happens due to the relatively distal location of the fusion site and due to the very high diffusion coefficient of NPY-pHluorin ($\sim 8 \mu\text{m}^2$), cargo molecules escape the measurement region. D. Illustration of (1) detectable diffusing cargo molecule in the course of dispersion that was noticed in some vesicular events as an increase in Gaussian SD (2) and sometimes also as an increase in signal offset (3), this happens due to the very proximal location of the fusion site to the cell membrane, resulting in a restricted space for the cargo molecules.

4.4 Schematic illustration of NPY-pHluorin release from LDCVs

Coalescing all the features of NPY-pHluorin release events, we can propose the following scenarios for vesicular exocytosis of NPY. As it was mentioned before, the

time course of NPY-pHluorin signal illustrates three different stages of fluorescence steps, such as rise-time, duration and decay. In the physiological perspective this can be translated into dequenching, variable open state of fusion pore often redirecting efflux of cargo molecules and final decay of the signal resulting from release of cargo molecule from the vesicle (discharge and dissipation). Altogether, variability in the open time of the fusion pore before its full dilation translated into this high degree of variability of the overall signal time course. NPY-pHluorin release events also fulfill the hallmarks of classical v-SNARE-mediated, Ca^{2+} -regulated release as they are elicited due to increase in the intracellular calcium, which are sensed by vesicular calcium sensing proteins, such as SytI and SytVII.

4.5 Syb- pHluorin, a tool to study exo-and endocytosis

To study vesicle recycling, pHluorin molecules were often fused to the intraluminal loop of vesicular proteins, such as SybII (Sankarnarayanan et al., 2000; Sankarnarayanan et al., 2001; Li et al., 2005; Burrone et al., 2007), Syt (Dean et al., 2012), Synaptophysin (Granseth et al., 2006), vesicular glutamate transporter [v-Glut] (Fernandez-Alfonso et al., 2008) and post-synaptic receptors (Rathje et al., 2013). By using an integral membrane protein as an anchor for pHluorin, the signal time course should reflect not only the initial opening (dequenching) of the fusion pore but also endocytosis and reacidification (Miesenböck et al., 1998; Vardjan et al., 2007). Vesicles must undergo few prerequisite steps in order to get endocytosed, such as cavcapture and retrieval. Capacitance measurements are capable to demonstrate the granular retrieval (Albillos et al., 1997; Ales et al., 1999; Henkel et al., 2001). To elucidate cavcapture, earlier investigations by Perrais et al., 2004, illustrated continuity of the granule with the external space by using tPA-EGFP and systematic alteration of the extracellular pH. The time course of Syb-pHluorin can be dissected within three stage, such as rise time, duration and decay that represents initial opening of fusion pore, open state or dilated state of fusion pore and dissipation of signal (might be due to SybII distribution, retrieval and reacidification). Hence, with the use of membrane bound Syb-pHluorin, we were able to report de-acidification (alkalization) due to initial opening of the fusion pore and reacidification together with endocytosis of the vesicle. This subsequent reacidification may be accompanied with undocking of vesicles from the plasma

membrane. In contrast to the NPY-pHluorin time course, Syb-pHluorin signal has exhibited a long lasting time-course of pHluorin (Fig. 23). Particularly the decay phase appeared to be longer, a notion that is consistent with the previously reported Syb-pHluorin time course from synaptic boutons, consisting clusters of small synaptic vesicles [SSV] (Sankarnarayanan et al., 2000; Sankarnarayanan et al., 2001; Li et al., 2005; Burrone et al., 2007). The extensive variability is best explained by the multiple factors that govern the decay kinetics of Syb-pHluorin.

4.6 Spatial reorganization of vesicular SybII at fusion site as a consequence of vesicular exocytosis

Lateral diffusion of SybII in form of Syb-pHluorin often accompanied with release processes like insulin release in pancreatic β cells (Tsuboi et al., 2003). Other exocytotic processes also demonstrated radial dispersion of SybII from bouton to the axon in synaptic boutons of hippocampal neurons upon 600 action potentials stimulation at 20Hz (Sankarnarayanan et al., 2000). Lastly, distribution of SybII (Syb-pHluorin) was also observed in the active zone of *Caenorhabditis elegans* motor neurons (Dittman et al., 2006). This study found that SybII equilibrates throughout the axon and surface SybII is enriched in the proximity of active zone. Consistent with these discoveries, short lasting events in our measurement exhibited a one-stage decay of the signal that was accompanied with spatial broadening of the signal over time, i.e. accumulation of fluorescent material around fusion site in complementary to vesicular release (Fig. 27). An attractive explanation for this observation could be that SybII only slowly distributes within the plasma membrane and might be further hindered during its passage through the neck of the fusion pore.

Given aforementioned simulation data (Fig. 32), assuming a 16-fold slower diffusion coefficient of Syb-pHluorin compared with that for NPY-pHluorin, our simulation results revealed that diffusional dispersion of released sybII molecules within the plasma membrane should be clearly detectable at a time resolution of 0.1 s/frame.

Altogether, based on the spatial and the temporal data set we can conclude that these Syb-pHluorin events should represent vesicles do completely merge with the

plasma membrane and thereby allow for dispersion of the membrane bound EGFP-tagged SybII molecules. In addition, if there is a scope of further loss of signal available after SybII distribution then it's primarily facilitated by reacidification (spike-like event).

Furthermore, another set of results suggest that blocking of reacidification (Bafilomycin treatment) affects both event types irrespective of whether they encompass more or less lateral spreading of the SybII molecules in the plasma membrane. This results also agrees with the observation that Bafilomycin shifts the entire frequency distribution for half-width to higher values without affecting specifically short (spike-like events) or long-lasting events (plateau-like events) (Fig. 30, 31).

On the other hand, long-lasting events have shown a usual quick uprise, a prolonged duration and highly variable decay phases. Coupling these features with no spatial broadening (Fig. 28), this sub-population of events demonstrate a different biological phenomenon that mainly comprised of three stages, *viz* vesicles are undocked from the vicinity of plasma membrane and subsequently vesicles are reacidified, and moved out of focal plane. This multi-factorial contribution transform decay phase of Syb-pHluorin time course highly heterogeneous.

Therefore, we intended to find an explanation to address this complicated scenario of huge variability. An attractive explanation for this diversity could be met that as these processes are single vesicular events governed by the stochastic processes, which are modulated by the molecular orchestration of few molecules. Alternatively, they might also be coordinated by multiple SNARE complexes as it was studied by Shi et al., 2012, illustrating 1 SNARE complex opens the fusion pore and multiple SNARE complex sustain the opening state of the fusion pore. Therefore, it is possible for our result that involvement of multiple SNARE complex in the process might lead to exocytosis and contribution of single SNARE complex might direct the process to endocytosis.

4.7 Bafilomycin treatment prolongs the time course of Syb-pHluorin events

The vesicular ATPase (v-ATPase) pump is known to consist of 2 main subunits V_0

and V_1 multi-subunit complex. The V_0 subunit comprises the main proteolipid pore complex in the membrane (Israël et al., 1986). Bafilomycin (Baf), the blocker of v-ATPase is known to inhibit the function V_0 complex with its interaction with the complex itself (Dröse et al. 1993; Zhang et al., 1994). Regarding binding efficiency of Baf to V_0 complex, an earlier study reported that bafilomycin A1 binds very tightly to the purified v-ATPase of chromaffin granules, with a dissociation constant of $\sim K_D \sim$ approximately $10^{-8} \text{ mol l}^{-1}$ (Hanada et al., 1990).

Our results illustrate that Baf prolongs the time course of Syb-pHluorin events as judged from an increase in the mean event half-width and tau (τ), and also from the shift in the frequency distribution to higher value. Therefore, we could conclude that bafilomycin induces a delay in the onset of reacidification (Fig. 30). The lateral dispersion of Syb-pHluorin remaining in presence of Baf suggests that the decay kinetics observed in the presence of Baf are most likely governed at least in part by diffusional dispersion of the labeled molecules in the plasma membrane (as shown in the increase of the SD values). Alternatively, it is possible that events that do not show such increase in SD may facilitate the signal decay by post-endocytotic transport of vesicles out of focal plane. This conclusion is particularly valid because the continuous presence of Baf (with higher $K_D \sim$ approximately $10^{-8} \text{ mol l}^{-1}$) makes it likely that the proton transport through the v-ATPase is efficiently blocked. In general, both vesicle populations have a similar fate, i.e. retrieval and reacidification.

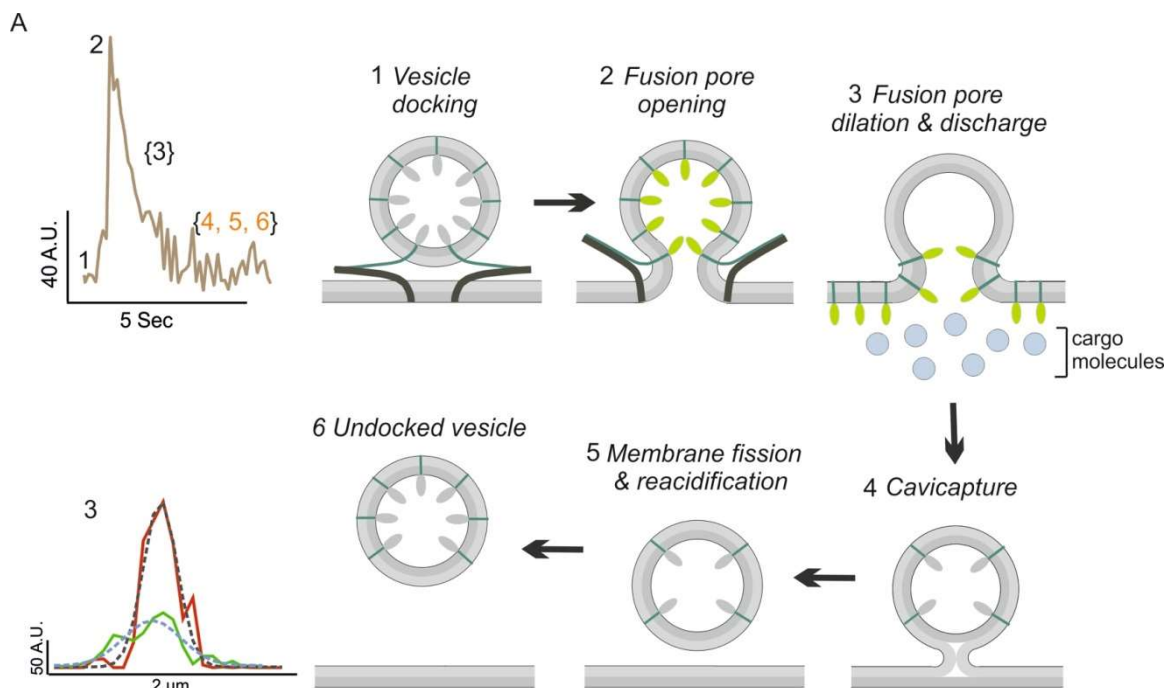
Interestingly, our findings exhibited similar pattern of Syb-pHluorin time course in presence of Baf compared with previously investigations in synaptic boutons that were used to determine the recycling synaptic vesicles, by using Baf-induced 'alkaline trapping' method, where bafilomycin blocks the reacidification of immediate endocytosed vesicles and traps them in an alkaline state (Sankarnarayanan et al., 2001; Li et al., 2005; Burrone et al., 2007).

Nonetheless, previous investigations with Baf and Syb-pHluorin in synaptic boutons observed a continuously fluorescent state of Syb-pHluorin or a strongly prolonged time course of decay at post fusion state (Sankarnarayanan et al., 2001; Burrone et al., 2007). This change in time course became even more prominent, with increasing the dose of Baf ($0.5 \mu\text{M}$ - $5 \mu\text{M}$) (Sankarnarayanan et al., 2001). This different behavior of Syb-pHluorin signal in our cells and neurons may be due

to the fact that Synaptic bouton represents clusters of small synaptic vesicles (~100-500 vesicles) that remain in the same focal plane. In our experiment importantly vesicles transport out of focal plane should contribute to the culmination of the Syb-pHluorin signal.

Taken together, we conclude that the Syb-pHluorin time course is mainly governed by three factors: (1) SybII distribution through the lipid-bridge formed between vesicle and plasma membrane, (2) reacidification of the vesicular lumen, and (3) undocking of vesicles following typical scenarios of the exocytosing vesicles have been displayed in Fig 36A for spike events and 37A for plateau event, comprising steps like cavicapture and subsequent membrane fission. Additionally, variability in the duration of the fusion pore also plays a modulatory factor in determining the signal time course.

In summary, our observations pinpoint differential opening modes of the fusion pore and also provide information on the fate of vesicles at a post-fusion state that is few seconds after the initiation of exocytosis. This time domain monitored in our method cannot be measured with other techniques, such as carbon fiber amperometry.



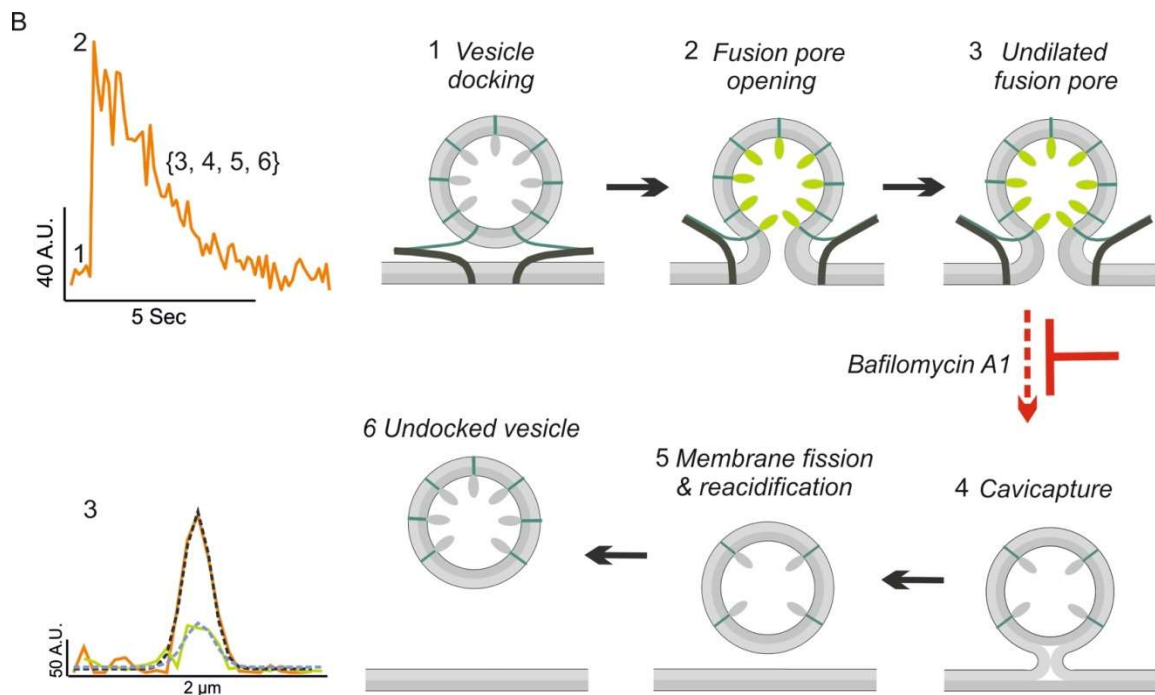


Fig. 36: Schematic model demonstrating stimulation-elicited Syb-pHluorin events from LDCVs in chromaffin cells: A. Stages of *spike event*. (1) Docking of vesicle in the proximity of plasma membrane. (2) Dequenching of pHluorin molecule, after opening of the fusion pore. (3) Discharge of cargo molecules in the extra-cellular milieu, alongside transfer of SybII through the neck of fusion pore into the plasma membrane. (4) Cavicapture and initiation of luminal reacidification. (5) Membrane fission that detaches vesicle from plasma membrane. (6) Undocking of vesicles that removes vesicles from the vicinity of plasma membrane, thus they are removed from the focal plane. **B. Stages of *plateau event*.** (1) Vesicles are docked in the proximity of plasma membrane. (2) Opening of fusion pore, leading to the dequenching of pHluorin molecule. (3) Opening of fusion pore with incomplete dilation, which hindered cargo efflux, giving adequate time for the initiation of cavicapture. (4) Initiation of luminal reacidification as cavicapture progresses, at this step Bafilomycin A1 acts to block the reacidification. (5) Complete detachment of vesicular structure as it undergoes membrane fission. (6) Lastly, vesicles were undocked for recycling process that removes them from the focal plane.

Compared to the electrochemical detection method to detect alternative cargo (catecholamine) release that provides a temporal duration of 1-50 ms, our measurements could resolve a time domain of few seconds (~10 folds higher than amperometric events) for peptidergic (NPY) cargo molecules and their diffusion at post vesicular fusion state. Given the diameter of an initial fusion pore (<3 nm) and the molecular dimension of NPY-pHluorin (4.6*3.2*3.1 nm), the expulsion of the cargo molecule is hindered due to restricting fusion pore. However, 400 dalton

sized catecholamines with a dimension of $1*0.4*0.4$ nm, can be expelled without any hindrance, as it was shown previously by our group Kesavan et al., 2007.

In addition to NPY-pHluorin, our study also addressed differential kinetics and spatial behaviors of a membrane bound slowly diffusing molecule, i.e. SynaptopHluorin (Syb-pHluorin). With Syb-pHluorin, we could unmask different physiological processes, such as vesicular exocytosis, and endocytosis and reacidification, based on their bafilomycin dependence of the Syb-pHluorin signal time course and distribution of SybII around the neck of fusion pore. However, elucidating the mechanistic components for these variations, with respect to different SNARE and accessory proteins and the context of their supra-molecular organization would be essential for better understanding neurotransmitter release and cellular trafficking.

5. References

Alberts, B., Johnson, A., Lewis, J., Raff, M., Roberts, K., Walter, P. (2002). *Molecular Biology of the Cell, 4th edition*. New York: Garland Science.

Alberts, P., Daumke, O., Deverson, E.V., Howard, J.C., Knittler, M.R. (2001). Distinct functional properties of the TAP subunits coordinate the nucleotide-dependent transport cycle. *Curr. Biol.* 11,242-251.

Albillos, A., Dernick, G., Horstmann, H., Almers, W., Alvarez de Toledo, G., Lindau, M. (1997). The exocytotic event in chromaffin cells revealed by patch amperometry. *Nature* 389, 509-512.

Alés, E., Tabares, L., Poyato, J.M., Valero, V., Lindau, M., Alvarez de Toledo, G. (1999). High calcium concentrations shift the mode of exocytosis to the kiss-and-run mechanism. *Nat. Cell Biol.* 1, 40-44.

Almers, W. (1990). Exocytosis. *Annual Review Physiology* 52, 607-624.

Alvarez de Toledo, G., Fernández-Chacón, R., Fernández, J.M. (1993). Release of secretory products during transient vesicle fusion. *Nature* 363, 554-558.

An, S.J., Grabner, C.P., Zenisek, D. (2010). Real-time visualization of Complexin during single exocytic events. *Nat. Neurosci.* 5, 577-583.

Archer, D.A., Graham, M.E., Burgoyne, R.D. (2002). Complexin regulates the closure of the fusion pore during regulated vesicle exocytosis. *J. Biol. Chem.* 277, 18249-18252.

Ashery, U., Varoqueaux, F., Voets, T., Betz, A., Thakur, P., Koch, H., Neher, E., Brose, N., Rettig, J. (2000). Munc13-1 acts as a priming factor for large dense-core vesicles in bovine chromaffin cells. *EMBO J.* 19, 3586-3596.

Augustine, G.J., Burns, M.E., DeBello, W.M., Hilfiker, S., Morgan, J.R., Schweizer, F.E., Tokumaru, H., Umayahara, K. (1999). Proteins involved in synaptic vesicle trafficking. *J. Physiol.* 520, 33-41.

- Banerjee, A., Barry, V.A., DasGupta, B.R., Martin, T.F. (1996). N-Ethylmaleimide-sensitive factor acts at a pre-fusion ATP-dependent step in Ca^{2+} -activated exocytosis. *J. Biol. Chem.* **271**, 20223-20226.
- Basu, J., Shen, N., Dulubova, I., Lu, J., Guan, R., Guryev, O., Grishin, N.V., Rosenmund, C., Rizo, J. (2005). A minimal domain responsible for Munc13 activity. *Nat. Struct. Mol. Biol.* **11**, 1017-1018.
- Baumert, M., Maycox, P.R., Navone, F., De Camilli, P., Jahn, R. (1989). Synaptobrevin: an integral membrane protein of 18,000 daltons present in small synaptic vesicles of rat brain. *EMBO J.* **8**, 379-384.
- Becherer, U., Rettig, J. (2006). Vesicle pools, docking, priming, and release. *Cell Tissue Res.* **326**, 393-407.
- Bittner M.A., Holz R.W. (1992) Kinetic analysis of secretion from permeabilized adrenal chromaffin cells reveals distinct components. *J. Biol. Chem.* **267**, 16219-16225.
- Borisovska, M., Schwarz, Y.N., Dhara, M., Yarzagaray, A., Hugo, S., Narzi, D., Siu, S.W., Kesavan, J., Mohrmann, R., Böckmann, R.A., Bruns, D. (2012). Membrane-proximal tryptophans of synaptobrevin II stabilize priming of secretory vesicles. *J. Neurosci.* **32**, 15983-15997.
- Borisovska, M., Zhao, Y., TSytsyura, Y., Glyvuk, N., Takamori, S., Matti, U., Rettig, J., Südhof, T., Bruns D. (2005). v-SNAREs control exocytosis of vesicles from priming to fusion. *EMBO J.* **24**, 2114-2126.
- Bowser, D.N., Khakh, B.S. (2007). Two forms of single-vesicle astrocyte exocytosis imaged with total internal reflection fluorescence microscopy. *Proc. Natl. Acad. Sci. U S A.* **104**, 4212-4217.
- Bracher, A., Kadlec, J., Betz, H., Weissenhorn, W. (2002). X-ray structure of a neuronal Complexin-SNARE complex from squid. *J. Biol. Chem.* **277**, 26517-26523.
- Brose, N., Hofmann, K., Hata, Y., Südhof, T.C. (1995). Mammalian homologues of *Caenorhabditis elegans* unc-13 gene define novel family of C2-domain proteins. *J Biol.*

Chem. 270, 25273-25280.

Brunger, A.T., Wenginger, K., Bowen, M., Chu, S. (2009). Single-molecule studies of the neuronal SNARE fusion machinery. *Annual Review Biochemistry* 78, 903-928.

Bruns, D. (2004). Detection of transmitter release with carbon fiber electrodes. *Methods* 33, 312-321.

Bruns, D., Jahn, R. (1995). Real-time measurement of transmitter release from single synaptic vesicles. *Nature* 377, 62-65.

Bruns, D., Riedel, D., Klingauf, J., Jahn, R. (2000). Quantal release of serotonin. *Neuron* 28, 205-220.

Burgess, T.L., Kelly, R.B. (1987). Constitutive and regulated secretion of proteins. *Annual Review Cell Biology* 3, 243-293.

Burgoyne, R.D., Clague, M.J. (2003). Calcium and calmodulin in membrane fusion. *Biochimica et Biophysica Acta* 1641, 137-143.

Burgoyne, R.D., Morgan, A. (2003). Secretory Granule Exocytosis. *Physiology Review* 83, 581-632.

Burrone, J., Li, Z., Murthy, V.N. (2006) Studying vesicle cycling in presynaptic terminals using the genetically encoded probe synaptopHluorin. *Nat. Protoc.* 1, 2970-2978.

Cao, P., Yang, X., Südhof, T.C. (2013). Complexin activates exocytosis of distinct secretory vesicles controlled by different Synaptotagmins. *J. Neurosci.* 33, 1714-1727.

Chapman, E.R. (2008). How does Synaptotagmin trigger neurotransmitter release? *Annual Review Biochemistry* 77, 615-41.

Chen, X., Tomchick, D.R., Kovrigin, E., Araç, D., Machius, M., Südhof, T.C., Rizo, J. (2002). Three-dimensional structure of the Complexin/SNARE complex. *Neuron* 33, 397-409.

Chilcote, T.J., Galli, T., Mundigl, O., Edelmann, L., McPherson, P.S., Takei, K., De Camilli, P. (1995). Cellubrevin and synaptobrevins: similar subcellular localization and biochemical properties in PC12 cells. *J. Cell. Biol.* **129**,219-231.

Cho, R.W., Song, Y., Littleton, J.T. (2010). Comparative analysis of *Drosophila* and mammalian complexins as fusion clamps and facilitators of neurotransmitter release. *Mol. Cell Neurosci.* **45**, 389-397.

Chow, R.H., Von Rüden, L., Neher, E. (1992). Delay in vesicle fusion revealed by electrochemical monitoring of single secretory events in adrenal chromaffin cells. *Nature* **356**, 60-63.

Chung, S.H., Takai, Y., Holz, R.W. (1995) Evidence that the Rab3a-binding protein, rabphilin3a, enhances regulated secretion. Studies in adrenal chromaffin cells. *J. Biol. Chem.* **270**, 16714-16718.

Coussens, L., Parker, P.J., Rhee L., Yang-Feng, T.L., Chen E., Waterfield, M.D., Francke, U., Ullrich A. (1986). Multiple, Distinct Forms of Bovine and Human Protein Kinase C Suggest Diversity in Cellular Signaling Pathways. *Science* **233**, 859-866.

Curran, M.J., Cohen, F.S., Chandler, D.E., Munson, P.J., Zimmerberg, J. (1993). Exocytotic fusion pores exhibit semi-stable states. *J. Membr. Biol.* **133**,61-75.

Davletov, B.A., Südhof, T.C. (1993) A single C2 domain from Synaptotagmin I is sufficient for high affinity Ca²⁺/phospholipid binding. *J. Biol. Chem.* **268**, 26386-26390.

Deák, F., Shin, O.H., Kavalali, E.T., Südhof, T.C. (2006). Structural determinants of synaptobrevin 2 function in synaptic vesicle fusion. *J. Neurosci.*, **26**,6668-6676.

Dean, C., Dunning, F.M., Liu, H., Bomba-Warczak, E., Martens, H., Bharat, V., Ahmed, S., Chapman, E.R. (2012). Axonal and dendritic synaptotagmin isoforms revealed by a pHluorin-syt functional screen. *Mol. Biol. Cell.* **23**1715-1727

Deitcher, D.L., Ueda, A., Stewart, B.A., Burgess, R.W., Kidokoro, Y., Schwarz, T.L. (1998). Distinct requirements for evoked and spontaneous release of neurotransmitter are revealed by mutations in the *Drosophila* gene neuronal-synaptobrevin. *J. Neurosci.* **18**, 2028-2039.

De Wit, H., Cornelisse, L.N., Toonen, R.F., Verhage, M. (2006). Docking of secretory vesicles is syntaxin dependent. *PLoS One*. *1*, e126.

De Wit H., Walter, A.M., Milosevic., I., Gulyás-Kovács, A., Riedel, D., Sørensen, J.B., Verhage, M., (2009). SynaptotagminI docks secretory vesicles to syntaxin-1/SNAP-25 acceptor complexes. *Cell* *138*, 935-946.

Dhara, M., Yarzagaray, A., Schwarz, Y., Dutta, S., Grabner, C., Moghadam, P.K., Bost, A., Schirra, C., Rettig, J., Reim, K., Brose, N., Mohrmann, R., Bruns, D. (2014). Complexin synchronizes primed vesicle exocytosis and regulates fusion pore dynamics. *J. Cell Biol.* *204*, 1123-1140.

Dittman, J.S., Kaplan, J.M. (2006). Factors regulating the abundance and localization of synaptobrevin in the plasma membrane. *Proc. Natl. Acad. Sci. U S A.* *103*, 11399-11404.

Dröse S1, Altendorf K. (1997). Bafilomycins and concanamycins as inhibitors of v-ATPases and P-ATPases. *J. Exp. Biol.* *200*, 1-8.

Dulubova, I., Sugita, S., Hill, S., Hosaka, M., Fernandez, I., Südhof, T.C., Rizo, J. (1999). A conformational switch in syntaxin during exocytosis: role of munc18. *EMBO J.* *18*, 4372-4382.

Edwardson, J.M., Daniels-Holgate, P.U. (1992). Reconstitution in vitro of a membrane-fusion event involved in constitutive exocytosis. A role for cytosolic proteins and a GTP-binding protein, but not for Ca²⁺. *Biochem. J.* *285*, 383-385.

Elferink, L.A., Trimble, W.S., Scheller, R.H. (1989). Two vesicle-associated membrane protein genes are differentially expressed in the rat central nervous system. *J. Biol. Chem.* *264*, 11061-11064.

Eberhard, D.A., Cooper, C.L., Low, M.G., Holz, R.W. (1990). Evidence that the inositol phospholipids are necessary for exocytosis. Loss of inositol phospholipids and inhibition of secretion in permeabilized cells caused by a bacterial phospholipase C and removal of ATP. *Biochem. J.* *268*, 15-25.

Fasshauer, D., Bruns, D., Shen, B., Jahn, R., Brünger, A.T. (1997). A structural change occurs upon binding of syntaxin to SNAP-25. *J. Biol Chem.*272, 4582-4590.

Fasshauer, D., Margittai, M. (2004). A transient N-terminal interaction of SNAP-25 and syntaxin nucleates SNARE assembly. *J. Biol. Chem.*,279,7613-7321.

Fasshauer, D., Otto, H., Eliason, W.K., Jahn, R., Brünger, A.T. (1997). Structural changes are associated with soluble N-ethylmaleimide-sensitive fusion protein attachment protein receptor complex formation. *J. Biol. Chem.*272, 28036-28041.

Fernandez-Alfonso, T., Ryan, T.A. (2008). A heterogeneous "resting" pool of synaptic vesicles that is dynamically interchanged across boutons in mammalian CNS synapses. *Brain Cell Biol.*36, 87-100.

Fernandez, J.M., Neher, E., Gomperts, B.D. (1984). Capacitance measurements reveal stepwise fusion events in degranulating mast cells. *Nature*312, 453-455.

Fernández-Chacón, R., Königstorfer, A., Gerber, S.H., García, J., Matos, M.F., Stevens, C.F., Brose, N., Rizo, J., Rosenmund, C., Südhof, T.C. (2001). SynaptotagminI functions as a calcium regulator of release probability. *Nature.* 410,41-49.

Friedrich, R., Yeheskel, A., Ashery, U. (2010). DOC2B, C2 domains, and calcium: A tale of intricate interactions. *Mol. Neurobiol.*41, 42-51.

Gaffield, M.A., Tabares, L., Betz, W.J. (2009). The spatial pattern of exocytosis and post-exocytic mobility of synaptopHluorin in mouse motor nerve terminals. *J. Physiol.*587,1187-1200.

Gandhi, S.P., Stevens, C.F. (2003). Three modes of synaptic vesicular recycling revealed by single-vesicle imaging. *Nature*423, 607-613.

Gentet, L.J., Stuart, G.J., Clements, J.D. (2000). Direct measurement of specific membrane capacitance in neurons. *Biophys J.*79, 314-320.

Geppert, M., Archer, B.T.III, Südhof TC. (1991). SynaptotagminII. A novel differentially distributed form of Synaptotgmin. *J. Biol. Chem.*266,13548-13552.

Geppert, M., Goda, Y., Hammer, R.E., Li, C., Rosahl, T.W., Stevens, C.F., Südhof, T.C. (1994). Synaptotagmin I: a major Ca²⁺ sensor for transmitter release at a central synapse. *Cell*79, 717-727.

Gerber, S.H., Rah, J.C., Min, S.W., Liu, X., De Wit, H., Dulubova, I., Meyer, A.C., Rizo, J., Arancillo, M., Hammer, R.E., Verhage, M., Rosenmund, C., Südhof, T.C. (2008). Conformational switch of syntaxin-1 controls synaptic vesicle fusion. *Science*321, 1507-1510.

Gillis, K.D., Pun, R.Y., Mislér, S. (1991). Long-term monitoring of depolarization-induced exocytosis from adrenal medullary chromaffin cells and pancreatic islet B cells using "perforated patch recording". *Ann. N. Y. Acad. Sci.*635, 464-467.

Gillis, K.D., Mislér, S. (1992). Single cell assay of exocytosis from pancreatic islet B cells. *Pflugers. Arch.*420, 121-123.

Gomi, H., Mizutani, S., Kasai, K., Itohara, S., Izumi, T. (2005). Granophilin molecularly docks insulin granules to the fusion machinery. *J. Cell Biol.*171, 99-109.

Gomperts, B.D. (1990). G_E: A GTP-binding protein mediating exocytosis. *Annual Review Physiology.* 52, 591- 606.

Granseth, B., Odermatt, B., Royle, S.J., Lagnado, L. (2006). Clathrin-mediated endocytosis is the dominant mechanism of vesicle retrieval at hippocampal synapses. *Neuron.*51, 773-786.

Groffen, A.J., Martens, S., Díez Arazola, R., Cornelisse, L.N., Lozovaya, N., de Jong, A.P., Goriounova, N.A., Habets, R.L., Takai, Y., Borst, J.G., Brose, N., McMahon, H.T., Verhage, M. (2010). Doc2b is a high-affinity Ca²⁺ sensor for spontaneous neurotransmitter release. *Science* 327, 1614-1618.

Guy, J., Li, S., Pelletier, G. (1988). Studies on the physiological role and mechanism of action of neuropeptide Y in the regulation of luteinizing hormone secretion in the rat. *Regul. Pept.*, 23, 209-216.

Hammarlund, M., Watanabe, S., Schuske, K., Jorgensen, E.M. (2008). CAPS and syntaxin dock dense core vesicles to the plasma membrane in neurons. *J. Cell Biol.* **180**, 483-491.

Hanada, H., Moriyama, Y., Maeda, M., Futai, M. (1990). Kinetic studies of chromaffin granule H⁺-ATPase and effects of bafilomycin A1. *Biochem. Biophys. Res. Commun.* **170**, 873-878.

Hansel, D.E., Eipper, B.A., Ronnett, G.V. (2001). Neuropeptide Y functions as a neuroproliferative factor. *Nature* **410**, 940-944.

Hata, Y., Slaughter, C.A., Südhof, T.C. (1993). Synaptic vesicle fusion complex contains unc-18 homologue bound to syntaxin. *Nature*, **366**, 347-351.

Hata, Y., Davletov, B., Petrenko, A.G., Jahn, R., Südhof, T.C. (1993). Interaction of Synaptotagmin with the cytoplasmic domains of neurexins. *Neuron*, **10**, 307-315.

Helms, J.B., Karrenbauer, A., Wirtz, K.W., Rothman J.E., Wieland, F.T. (1990) Reconstitution of steps in the constitutive secretory pathway in permeabilized cells. Secretion of glycosylated tripeptide and truncated sphingomyelin. *J. Biol. Chem.*, **265**, 20027-20032.

Hay, J.C., Martin, T.F. (1992). Resolution of regulated secretion into sequential MgATP-dependent and calcium-dependent stages mediated by distinct cytosolic proteins. *J. Cell Biol.*, **119**, 139-151.

Hay, J.C., Fisette, P.L., Jenkins, G.H., Fukami, K., Takenawa, T., Anderson, R.A., Martin, T.F. (1995). ATP-dependent inositide phosphorylation required for Ca²⁺-activated secretion. *Nature*, **374**, 173-177.

Hiesinger, P.R., Fayyazuddin, A., Mehta, S.Q., Rosenmund, T., Schulze, K.L., Zhai, R.G., Verstreken, P., Cao, Y., Zhou, Y., Kunz, J., Bellen, H.J. (2005). The v-ATPase V0 subunit a1 is required for a late step in synaptic vesicle exocytosis in *Drosophila*. *Cell* **121**, 607-620.

Hobson, R.J., Liu, Q., Watanabe, S., Jorgensen, E.M. (2011). Complexin maintains

vesicles in the primed state in *C. elegans*. *Curr. Biol.* *21*, 106-113.

Holz, R.W., Bittner, M.A., Peppers, S.C., Senter, R.A., Eberhard, D.A. (1989). MgATP-independent and MgATP-dependent exocytosis. Evidence that MgATP primes adrenal chromaffin cells to undergo exocytosis. *J. Biol. Chem.* *264*, 5412-5419.

Hoopmann P, Rizzoli SO, Betz WJ. (2012). Imaging synaptic vesicle recycling by staining and destaining vesicles with FM dyes. *Cold Spring Harb. Protoc.* *Jan 1;2012*, 77-83.

Hua, Y., Scheller, R.H. (2001). Three SNARE complexes cooperate to mediate membrane fusion. *Proc. Natl. Acad. Sci. U S A.* *98*, 8065-8070.

Israël, M., Morel, N., Lesbats, B., Birman, S., Manaranche, R. (1986). Purification of a presynaptic membrane protein that mediates a calcium-dependent translocation of acetylcholine. *Proc. Natl. Acad. Sci. U S A.* *83*, 9226-9230.

Jackson, M.B., Chapman, E.R. (2006). Fusion pores and fusion machines in Ca²⁺-triggered exocytosis. *Annu Rev Biophys Biomol Struct.*; *35*:135-60.

Jackson, M.B., Chapman, E.R. (2008). The fusion pores of Ca²⁺-triggered exocytosis. *Nat. Struct. Mol. Biol.* *15*, 684-689.

Jahn, R., Fasshauer, D. (2012). Molecular machines governing exocytosis of synaptic vesicles. *Nature* *490*, 201-207.

Jockusch, W.J., Speidel, D., Sigler, A., Sørensen, J.B., Varoqueaux, F., Rhee, J.S., Brose, N. (2007). CAPS-1 and CAPS-2 are essential synaptic vesicle priming proteins. *Cell* *131*, 796-808.

Kaesler-Woo, Y.J., Yang, X., Südhof, T.C. (2012). C-terminal Complexin sequence is selectively required for clamping and priming but not for Ca²⁺ triggering of synaptic exocytosis. *J. Neurosci.* *32*, 2877-2885.

Kalra, S.P., Kalra, P.S. (2004). NPY and cohorts in regulating appetite, obesity and metabolic syndrome: beneficial effects of gene therapy. *Neuropeptides.* *38*, 201-211.

- Kelly, R.B. (1991). Storage and Release of Neurotransmitters. *Curr. Opin. Cell Biol.*3, 654-660.
- Kesavan, J., Borisovska, M., Bruns, D. (2007). v-SNARE actions during Ca(2+)-triggered exocytosis. *Cell*131, 351-363.
- Klyachko, V.A., Jackson, M.B. (2002). Capacitance steps and fusion pores of small and large-dense-core vesicles in nerve terminals. *Nature*418, 89-92.
- Koushika, S.P., Richmond, J.E., Hadwiger, G., Weimer, R.M., Jorgensen, E.M., Nonet, M.L. (2001). A post-docking role for active zone protein Rim. *Nat. Neurosci.*4, 997-1005.
- Kümmel, D., Krishnakumar, S.S., Radoff, D.T., Li, F., Giraudo, C.G., Pincet, F., Rothman, J.E., Reinisch, K.M. (2011). Complexin cross-links prefusion SNAREs into a zigzag array. *Nat. Struct. Mol. Biol.*18, 927-933.
- Lai, A.L., Huang, H., Herrick, D.Z., Epp, N., Cafiso, D.S. (2011). Synaptotagmin1 and SNAREs form a complex that is structurally heterogeneous. *J. Mol. Biol.*405, 696-706.
- Li, F., Pincet, F., Perez, E., Eng, W.S., Melia, T.J., Rothman, J.E., Tareste, D., (2007). Energetics and dynamics of SNAREpin folding across lipid bilayers. *Nat. Struct. Mol. Biol.*14, 890-896.
- Lindau, M., Almers, W. (1995). Structure and function of fusion pores in exocytosis and ectoplasmic membrane fusion. *Curr. Opin. Cell Biol.*7,509-517.
- Lindau, M., Alvarez de Toledo, G. (2003). The fusion pore. *Biochim. Biophys. Acta*1641, 167-173.
- Li, W., Ma, C., Guan, R., Xu, Y., Tomchick, D.R., Rizo, J. (2011). The crystal structure of a Munc13 C-terminal module exhibits a remarkable similarity to vesicle tethering factors. *Structure.*19, 1443-1455.
- Li, Z., Burrone, J., Tyler, W.J., Hartman, K.N., Albeanu, D.F., Murthy, V.N. (2005). Synaptic vesicle recycling studied in transgenic mice expressing synaptotHluorin. *Proc. Natl. Acad. Sci. U S A.*102,6131-6136.

Lodish, H. et al., (2008). *Molecular Cell Biology, Sixth edition*. W. H. Freeman and company

McNew, J.A., Weber, T., Engelman, D.M., Söllner, T.H., Rothman, J.E. (1999). The length of the flexible SNAREpin juxtamembrane region is a critical determinant of SNARE-dependent fusion. *Mol. Cell*, *4*, 415-421.

McNew, J.A., Weber, T., Parlati, F., Johnston, R.J., Melia, T.J., Söllner, T.H., Rothman, J.E. (2000). Close is not enough: SNARE-dependent membrane fusion requires an active mechanism that transduces force to membrane anchors. *J. Cell Biol.*, *150*, 105-117.

Ma, C., Li, W., Xu, Y., Rizo, J. (2011). Munc13 mediates the transition from the closed syntaxin-Munc18 complex to the SNARE complex. *Nat. Struct. Mol. Biol.* *18*, 542-549.

Malsam, J., Seiler, F., Schollmeier, Y., Rusu, P., Krause, J.M., Söllner, T.H. (2009). The carboxy-terminal domain of ComplexinI stimulates liposome fusion. *Proc. Natl. Acad. Sci. U S A.* *106*, 2001-2006.

Manabe, T., Yoshimori, T., Henomatsu, N., Tashiro, Y. (1993). Inhibitors of vacuolar-type H(+)-ATPase suppresses proliferation of cultured cells. *J Cell Physiol.* *157*, 445-452.

Martin, J.A., Hu, Z., Fenz, K.M., Fernandez, J., Dittman, J.S. (2011). Complexin has opposite effects on two modes of synaptic vesicle fusion. *Curr. Biol.* *21*, 97-105.

Martin, T.F. (2002). Prime movers of synaptic vesicle exocytosis. *Neuron* *34*, 9-12.

Maruyama, I.N., Brenner, S. (1991). A phorbol ester/diacylglycerol-binding protein encoded by the unc-13 gene of *Caenorhabditis elegans*. *Proc. Natl. Acad. Sci. U S A.* *88*, 5729-5733.

Matthew WD, Tsavaler L, Reichardt LF. (1981). Identification of a synaptic vesicle-specific membrane protein with a wide distribution in neuronal and neurosecretory tissue. *J. Cell. Biol.* *91*, 257-269.

Mattsson, J.P., Keeling, D.J. (1996). [³H]Bafilomycin as a probe for the transmembrane proton channel of the osteoclast vacuolar H(+)-ATPase. *Biochim. Biophys. Acta.* *1280*, 98-

106.

Maximov, A., Südhof, T.C. (2005). Autonomous function of Synaptotagmin1 in triggering synchronous release independent of asynchronous release. *Neuron* **48**, 547-554.

Maximov, A., Tang, J., Yang, X., Pang, Z.P., Südhof, T.C. (2009). Complexin controls the force transfer from SNARE complexes to membranes in fusion. *Science* **323**, 516-521.

McMahon, H.T., Missler, M., Li, C., Südhof, T.C. (1995). Complexins: cytosolic proteins that regulate SNAP receptor function. *Cell* **83**, 111-119.

McMahon, H.T., Ushkaryov, Y.A., Edelman, L., Link, E., Binz, T., Niemann, H., Jahn, R., Südhof, T.C. (1993). Cellubrevin is a ubiquitous tetanus-toxin substrate homologous to a putative synaptic vesicle fusion protein. *Nature* **364**, 346-349.

McNew, J.A., Parlati, F., Fukuda, R., Johnston, R.J., Paz, K., Paumet, F., Söllner, T.H., Rothman, J.E. (2000). Compartmental specificity of cellular membrane fusion encoded in SNARE proteins. *Nature* **407**, 153-159.

McNew, J.A., Weber, T., Parlati, F., Johnston, R.J., Melia, T.J., Söllner, T.H., Rothman, J.E. (2000). Close is not enough: SNARE-dependent membrane fusion requires an active mechanism that transduces force to membrane anchors. *J. Cell Biol.* **150**, 105-117.

Mochida, S., Orita, S., Sakaguchi, G., Sasaki, T., Takai, Y. (1998). Role of the Doc2 alpha-Munc13-1 interaction in the neurotransmitter release process. *Proc. Natl. Acad. Sci. U S A.* **95**, 11418-11422.

Neher, E., Marty, A. (1982). Discrete changes of cell membrane capacitance observed under conditions of enhanced secretion in bovine adrenal chromaffin cells. *Proc. Natl. Acad. Sci. U S A.* **79**, 6712-6716.

Nofal, S., Becherer, U., Hof, D., Matti, U., Rettig, J. (2007). Primed vesicles can be distinguished from docked vesicles by analyzing their mobility. *J. Neurosci.* **27**, 1386-1395.

Orita, S., Sasaki, T., Komuro, R., Sakaguchi, G., Maeda, M., Igarashi, H., Takai, Y. (1996). Doc2 enhances Ca²⁺-dependent exocytosis from PC12 cells. *J. Biol. Chem.* **271**, 7257-

7260.

Orita, S., Naito, A., Sakaguchi, G., Maeda, M., Igarashi, H., Sasaki, T., Takai, Y. (1997). Physical and functional interactions of Doc2 and Munc13 in Ca²⁺-dependent exocytotic machinery. *J. Biol. Chem.* 272, 16081-16084.

Ornberg, R.L., Reese, T.S. (1981). Beginning of exocytosis captured by rapid-freezing of *Limulus* amoebocytes. *J. Cell. Biol.* 90, 40-54.

Palade G. (1975). Intracellular aspects of the process of protein synthesis. *Science* 189, 347-358.

Pang, Z.P., Südhof, T.C. (2010). Cell biology of Ca²⁺-triggered exocytosis. *Curr. Opin. Cell Biol.* 22, 496-505.

Pasche, M., Matti, U., Hof, D., Rettig, J., Becherer, U. (2012). Docking of LDCVs is modulated by lower intracellular [Ca²⁺] than priming. *PLoS One*. 7, e36416.

Perin, M.S., Fried, V.A., Mignery, G.A., Jahn, R., Südhof, T.C. (1990). Phospholipid binding by a synaptic vesicle protein homologous to the regulatory region of protein kinase C. *Nature*. 345, 260-263.

Perrais, D., Kleppe, I.C., Taraska, J.W., Almers, W. (2004). Recapture after exocytosis causes differential retention of protein in granules of bovine chromaffin cells. *J. Physiol.* 560, 413-428.

Pinheiro, P.S., de Wit, H., Walter, A.M., Groffen, A.J., Verhage, M., Sørensen, J.B. (2013). Doc2b synchronizes secretion from chromaffin cells by stimulating fast and inhibiting sustained release. *J. Neurosci.* 33, 16459-16470.

Pothos, E.N., Davila, V., Sulzer, D. (1998). Presynaptic recording of quanta from midbrain dopamine neurons and modulation of the quantal size. *J. Neurosci.* 18, 4106-4118.

Pouli, A.E., Emmanouilidou, E., Zhao, C., Wasmeier, C., Hutton, J.C., Rutter, G.A. (1998). Secretory-granule dynamics visualized in vivo with a phogrin-green fluorescent protein chimera. *Biochem. J.*, 333, 193-199.

Rathje, M., Fang, H., Bachman, J.L., Anggono, V., Gether, U., Huganir, R.L., Madsen, K.L. (2013). AMPA receptor pHluorin-GluA2 reports NMDA receptor-induced intracellular acidification in hippocampal neurons. *Proc. Natl. Acad. Sci. U. S. A.* *110*, 14426-14431.

Renshaw, D., Hinson, J.P. Neuropeptide Y and the adrenal gland: a review. *Peptides*. 2001 *22*, 429-438.

Rettig, J., Neher, E. (2002). Emerging roles of presynaptic proteins in Ca⁺⁺-triggered exocytosis. *Science* *298*, 781-785.

Rizo, J., Chen, X., Araç, D. (2006). Unraveling the mechanisms of Synaptotagmin and SNARE function in neurotransmitter release. *Trends Cell Biol.*, *16*, 339-350.

Rothman, J.E., Wieland, F.T. (1996). Protein sorting by transport vesicles. *Science* *272*, 227-234.

Sankaranarayanan, S., De Angelis, D., Rothman, J.E., Ryan, T.A. (2000). The use of pHluorins for optical measurements of presynaptic activity. *Biophys. J.* *79*, 2199-2208.

Sankaranarayanan, S., Ryan, T.A. (2000). Real-time measurements of vesicle-SNARE recycling in synapses of the central nervous system. *Nat. Cell Biol.* *2*, 197-204.

Sankaranarayanan, S., Ryan, T.A. (2001). Calcium accelerates endocytosis of vSNAREs at hippocampal synapses. *Nat. Neurosci.* *4*, 129-136.

Schlüter, O.M., Schnell, E., Verhage, M., Tzonopoulos, T., Nicoll, R.A., Janz, R., Malenka, R.C., Geppert, M., Südhof, T.C. (1999). Rabphilin knock-out mice reveal that rabphilin is not required for rab3 function in regulating neurotransmitter release. *J. Neurosci.* *19*, 5834-5846.

Schoch, S., Castillo, P.E., Jo, T., Mukherjee, K., Geppert, M., Wang, Y., Schmitz, F., Malenka, R.C., Südhof, T.C. (2002). RIM1alpha forms a protein scaffold for regulating neurotransmitter release at the active zone. *Nature* *415*, 321-326.

Schonn, J.S., Maximov, A., Lao, Y., Südhof, T.C., Sørensen, J.B. (2008). Synaptotagmin-

1 and -7 are functionally overlapping Ca²⁺ sensors for exocytosis in adrenal chromaffin cells. *Proc. Natl. Acad. Sci. U S A.* *105*, 3998-4003.

Schroeder, T.J., Borges, R., Finnegan, J.M., Pihel, K., Amatore, C., Wightman, R.M. (1996). Temporally resolved, independent stages of individual exocytotic secretion events. *Biophys. J.* *70*, 1061-1068.

Schütz, D., Zilly, F., Lang, T., Jahn, R., Bruns, D. (2005). A dual function for Munc-18 in exocytosis of PC12 cells. *Eur. J. Neurosci.* *21*, 2419-2432.

Seiler, F., Malsam, J., Krause, J.M., Söllner, T.H. (2009). A role of Complexon-lipid interactions in membrane fusion. *FEBS Lett.* *583*, 2343-2348.

Shi, L., Shen, Q.T., Kiel, A., Wang, J., Wang, H.W., Melia, T.J., Rothman, J.E., Pincet, F. (2012). SNARE proteins: one to fuse and three to keep the nascent fusion pore open. *Science.* *335*, 1355-1359.

Sørensen, J.B., Nagy, G., Varoqueaux, F., Nehring, R.B., Brose, N., Wilson, M.C., Neher, E. (2003). Differential control of the releasable vesicle pools by SNAP-25 splice variants and SNAP-23. *Cell* *114*, 75-86.

Spruce, A.E., Breckenridge, L.J., Lee, A.K., Almers, W. (1990). Properties of the fusion pore that forms during exocytosis of a mast cell secretory vesicle. *Neuron* *4*, 643-654.

Staal, R.G., Mosharov, E.V., Sulzer, D. (2004). Dopamine neurons release transmitter via a flickering fusion pore. *Nat. Neurosci.* *7*, 341-346.

Steiner, H. J., Schmid, K. W., Fischer-Colbrie, R., Sperk, G., Winkler, G. (1989). Co-localization of chromogranin A and B, secretogranin II and neuropeptide Y in chromaffin granules of rat adrenal medulla studied by electron microscopic immunocytochemistry. *Histochemistry* *91*, 473-477.

Steyer, J.A., Horstmann, H., Almers, W. (1997). Transport, docking and exocytosis of single secretory granules in live chromaffin cells. *Nature* *388*, 474-478.

Südhof, T.C. (2012). The presynaptic active zone. *Neuron* *75*, 11-25.

Südhof, T.C., Rothman, J.E. (2009). Membrane fusion: grappling with SNARE and SM proteins. *Science* **323**, 474-477.

Südhof, T.C., Rizo, J. (2011). Synaptic vesicle exocytosis. *Cold Spring Harb. Perspect. Biol.* **1**;3. pii: a005637.

Südhof, T.C. (1995). The synaptic vesicle cycle: a cascade of protein-protein interactions. *Nature* **375**, 645-653.

Swaminathan, R., Hoang, C.P., Verkman, A.S. (1997). Photobleaching recovery and anisotropy decay of green fluorescent protein GFP-S65T in solution and cells: cytoplasmic viscosity probed by green fluorescent protein translational and rotational diffusion. *Biophys. J.* **72**, 1900-1907.

Taraska, J.W., Almers, W. (2004). Bilayers merge even when exocytosis is transient. *Proc. Natl. Acad. Sci. U S A.* **101**, 8780-8785.

Taraska, J.W., Perrais, D., Ohara-Imaizumi, M., Nagamatsu, S., Almers, W. (2003). Secretory granules are recaptured largely intact after stimulated exocytosis in cultured endocrine cells. *Proc. Natl. Acad. Sci. U S A.* **100**, 2070-2075.

Tatemoto, K. (1982). Isolation and characterization of peptide YY (PYY), a candidate gut hormone that inhibits pancreatic exocrine secretion. *Proc. Natl. Acad. Sci. U S A.* **79**, 2514-2518.

Tatemoto, K. (1982). Neuropeptide Y: complete amino acid sequence of the brain peptide. *Proc. Natl. Acad. Sci. U S A.* **79**, 5485-5489.

Tokumaru, H., Shimizu-Okabe, C., Abe, T. (2008). Direct interaction of SNARE complex binding protein synaphin/Complexin with calcium sensor Synaptotagmin 1. *Brain Cell Biol.* **36**, 173-189.

Toonen, R.F., Kochubey, O., de Wit, H., Gulyas-Kovacs, A., Konijnenburg, B., Sørensen, J.B., Klingauf, J., Verhage, M. (2006). Dissecting docking and tethering of secretory vesicles at the target membrane. *EMBO J.* **25**, 3725-3737.

Toonen, R.F., Wierda, K., Sons, M.S., de Wit, H., Cornelisse, L.N., Brussaard, A., Plomp, J.J., Verhage, M. (2006). Munc18-1 expression levels control synapse recovery by regulating readily releasable pool size. *Proc. Natl. Acad. Sci. U S A.* *103*, 18332-18337.

Torii, S., Zhao, S., Yi, Z., Takeuchi, T., Izumi, T. (2002). Granuphilin modulates the exocytosis of secretory granules through interaction with syntaxin 1a. *Mol. Cell Biol.* *22*, 5518-5526.

Tsuboi T1, Rutter GA. (2003). Insulin secretion by 'kiss-and-run' exocytosis in clonal pancreatic islet beta-cells. *Biochem. Soc. Trans.* *31*, 833-836.

Tsuboi, T., McMahon, H.T., Rutter, G.A. (2004). Mechanisms of dense core vesicle recapture following "kiss and run" ("cavicapture") exocytosis in insulin-secreting cells. *J. Biol. Chem.* *279*, 47115-47124.

Tsuboi, T., Fukuda, M. (2005). The C2B domain of rabphilin directly interacts with SNAP-25 and regulates the docking step of dense core vesicle exocytosis in PC12 cells. *J. Biol. Chem.* *280*, 39253-39259.

Tsuboi, T., Fukuda, M. (2006). Rab3A and Rab27A cooperatively regulate the docking step of dense-core vesicle exocytosis in PC12 cells. *J. Cell Sci.* *119*, 2196-2203.

Tsuboi, T., Zhao, C., Terakawa, S., Rutter, G.A. (2000). Simultaneous evanescent wave imaging of insulin vesicle membrane and cargo during a single exocytotic event. *Curr. Biol.*, *10*, 1307-1310.

Umata, T., Moriyama, Y., Futai, M., Mekada, E. (1990). The cytotoxic action of diphtheria toxin and its degradation in intact Vero cells are inhibited by bafilomycin A1, a specific inhibitor of vacuolar-type H(+)-ATPase. *J. Biol. Chem.* *265*, 21940-21945.

Ureña, J., Fernández-Chacón, R., Benot, A.R., Alvarez de Toledo, G.A., López-Barneo, J. (1994). Hypoxia induces voltage-dependent Ca²⁺ entry and quantal dopamine secretion in carotid body glomus cells. *Proc. Natl. Acad. Sci. U S A.* *91*, 10208-10211.

Vardjan, N., Stenovc, M., Jorgacevski, J., Kreft, M., Zorec, R. (2007). Subnanometer

fusion pores in spontaneous exocytosis of peptidergic vesicles. *J. Neurosci.* **27**, 4737-4746.

Vardjan, N., Stenovec, M., Jorgacevski, J., Kreft, M., Zorec, R. (2007). Elementary properties of spontaneous fusion of peptidergic vesicles: fusion pore gating. *J. Physiol.* **585**, 655-661.

Varoqueaux, F., Sigler, A., Rhee, J.S., Brose, N., Enk, C., Reim, K., Rosenmund, C. (2002). Total arrest of spontaneous and evoked synaptic transmission but normal synaptogenesis in the absence of Munc13-mediated vesicle priming. *Proc. Natl. Acad. Sci. U S A.* **99**, 9037-9042.

Verhage, M., Sørensen, J.B. (2008). Vesicle docking in regulated exocytosis. *Traffic.* **9**, 1414-1424.

Verhage, M., Maia, A.S., Plomp, J.J., Brussaard, A.B., Heeroma, J.H., Vermeer, H., Toonen, R.F., Hammer, R.E., van den Berg, T.K., Missler, M., Geuze, H.J., Südhof, T.C. (2000). Synaptic assembly of the brain in the absence of neurotransmitter secretion. *Science* **287**, 864-869.

Voets, T., Moser, T., Lund, P.E., Chow, R.H., Geppert, M., Südhof, T.C., Neher, E. (2001). Intracellular calcium dependence of large dense-core vesicle exocytosis in the absence of Synaptotagmin I. *Proc. Natl. Acad. Sci. U S A.* **98**, 11680-11685.

Voets T1, Toonen RF, Brian EC, de Wit H, Moser T, Rettig J, Südhof TC, Neher E, Verhage M. (2001). Munc18-1 promotes large dense-core vesicle docking. *Neuron* **31**, 581-591.

Vrljic, M., Strop, P., Ernst, J.A., Sutton, R.B., Chu, S., Brunger, A.T. (2010). Molecular mechanism of the Synaptotagmin-SNARE interaction in Ca²⁺-triggered vesicle fusion. *Nat. Struct. Mol. Biol.* **17**, 325-331.

Wang, C.T., Grishanin, R., Earles, C.A., Chang, P.Y., Martin, T.F., Chapman, E.R., Jackson, M.B. (2001). Synaptotagmin modulation of fusion pore kinetics in regulated exocytosis of dense-core vesicles. *Science* **294**, 1111-1115.

- Wang, C.T., Lu, J.C., Bai, J., Chang, P.Y., Martin, T.F., Chapman, E.R., Jackson, M.B. (2003). Different domains of Synaptotagmin control the choice between kiss-and-run and full fusion. *Nature* **424**, 943-947.
- Weber, T., Zemelman, B.V., McNew, J.A., Westermann, B., Gmachl, M., Parlati, F., Söllner, T.H., Rothman, J.E. (1998). SNAREpins: minimal machinery for membrane fusion. *Cell*, **92**, 759-772.
- Weimer, R.M., Gracheva, E.O., Meyrignac, O., Miller, K.G., Richmond, J.E., Bessereau, J.L. (2006). UNC-13 and UNC-10/rim localize synaptic vesicles to specific membrane domains. *J. Neurosci.* **26**, 8040-8047.
- Wojcik, S.M., Brose, N. (2007). Regulation of membrane fusion in synaptic excitation-secretion coupling: speed and accuracy matter. *Neuron* **55**, 11-24.
- Xiao, W., Poirier, M.A., Bennett, M.K., Shin, Y.K. (2001). The neuronal t-SNARE complex is a parallel four-helix bundle. *Nat. Struct. Biol.* **8**, 308-311.
- Xue, M., Craig, T.K., Xu, J., Chao, H.T., Rizo, J., Rosenmund, C. (2010). Binding of the Complexin N terminus to the SNARE complex potentiates synaptic-vesicle fusogenicity. *Nat. Struct. Mol. Biol.* **17**, 568-575.
- Xue, M., Giagtzoglou, N., Bellen, H.J. (2011). Dueling Ca²⁺ sensors in neurotransmitter release. *Cell* **147**, 491-493.
- Xue, M., Reim, K., Chen, X., Chao, H.T., Deng, H., Rizo, J., Brose, N., Rosenmund, C. (2007). Distinct domains of Complexin I differentially regulate neurotransmitter release. *Nat. Struct. Mol. Biol.* **14**, 949-958.
- Yang, X., Kaeser-Woo, Y.J., Pang, Z.P., Xu, W., Südhof, T.C. (2010). Complexin clamps asynchronous release by blocking a secondary Ca²⁺ sensor via its accessory α helix. *Neuron* **68**, 907-920.
- Yao, J., Gaffaney, J.D., Kwon, S.E., Chapman, E.R. (2011). Doc2 is a Ca²⁺ sensor required for asynchronous neurotransmitter release. *Cell* **147**, 666-677.

- Yizhar, O., Ashery, U. (2008). Modulating vesicle priming reveals that vesicle immobilization is necessary but not sufficient for fusion-competence. *PLoS One*.3, e2694.
- Yoshihara, M., Littleton, J.T. (2002). SynaptotagminI functions as a calcium sensor to synchronize neurotransmitter release. *Neuron*36, 897-908.
- Yu, M., Kasai, K., Nagashima, K., Torii, S., Yokota-Hashimoto, H., Okamoto, K., Takeuchi, T., Gomi, H., Izumi, T. (2007). Exophilin4/Slp2-a targets glucagon granules to the plasma membrane through unique Ca²⁺-inhibitory phospholipid-binding activity of the C2A domain. *Mol. Biol. Cell*18, 688-696.
- Zhang, J., Feng, Y., Forgac, M. (1994). Proton conduction and bafilomycin binding by the V0 domain of the coated vesicle v-ATPase. *J. Biol. Chem.*269,23518-23523.
- Zhou, Z., Mislis, S., Chow, R.H. (1996). Rapid fluctuations in transmitter release from single vesicles in bovine adrenal chromaffin cells. *Biophys. J.*70, 1543-1552.
- Zhou, K.M., Dong, Y.M., Ge, Q., Zhu, D., Zhou, W., Lin, X.G., Liang, T., Wu, Z.X., Xu, T. (2007). PKA activation bypasses the requirement for UNC-31 in the docking of dense core vesicles from *C. elegans* neurons. *Neuron*56, 657-669.
- Zhu, D., Zhou, W., Liang, T., Yang, F., Zhang, R.Y., Wu, Z.X., Xu, T.(2007).Synaptotagmin 1 and 9 function redundantly in controlling fusion pore of large dense core vesicles. *Biochem. Biophys. Res. Commun.*361, 922-927.
- Zilly, F.E., Sørensen, J.B., Jahn, R., Lang, T. (2006). Munc18-Bound Syntaxin Readily Forms SNARE Complexes with Synaptobrevin in Native Plasma Membranes. *PLoS Biol.*4, e33.

Appendix

Source Invitrogen

[<http://tools.lifetechnologies.com/content/sfs/manuals/18448019.pdf>]

